

Topological Methods for the Analysis of Solar Magnetic Fields

Dana W. Longcope

Department of Physics
Montana State University
Bozeman, Montana 59717
U.S.A.

email: dana@solar.physics.montana.edu
<http://solar.physics.montana.edu/dana>

Accepted on 28 June 2005

Published on 29 November 2005

Living Reviews in Solar Physics

Published by the
Max Planck Institute for Solar System Research
Max-Planck-Str. 2, 37191 Katlenburg-Lindau, Germany
ISSN 1614-4961

Abstract

The solar coronal magnetic field is anchored to a complex distribution of photospheric flux consisting of sunspots and magnetic elements. Coronal activity such as flares, eruptions and general heating is often attributed to the manner in which the coronal field responds to photospheric motions. A number of powerful techniques have been developed to characterize the response of the coronal field by describing its *topology*. According to such analyses, activity will be concentrated around topological features in the coronal field such as separatrices, null points or bald patches. Such topological properties are insensitive to the detailed geometry of the magnetic field and thereby create an analytic tool powerful and robust enough to be useful on complex observations with limited resolution. This article reviews those topological techniques, their developments and applications to observations.

How to cite this article

Owing to the fact that a *Living Reviews* article can evolve over time, we recommend to cite the article as follows:

Dana W. Longcope,
“Topological Methods for the Analysis of Solar Magnetic Fields”,
Living Rev. Solar Phys., **2**, (2005), 7. [Online Article]: cited [<date>],
<http://www.livingreviews.org/lrsp-2005-7>

The date given as <date> then uniquely identifies the version of the article you are referring to.

Article Revisions

Living Reviews supports two different ways to keep its articles up-to-date:

Fast-track revision A fast-track revision provides the author with the opportunity to add short notices of current research results, trends and developments, or important publications to the article. A fast-track revision is refereed by the responsible subject editor. If an article has undergone a fast-track revision, a summary of changes will be listed here.

Major update A major update will include substantial changes and additions and is subject to full external refereeing. It is published with a new publication number.

For detailed documentation of an article’s evolution, please refer always to the history document of the article’s online version at <http://www.livingreviews.org/lrsp-2005-7>.

Contents

1	Introduction	5
2	Field Lines and Null Points	8
2.1	Magnetic field lines	8
2.2	Physical significance of magnetic field lines	9
2.3	Magnetic discontinuities	14
2.4	Null points	14
2.5	Topological changes: Reconnection	18
3	Footpoints and Footpoint Mappings	20
3.1	Anchoring and line tying	20
3.2	Field extrapolation	21
3.3	Footpoint mapping as a dynamical constraint	22
3.4	Topological models of anchored fields	23
4	Magnetic Charge Topology Models	26
4.1	The photospheric field	28
4.2	Skeletons	29
4.3	Connectivity	32
4.4	Applications	33
5	Pointwise Mapping Models	35
5.1	Mapping discontinuities: Coronal fans and bald patches	35
5.2	Quasi-separatrix layers	40
6	Submerged Poles Models	42
6.1	The method	42
6.2	Comparisons with observations	45
6.3	Separatrices and QSLs	47
7	Coronal Null Points	48
8	Topology of the Heliospheric Magnetic Field	52
8.1	The solar wind	52
8.2	Open/closed boundaries	53
8.3	Magnetic clouds and coronal mass ejections	59
9	Conclusion	60
10	Acknowledgements	61
	References	72

1 Introduction

In 1958, Sweet proposed a model for solar flares in which four sunspots interacted by transferring flux across a common magnetic field (Sweet, 1958b). The years following this proposal saw extensive developments fleshing out the theoretical underpinnings of the flux transfer in this hypothesized scenario: magnetic reconnection (Sweet, 1958a; Parker, 1957; Petschek, 1964; Sonnerup, 1970; Vasyliunas, 1975). Reconnection is a process whereby topological change in some magnetic field lines facilitates the release of magnetic energy. The vast majority of these initial investigations considered a simplified two-dimensional geometry in which topological change occurred at an isolated X-point or neutral point (see Panel a of Figure 1). As two field lines were brought into contact with the X-point they appeared to “break” into two pieces each to form four *separatrices*. New field lines were then forged by joining together pieces from opposite originals. The rate at which this topological change was performed was the rate of flux transfer across the X-point, equivalent to the electric field in the ignorable direction at that point.

It was not until 1980, that Baum and Bratenahl revived Sweet’s original three-dimensional quadrupolar configuration to reveal the subtle inter-relation between its two separatrix surfaces, from the field’s positive and negative magnetic null points, intersecting along a single field line, called *the separator* (Baum and Bratenahl, 1980). While this inter-relation and the terms for the constituents were already being used in the magnetospheric literature (Stern, 1973; Yeh, 1976), Baum and Bratenahl’s computational investigation marked their introduction to solar physics. They used Sweet’s configuration to show how much more complex was the structure of the separator than the simple X-point which was its two-dimensional analog. To understand reconnection it would therefore be necessary to understand how the simple topological change characterized in two-dimensional models was manifest in three dimensions.

The detailed kinematics of reconnection along a separator were tackled in various papers appearing at the end of that decade (Greene, 1988; Gorbachev *et al.*, 1988; Lau and Finn, 1990). Perhaps the most surprising contrast to two-dimensional models was that reconnection in Sweet’s model did not occur at the field’s null point but rather along the separator field line in the corona. There followed an accelerating flow of investigations using this three-dimensional topological picture to interpret solar flares (Gorbachev and Somov, 1988, 1989; Mandrini *et al.*, 1991, 1993; Démoulin *et al.*, 1993, 1994; Bagalá *et al.*, 1995; Longcope, 1996). These studies clarified how the morphology of solar flares could be interpreted in terms of topology of a three-dimensional magnetic field.

It is not surprising that three-dimensional magnetic fields are more complex than two-dimensional fields. Indeed, even two-dimensional fields can be called complex if they contain structures over a wide range of length scales. Figure 1 shows two instances of hypothetical two-dimensional field lines. The first (Panel a) is a potential field, while the second (Panel b) is more finely structured, containing current on fine scales and is therefore *geometrically* more complex. The two fields are, however, topologically equivalent since field lines of one may be deformed into the other without breaking them. The topologies of both fields are characterized by one X-point and four separatrices (dark lines) which separate the other field lines into four distinct classes. As the work begun by Sweet has demonstrated, the analogous topological characterization of a three-dimensional field, even one which is geometrically simple, is far more complex than in two dimensions.

The ever-increasing resolution and cadence of coronal imaging instruments, SMM, *Yohkoh*, SOHO/EIT and TRACE, have revealed the coronal field to be extremely complex. In a parallel development, the increasing power of computers has opened the way to numerical investigation of three-dimensional magnetic fields at ever-increasing resolution. This combination has led to consideration of solar magnetic fields which are ever more complicated both geometrically and topologically. The increased topological complexity poses a challenge rather different from the increasing geometrical complexity, which reflects only a greater range of scales resolved either

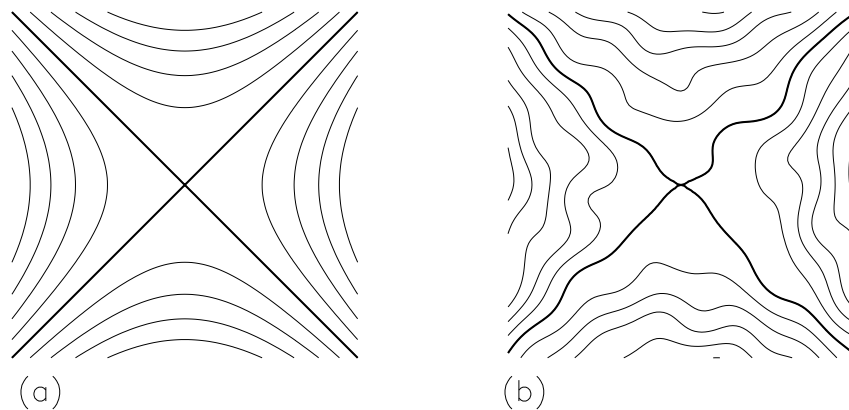


Figure 1: Two-dimensional magnetic fields which are topologically equivalent. Curves show magnetic field lines, and the dark field lines are the separatrices from a magnetic null point (X-point). Panel a: a null point in a potential magnetic field. Panel b: a non-potential field with small scale structure and current, which is nevertheless topologically equivalent to the potential field in Panel a.

observationally or computationally. As these challenges of increased topological complexity are met, by the previously arcane terminology of topological field models, terms such as “spine”, “fan”, “separator”, “bald patch” and “quasi-separatrix layer” are gaining broad use among solar physicists of all descriptions.

This article is intended to review and organize the existing body of literature pertinent to the topological analysis of magnetic fields in the solar corona. In its broadest sense “magnetic topology” encompasses a wide range of purely mathematical work, as well as investigations of magnetic fields in the magnetosphere, astrophysical contexts and laboratory experiments. This review will be limited, however, to applications of direct relevance to solar physics. With that aim in mind, an attempt is made to bypass mathematical rigor with an eye toward results and their applications. In most cases the cited literature can provide caveats and justifications whenever they might be desired.

The scope of the article is intentionally limited to topology, and excludes matters of dynamics and energetics whenever possible. This narrow scope is adopted in the interest of providing a thorough and comprehensive treatment of one subject. The field’s topology does play a critical role in determining its dynamics. This relationship is a complex one and is essential to understanding the significance of topology. Nevertheless, the topology itself is complex enough that it is worth reviewing it alone, before considering its possible influence on energetics or dynamics.

By its very definition, the topology of a field is a robust property which will persist when the field is made more geometrically complex through equilibrium and dynamical currents. The topology may be illustrated in simple fields, such as potential magnetic fields, and still be applicable to fields of far greater sophistication. Thus, while much of the literature invokes simple fields for illustration, the topological analyses reviewed here are applicable to a far wider set of magnetic fields. It is this broad applicability which makes topological field analysis so powerful.

The review is intended to be comprehensive in its coverage of topology of three-dimensional fields, since this is the present state of the art. Two-dimensional or two-and-a-half-dimensional fields are essentially special cases of three dimensions, obtained by invoking an additional symmetry. Topological aspects unique to two dimensions are specifically mentioned where there is particular need.

In an effort to be comprehensive and to be useful to students and non-specialists, Sections 2

and 3 review basic elements of magnetic fields and their topology. This review includes a definition of field lines and various types of magnetic null points, and a summary of circumstances where these theoretical concepts are physically significant. It also reviews the methods of field extrapolation by which model fields are usually constructed. This leads naturally to a discussion of field line mapping and to discontinuities in magnetic fields.

The review introduces an organizing framework which accommodates as much existing literature as possible as one coherent body. Such a comprehensive framework has not, as far as can be determined, been presented before. Existing models are sorted into two broad categories according to their modeling of the photospheric field. In one class, termed here *magnetic charge topology*, the photospheric field is modeled as an intermittent collection of discrete source regions. Field lines anchored in common sources are deemed topologically equivalent. The other class, called here *pointwise mapping models*, considers a non-intermittent photospheric field which defines a mapping between photospheric footpoints. The two classes have subtly different definitions of such topological features as separatrices. Prior to drawing this distinction it is difficult to reconcile the uses of these terms across the existing literature.

Sections 4 and 5 review literature on the two classes of models, magnetic charge topology and pointwise mapping model, respectively. An important group of models, which we call *submerged poles models*, combine elements of both types. We review these separately in Section 6. Section 7 reviews literature concerning coronal magnetic null points, which are features common to all three types of models. Finally, Section 8 reviews, very briefly, those topological elements unique to open field lines, as typically found in global coronal models or heliospheric models.

2 Field Lines and Null Points

2.1 Magnetic field lines

Magnetic field lines are the fundamental element in all discussions of magnetic topology. A field line, sometimes called a line of force, is a space-curve $\mathbf{r}(\ell)$ which is everywhere tangent to the local magnetic field vector $\mathbf{B}(\mathbf{x})$. It satisfies the differential equation

$$\frac{d\mathbf{r}}{d\ell} = \frac{\mathbf{B}[\mathbf{r}(\ell)]}{|\mathbf{B}[\mathbf{r}(\ell)]|}. \quad (1)$$

(It can be seen that this definition yields $|d\mathbf{r}/d\ell| = 1$, demonstrating that the parameter ℓ is the arc-length along the field line, measured forward¹ from the point $\mathbf{r}(0)$.) The field line is a curve, and therefore has volume zero. A *flux tube* may be constructed by bundling together a group of field lines with net flux Φ . The tube's net flux is found by integrating $\int \mathbf{B} \cdot d\mathbf{a}$ over any surface pierced by the entire tube.

As with any equation of its form, Equation (1) may be solved either forward or backward from any "initial" point $\mathbf{r}(0)$, except from so-called singular points where $\mathbf{B}(\mathbf{x}) = 0$, since the vector's direction would not be defined there (Arnold, 1973). Any volume where $|\mathbf{B}(\mathbf{x})| > 0$ may, in principle, be completely filled with field lines such that a unique field line passes through each point.

In general circumstances, the only way to find a field line is to integrate Equation (1). A useful shortcut is available, however, in cases with one symmetry dimension (i.e. in two dimensions). In these special circumstances a general magnetic field satisfying $\nabla \cdot \mathbf{B} = 0$ can be written in terms of a scalar function called the flux function, and an arbitrary component in the ignorable direction, both depending only on two coordinates². When z is the ignorable coordinate (planar symmetry), the expression is

$$\mathbf{B}(x, y) = \nabla A \times \hat{\mathbf{z}} + B_z(x, y)\hat{\mathbf{z}}, \quad (2)$$

and the flux function $A(x, y)$ is the $\hat{\mathbf{z}}$ component of the magnetic vector potential. In the case where ϕ is ignorable (azimuthal symmetry) the field takes the form

$$\mathbf{B}(r, z) = \nabla f \times \nabla \phi + B_\phi(r, z)\hat{\phi} = r^{-1}\nabla f \times \hat{\phi} + B_\phi(r, z)\hat{\phi}, \quad (3)$$

where the flux function f is related to the vector potential as $A_\phi(r, z) = r^{-1}f(r, z)$.

In either geometry the flux function has the useful property that it is constant along field lines, since its derivative

$$\frac{dA}{d\ell} = |\mathbf{B}|^{-1} \mathbf{B} \cdot \nabla A = 0, \quad (4)$$

or similarly for $df/d\ell$. In two-and-a-half dimensional cases, i.e. $B_z \neq 0$, a field line equation like Equation (1) must still be solved within the flux surface $A = \text{constant}$. It is often the case, however, that the topology of the flux surface defines the topology of its field lines. Part of the appeal of working with two-dimensional models is the ability to easily draw a selection of field lines by contouring the flux function.

The analog of a flux function in three dimensions are the Euler potentials³ $u(\mathbf{x})$ and $v(\mathbf{x})$, which generate the magnetic field⁴ (Sweet, 1950; Dungey, 1953; Stern, 1966; Sturrock and Woodbury, 1967)

$$\mathbf{B}(\mathbf{x}) = \nabla u \times \nabla v = \nabla \times (u\nabla v) = -\nabla \times (v\nabla u). \quad (5)$$

¹By convention, we will use the term *forward* to denote the direction pointed by the magnetic field vector.

²The inclusion of vector components in the ignorable direction is referred to as two-and-a-half dimensions.

³This representation is analogous to the use of Clebsch variables, also called a Clebsch transformation, to express vortex lines in hydrodynamics (Lamb, 1932).

⁴While α and β are more frequent choices for denoting these, α is used for too many other things in MHD already.

The two expressions on the right show that the field is automatically divergence-free and that its vector potential can be written as $\mathbf{A} = u\nabla v$ or through the gauge transformation $-\nabla(uv)$ as $\mathbf{A} = -v\nabla u$. It is easily verified that both potentials are constant along field lines, so a given field line may be identified by the pair of values (u, v) . Finding potentials to generate a given magnetic field requires the solution non-linear differential equations. These can prove difficult even for simple cases such as a potential field, $\nabla \cdot \mathbf{B} = 0$. Indeed, many useful magnetic fields cannot be even written in the form given by Equation (5) at all. This very powerful method is therefore used far less frequently than are flux functions.

2.2 Physical significance of magnetic field lines

Many of the statements collected under the heading *magnetic topology* are simply mathematical consequences of the first-order ordinary differential equation (1). These same properties apply to integral curves found in other areas of physics, such as phase-space trajectories, flow stream lines or vortex lines. Unlike these more abstract curves, however, magnetic field lines are often closely related to physical structures, so that their topological properties can have direct physical significance.

It goes without saying that the magnetic field is physically significant in many situations. It is not so clear, however, how magnetic field lines themselves, the integral curves satisfying Equation (1) at a single instant, have physical significance. Indeed, elementary physics texts often contain the warning that lines of force (i.e. field lines) are *not* physically meaningful. There are certain circumstances in space physics, however, in which this warning may be disregarded and field lines are related to physical properties of the plasma. The list below mentions a few mechanisms by which field lines are rendered physically meaningful. We will have occasion to revisit these circumstances in order to decide which topological properties are truly relevant.

Single particle motion

A charged particle subject to no other forces will remain close to a single field line. Drifts will displace the particle's guiding center by several gyro-radii after it has traversed a length comparable to the field's curvature radius or gradient scale. Most space plasmas are characterized by global scales much, much greater than the gyro-radii of their particles, especially their electrons. Field lines are therefore excellent approximations to the electron orbits, at least between scattering events.

The heliosphere, for example, includes a population of high-energy electrons (halo electrons) for which collisions are so rare that each one remains effectively confined to a single field line from the Sun to beyond 1 AU (Feldman *et al.*, 1975). The properties of the electrons at a given point may therefore be attributed to events occurring elsewhere on that field line. Electrons flowing in both directions along the field lines imply that both ends of the field line are connected to the Sun (Gosling *et al.*, 1987; McComas *et al.*, 1995).

Solar flares produce an accelerated population of electrons which follow the field line on which they are produced until they impact the dense chromosphere. This impact produces signatures such as H α ribbons and hard X-ray footpoint emission, which betray the magnetic field configuration above. When footpoints or ribbons appear in pairs they are assumed to be conjugate footpoints of a single magnetic field line.

As a beam of flare-accelerated electrons passes through the ambient plasma, they excite radio waves at the local plasma frequency. The radio frequency changes as the beam propagates into regions of higher or lower ambient density, producing a characteristic emission pattern known as a type-III radio burst (Bastian *et al.*, 1998). Frequencies decreasing below ~ 10 MHz are taken as evidence that the electrons are propagating on open field lines, while those which remain at higher frequencies are assumed to be trapped on closed field lines.

Thermal conductivity and coronal loops

In a diffuse, high temperature plasma thermal energy is conducted principally by electrons. When electrons are strongly magnetized ($\Omega_e \gg \nu_{ei}$) their orbits will follow field lines between collisions making thermal conductivity highly anisotropic (Braginskii, 1965). Heat is conducted parallel to the magnetic field far more readily than perpendicular to the field.

Due to this anisotropic conductivity, heat deposited somewhere in a plasma is rapidly and efficiently conducted to all points on the same field line. Plasma flows are also mechanically confined by the field, so a bundle of field lines will behave as one-dimensional autonomous atmosphere (Rosner *et al.*, 1978). High resolution images of the corona made in soft X-ray (SXR) or extreme ultraviolet (EUV) are characterized by thin *coronal loops* which are each assumed to be a single bundle of field lines for the reasons just mentioned.

Figure 2 shows an example of an image made at the EUV wavelength 171 Å by the TRACE spacecraft (Handy *et al.*, 1999). The majority of emission at this wavelength is believed to originate in coronal plasma around $T \simeq 10^6$ K. The numerous dark, thin curves are coronal loops, which are believed to follow bundles of coronal field lines. The coronal loops in this figure appear to connect polarity regions from three different active regions located at the center, left and lower-left of the field of view.

Coronal loop images in SXR or EUV provide one of the best observational indicators of magnetic topology in the corona. In the end, though, a coronal loop is not a magnetic field line, but is a column of plasma characterized by its excess emission. The neighboring corona is filled with other field lines which, as far as we know, are magnetically identical but which do not appear in these images. Partly this is due to the temperature response of the particular instrument, especially for narrow-band EUV images such as Figure 2. Here we are seeing only that plasma which happens to be within a narrow range of temperatures. Isolated loops also appear in broad-band instruments, such as *Yohkoh* SXT, which are sensitive to a much broader range of temperatures. Indeed, these same loops are sometimes observed in narrow-band EUV images at a slightly later time (Winebarger and Warren, 2005), so temperature response alone cannot explain why so much of the coronal magnetic field is free of loops at a given time.

One interpretation of various multi-temperature observational studies is that the corona has a tendency to form density enhancements along selected bundles of field lines, which then appear in imaging instruments as loops. No complete explanation has yet emerged as to why some bundles are selected while the majority are not (see Litwin and Rosner, 1993, for one proposed explanation). We henceforth assume only that coronal images reveal a sampling (perhaps rather sparse) of field-line bundles from the coronal magnetic field. It is also difficult to associate the time evolution of a loop with the motion of a given field line, since it is always possible that a pattern of sequential brightenings on neighboring loops has produced an apparent motion in a stationary magnetic field.

Alfvén wave propagation

Low-frequency waves in a magnetized plasma comprise three branches: slow magnetosonic, fast magnetosonic and shear Alfvén waves. The group velocity of the shear Alfvén wave is exactly parallel to the local magnetic field. Within the WKB limit any small localized disturbance will therefore propagate along a path following a magnetic field line. This means that a given field line will “learn” of perturbations anywhere along its arc at the Alfvén speed.

When equilibrium is established in a magnetic field, the distribution of current and pressure is dictated by equations whose characteristics are the field lines. For example, in a force-free

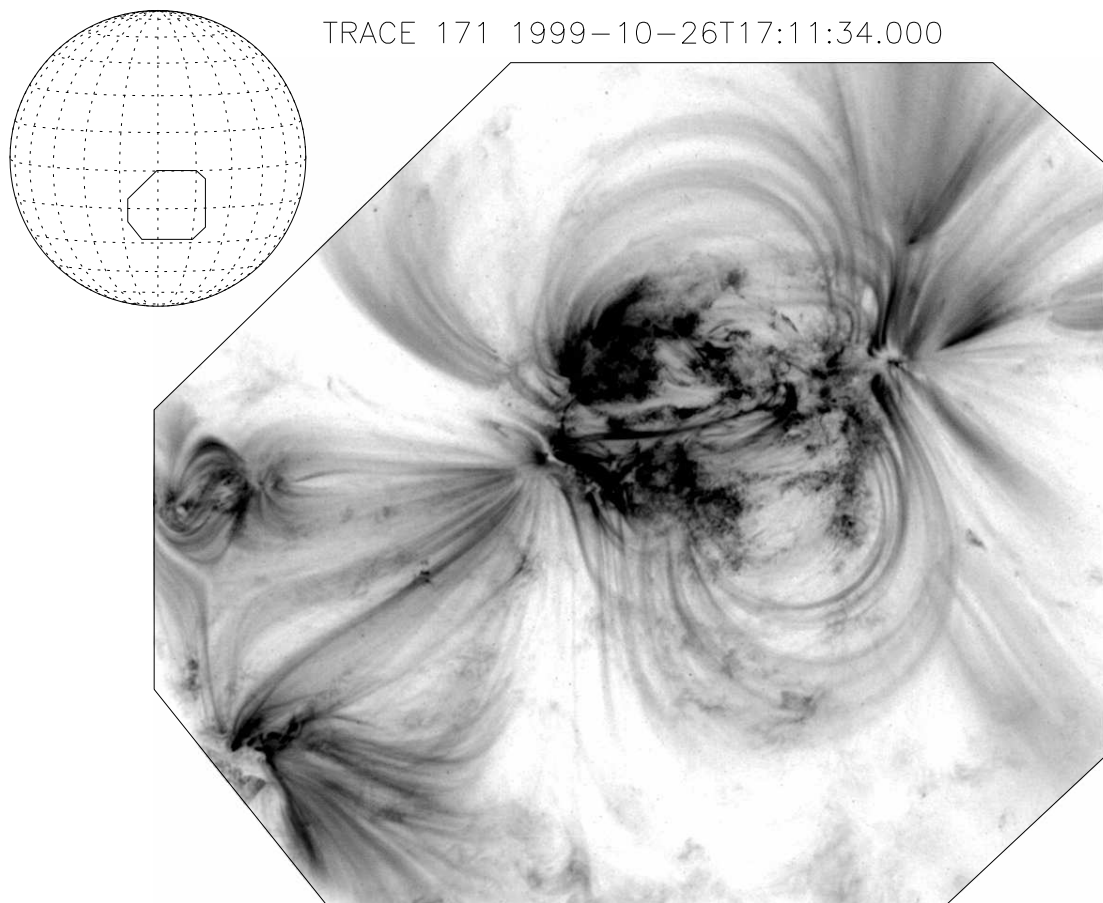


Figure 2: An EUV image of the coronal plasma made by TRACE at 171 \AA on October 26, 1999. The intensity of 171 \AA emission from a small portion of the solar disk is indicated by a reverse color table (darker indicates higher emission). An inset shows the location of the irregular field of view on the solar disk.

equilibrium, the current is proportional to the field: $\nabla \times \mathbf{B} = \alpha \mathbf{B}$, where $\mathbf{B} \cdot \nabla \alpha = 0$. This means that the field line twist parameter $\alpha(\mathbf{x})$ must be constant along each field line. In this way the field lines are the mathematical characteristics for the equilibrium equation (see Parker, 1979, for a discussion of characteristics in magnetostatic equations).

Frozen field lines

Space plasmas are often approximated as perfect conductors, meaning that the electric field vanishes in a frame moving with the plasma's local center of mass, $\mathbf{E}' = 0$. Expressing this fact in terms of the corresponding laboratory electric field $\mathbf{E} = -(\mathbf{v} \times \mathbf{B})/c$, and using it in Faraday's law yields the *ideal induction equation*,

$$\frac{\partial \mathbf{B}}{\partial t} - \nabla \times (\mathbf{v} \times \mathbf{B}) = 0, \quad (6)$$

governing the evolution of the magnetic field $\mathbf{B}(\mathbf{x}, t)$ under the influence of a plasma flow $\mathbf{v}(\mathbf{x}, t)$ ⁵.

Equation (6) provides a recipe for updating the magnetic vector field at all points in space under the influence of a perfectly conducting fluid with velocity field $\mathbf{v}(\mathbf{x}, t)$. It is one of the basic equations of magnetohydrodynamics (MHD); the others being mass continuity equation, momentum equation and some form of energy equation. Considerations of magnetic field topology and its evolution concern only the consequences of Equations (1, 6), independent of the other equations. Among the direct consequences of these two equations are the fact that field lines move with the plasma, and that flux is frozen into the plasma. First put forward by Alfvén (1943), developed further in following years (Sweet, 1950; Dungey, 1953), and rigorously formulated by Newcomb (1958), versions of these relationships are derived in most plasma physics texts (Moffatt, 1978; Parker, 1979; Priest, 1982; Sturrock, 1994), in many review papers (Stern, 1966; Axford, 1984; Greene, 1993), and among the preliminaries of topologically-oriented investigations (Vasyliunas, 1975; Hesse and Schindler, 1988; Hornig and Schindler, 1996). We present still another derivation below since these concepts are central to all that follows.

The relation between plasma motion and magnetic field lines follows from the manner by which Equation (6) relates the magnetic field and the velocity field. This inter-relation leads to an inter-relation between field lines, defined by Equation (1), and fluid *trajectories*. A particle moving at the plasma's flow velocity, i.e. a fluid element, follows a trajectory $\mathbf{r}(t)$ satisfying

$$\frac{d\mathbf{r}}{dt} = \mathbf{v}[\mathbf{r}(t), t]. \quad (7)$$

Parameterizing field lines by mass-column $\mu = \int (\rho/|\mathbf{B}|) d\ell$, rather than arc length ℓ , transforms the field line equation (1) into

$$\frac{d\mathbf{r}}{d\mu} = \frac{\mathbf{B}[\mathbf{r}(\mu), t]}{\rho[\mathbf{r}(\mu), t]}. \quad (8)$$

The reality of field lines follows from the fact that the field line equation (8) may be integrated either before or after trajectories of the fluid elements forming that field line are followed. Consider following a field line for $\delta\mu$ from a point \mathbf{r}_0 to a point \mathbf{r}_μ . Next follow the trajectory from \mathbf{r}_μ for an interval δt to a point $\mathbf{r}_{\mu t}$. This point is displaced by $\delta^2 \mathbf{r}_{\mu t}$ from \mathbf{r}_0 as shown in Figure 3.

⁵The initial condition $\mathbf{B}(\mathbf{x}, 0)$ must be divergence-free in order that $\nabla \cdot \mathbf{B} = 0$ for all time.

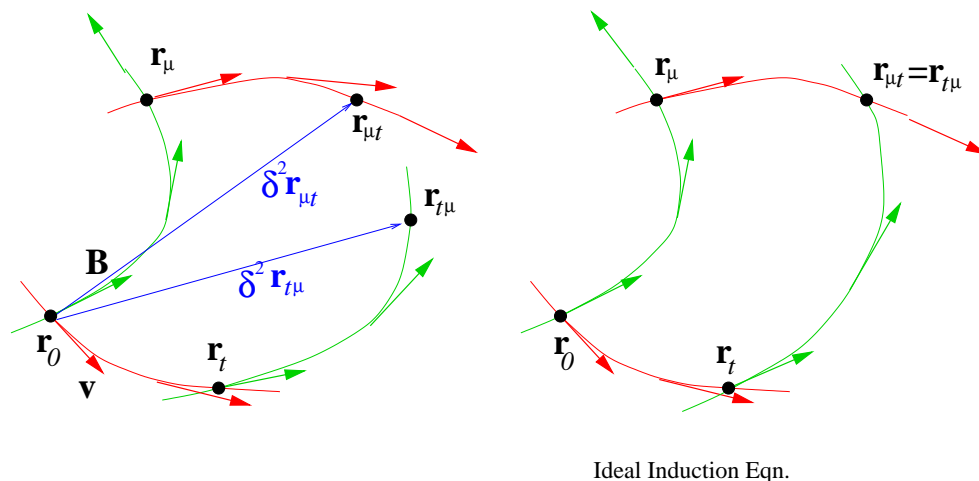
The two operations may be performed in the opposite order by first following, for δt , the trajectory of \mathbf{r}_0 , and denoting by $\mathbf{r}_{t\mu}$ the point $\delta\mu$ along the later field line. The difference in separations resulting from these two processes can be shown to be

$$\begin{aligned}\delta^2\mathbf{r}_{\mu t} - \delta^2\mathbf{r}_{t\mu} &= \delta t \delta\mu \left(\frac{d}{dt} \frac{d\mathbf{r}}{d\mu} - \frac{d}{d\mu} \frac{d\mathbf{r}}{dt} \right) \\ &= \delta t \delta\mu \left[\left(\frac{\partial}{\partial t} + \mathbf{v} \cdot \nabla \right) \frac{\mathbf{B}}{\rho} - \left(\frac{\mathbf{B}}{\rho} \cdot \nabla \right) \mathbf{v} \right]\end{aligned}\quad (9)$$

to leading order in $\delta\mu$ and δt . The term in square brackets can be written, after using mass continuity, as the left hand side of Equation (6) divided by ρ . This means that for a perfectly conducting plasma, i.e. $\mathbf{E}' = 0$, the displacement difference vanishes to second order, proving that the processes of field line tracing and trajectory following commute with one another.

The calculation above can be integrated to finite Δt and $\Delta\mu$ to show that two fluid elements on the same field line at one time, will also be on the same field line at all later times. Following this reasoning, we see that a field line evolves in time exactly like the curve of fluid elements initially lying along it. So long as the fluid velocity $\mathbf{v}(\mathbf{x}, t)$ remains bounded and continuous then it will transform the field line continuously, *without* breaking it.

The *frozen field line* theorem reviewed above is related to, but not the same as, the *frozen-flux theorem*. The latter is the magnetic analogue of Kelvin's circulation theorem for inviscid fluid flow. According to the frozen-flux theorem, the magnetic flux, $\Phi = \int \mathbf{B} \cdot d\mathbf{a}$, enclosed by a closed loop of fluid elements (not necessarily a field line) will not change as the loop moves. This is a straightforward consequence of the fact that the electromotive force, $\oint \mathbf{E}' \cdot d\mathbf{l}$, must vanish in any perfect conductor, since $\mathbf{E}' = 0$.



Ideal Induction Eqn.

Figure 3: An illustration of how the ideal induction equation implies that the operations of tracing field lines and following trajectories commute with one another. Field lines (green lines) are tangent to the magnetic field vectors (green arrows), while trajectories (red lines) are tangent to velocity vectors (red arrows). These are followed beginning with the point \mathbf{r}_0 in both orders to the points $\mathbf{r}_{\mu t}$ and $\mathbf{r}_{t\mu}$. The net displacements $\delta^2\mathbf{r}_{\mu t}$ and $\delta^2\mathbf{r}_{t\mu}$ are shown by blue arrows (they are not infinitesimal in the figure). In the case that \mathbf{B} and \mathbf{v} are related through the ideal induction equation, shown on the right, $\mathbf{r}_{\mu t} = \mathbf{r}_{t\mu}$, so the order of operations does not matter.

It is important to note that the final item, concerning frozen field lines, provides the only sense in which field lines are persistent. To be sure, field lines may be found for the magnetic field $\mathbf{B}(\mathbf{x})$ at a given instant and these will be physically significant for any of the other reasons presented above. In order to consider the evolution of a given field line, however, one must be able to track field lines in time. This tracking is unambiguous only when the field evolves according to the ideal induction equation (6). There are a slightly broader set of circumstances where it is possible to formally define field evolution (Hesse and Schindler, 1988; Hornig and Schindler, 1996), however, this definition will not be physically meaningful unless it coincides with the motion of something physical such as the plasma or the electron fluid. That is to say, while it is mathematically possible to define rules for tracking field lines, these rules are not observed by objects such as electrons or Alfvén waves.

2.3 Magnetic discontinuities

Unless otherwise noted we will assume that the magnetic field is spatially continuous in the sense that each of its spatial derivatives $\partial B_i/\partial x_j$ is defined and finite everywhere in space. The most important exception occurs at a surface of magnetic discontinuity. The general theory of such discontinuities is well documented in basic texts and reviews (see, e.g., Priest, 1982; Cowley *et al.*, 1997). Due to the solenoidal condition, $\nabla \cdot \mathbf{B} = 0$, the component of \mathbf{B} normal to this surface must be continuous, and the discontinuity must be in the tangential components, giving rise to a surface current

$$\mathbf{K} = \frac{c}{4\pi} \llbracket \mathbf{B} \rrbracket \times \hat{\mathbf{n}}, \quad (10)$$

where $\hat{\mathbf{n}}$ is the surface normal and $\llbracket \mathbf{B} \rrbracket \equiv \mathbf{B}(\mathbf{x} + \epsilon \hat{\mathbf{n}}) - \mathbf{B}(\mathbf{x} - \epsilon \hat{\mathbf{n}})$ is the discontinuity across the surface at a particular point.

Magnetic discontinuities occur across both fast shocks and slow shocks. In each shock there is a non-zero normal component so each field lines contains an angular bend. Such a discontinuity may be removed by local continuous deformation (essentially rounding the corners), and therefore is not an essential element of the field's topology. The third possibility, called a *tangential discontinuity* (TD) is one where $\hat{\mathbf{n}} \cdot \mathbf{B} = 0$ at the surface. Such a structure may be an equilibrium provided $\llbracket B^2 \rrbracket = 0$ so that there is pressure balance across the sheet (Cowley *et al.*, 1997). The occurrence of TDs under various circumstances is one of the key elements of topological field models. These are the most prevalent examples of equilibrium current sheets, and so the term “current sheet” is sometimes used to mean TD.

2.4 Null points

For a continuous magnetic field the field line equation (1) is singular only where the magnetic field vector vanishes (Arnold, 1973). In a general field, $\mathbf{B}(\mathbf{x})$ will vanish only at isolated points called *null points* \mathbf{x}_0 , in the vicinity of which it has the generic form

$$B_i(\mathbf{x}) = \sum_{j=1}^3 (x_j - x_{o,j}) M_{ij} + \dots, \quad (11)$$

where $M_{ij} \equiv \partial B_i/\partial x_j|_{\mathbf{x}_0}$ is the field's Jacobian matrix. A null point for which the matrix M_{ij} vanishes entirely is termed *higher order*, and will occur only in special circumstances. In the generic case⁶ where M_{ij} does not vanish identically the field lines have simple behavior in the

⁶The term *generic* and the related term *structurally stable* will be used repeatedly in a very precise mathematical sense. A full definition, as given in, e.g., Guckenheimer and Holmes (1983), is not possible here. The terms basically refer to situations whose qualitative form (i.e. topology) will not be destroyed by small changes. It is invoked to rule out specially constructed cases such as a perfect symmetry, to which a given statement will not apply.

neighborhood of the null, analogous the behavior of a general vector field in the vicinity of null points. The behavior may be characterized entirely from the eigenvectors and eigenvalues of the Jacobian matrix. In particular, it is possible to assign any null (excepting non-generic cases) to one of two categories, positive or negative, according to the number of its eigenvalues with positive real parts. A thorough analysis of this categorization is given by Parnell *et al.* (1996), from which we briefly report some of the main conclusions.

The matrix \mathbf{M} will have three eigenvalues which may be all real or may include complex eigenvalues. In the first case the eigenvalues may be ordered, $\lambda_1 \leq \lambda_2 \leq \lambda_3$; in the second there must be one real eigenvalue λ_r and a complex conjugate pair λ_c and λ_c^* . Since $\nabla \cdot \mathbf{B} = \sum_i M_{ii} = 0$, the three eigenvalues must sum to zero. A null point for which one eigenvalue is negative and the other two are positive (or have positive real parts) is called a *positive* null point (Priest and Titov, 1996)⁷. (The null is therefore called positive if $\det \mathbf{M} < 0$, which is confusing until one considers the sense of field lines in the fan surface.) The real and imaginary parts of the eigenvectors from the two positive eigenvalues span a plane within which all field lines originate at the null point. Following these field lines beyond the immediate neighborhood they form a surface called the *fan surface* of the null. There are also two *spine field lines* which terminate at the null in directions both parallel and anti-parallel to the eigenvector of the negative eigenvalue (see Figure 4). A *negative null* is one with the opposite structure: one positive eigenvalue and two with negative real parts, a fan surface of field lines ending at the null, and two spine field lines originating at the null.

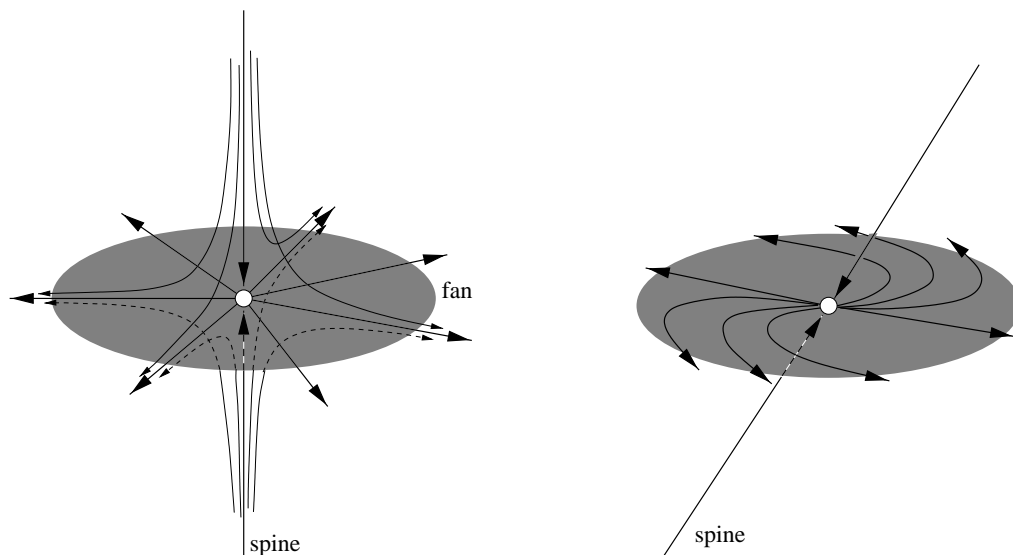


Figure 4: Schematic depictions of positive null points. Two spine field lines directed toward the null (white circle) appear as dark lines with arrow heads next to the null. The central portion of the horizontal fan surface is colored grey, and contains fan field lines directed outward like spokes on a wheel. The left case is the simplest: a potential null point which is cylindrically symmetric ($\lambda_2 = \lambda_3$). Thinner lines show a few of the field lines on either side of the fan surface. The right case is a non-potential null whose fan is spanned by eigenvectors of complex eigenvalues and whose spines are not orthogonal to the fan surface.

⁷An alternative term, *B-type null*, first appeared in the magnetospheric literature (Yeh, 1976) and has also been used in the solar physics literature (Greene, 1988; Lau and Finn, 1990). The term “positive null” is used here since it is more descriptive than “B-type”. Field lines within the fan surface are directed outward from the null as from a positive charge.

Cases where one or more eigenvalue real parts vanish cannot be classified as either positive or negative. Such cases are not generic (they will not survive a small but arbitrary perturbation to the field) but do occur in cases of symmetry, such as two-dimensional models, or at the instant of bifurcation (discussed in Section 7). An X-type null is one where one eigenvalue vanishes, namely λ_2 , and the other two have equal magnitude and opposite sign: $\lambda_1 = -\lambda_3$. This is the standard heteroclinic point in two-dimensional fields, however, as alluded to, they do not generally occur as such in three-dimensional fields. If the real parts of two eigenvalues vanish then so must the third, since they must sum to zero, barring a higher-order null (all three eigenvalues are identically zero) this must be an O-type null with two purely complex eigenvalues $\lambda_c = i\gamma$.

Fan field lines and spine field lines are notable exceptions to the general tenet that field lines have no beginning or ending – it seems that certain field lines terminate at null points. A fan surface divides the volume of field lines in two regions (or domains), thereby serving as one form of *separatrix* in three-dimensional magnetic fields. The spines, on the other hand, are one-dimensional curves and therefore do not form separatrices. This makes three-dimensional null points topologically different from two-dimensional X-points, since all four field lines connecting to an X-point are dubbed separatrices, regardless of their orientation. If a three-dimensional null is transformed continuously into an X-point by taking its intermediate eigenvalue to zero, then the spine and fan both become separatrices in the limit $\lambda_2 = 0$. Which of the X-point’s separatrices was formerly a spine depends on the former null type and which direction $\lambda_2 \rightarrow 0$.

An even more exotic kind of field line occurs when the fan surface of a positive null intersects the fan surface of a negative null, as shown in Figure 5. When the intersection is transversal it forms a *null-null line* (Lau and Finn, 1990). Intersections of separatrices are called *separators*, in general, and since a fan surface is one form of separatrix, null-null lines are one form of separator. There are, however, other forms of separators including finite-width TDs called current ribbons when the separatrix intersection is not transversal (Longcope and Cowley, 1996).

A null-null line has two termini since it must both begin at a positive null and end at a negative null. Since they lie at the intersection of separatrices, null-null lines are a more natural analog of two-dimensional X-points than are the three-dimensional null points themselves. In this analogy, however, it must be borne in mind that while an X-point may be identified locally, a null-null line is locally indistinguishable from nearby field lines; its uniqueness derives from only global topology. It is often, although not always, the case that the field vectors in the vicinity of the null-null line have an X-type shape (see inset of Figure 5). The exact location of the X in such a slice depends critically on the orientation of the plane, and each field line in some neighborhood may play the same role in a different plane. This local criterion may not, therefore, be used to identify a null-null line; the only way to locate it is by following field lines in both directions. (Longcope, 1996, presents a numerical algorithm for this.)

Substituting the local field (11) into the ideal induction equation (6) yields, to lowest order in distance from the null point, the requirement that the null point move with the flow: $\dot{\mathbf{x}}_0 = \mathbf{v}(\mathbf{x}_0)$. Continuing to next order in distance yields an equation for the evolution of the Jacobian matrix

$$\frac{dM_{ij}}{dt} = \sum_{k=1}^3 \left(\frac{\partial v_k}{\partial x_i} - \nabla \cdot \mathbf{v} \delta_{ik} \right) \Big|_{\mathbf{x}_0} M_{kj}. \quad (12)$$

The matrix in parentheses, call it V_{ki} , is related to the plasma’s local rate of strain at the null point. This can be used to show that each eigenvalue evolves according to $\dot{\lambda}_\nu = V_{\nu\nu} \lambda_\nu$ where $V_{\nu\nu}$ is a product of V_{ki} with the corresponding left and right eigenvectors. The most significant point is that, barring a singular flow field, an eigenvalue which is non-zero will remain non-zero and can never change sign. Under ideal induction, therefore, null points of a given type will move with the plasma flow but cannot change type and can be neither created nor destroyed (Hornig and Schindler, 1996).

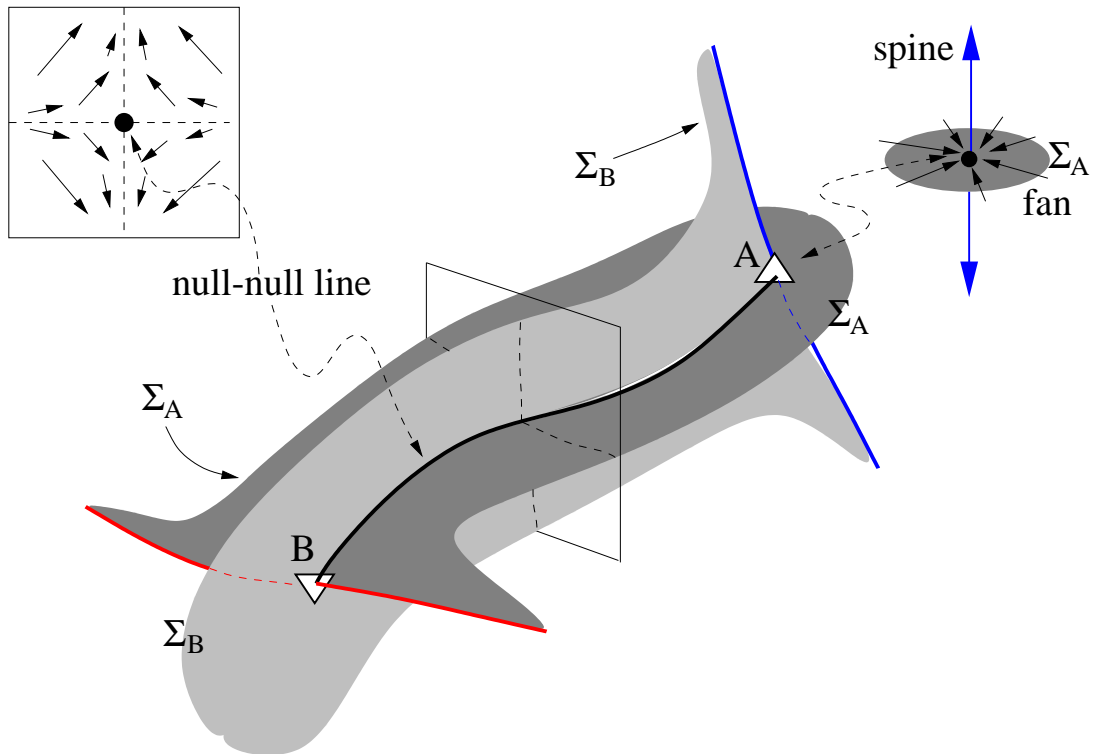


Figure 5: The structure of a null-null line. Positive and negative null points B and A have fan surfaces Σ_B and Σ_A shown in light and dark shades of grey, respectively. These intersect transversally along the null-null line shown as a thick black line. Surface Σ_B is then bounded by the two spines from null point A (blue), and similarly for Σ_A and the spines from B (red). The neighborhood of the null-null line is illustrated by the inset. This shows the direction of \mathbf{B} within a plane pierced normally by the null-null line at the dark circle. The fan surfaces cross the plane along the dotted lines.

It is also possible for the edge of a tangential discontinuity (TD) to include a null point which is locally Y-shaped. Such a null cannot be characterized by its derivative matrix M_{ij} , since derivatives are not defined at the discontinuity. If the TD occurs on a smooth sheet, however, the Y-type null will locally resemble one from a field which is otherwise current-free. It will therefore resemble the two-dimensional configuration first studied by Green (1965) and Syrovatskii (1971), and shown in Figure 6, except that field lines following the edge of the TD will either diverge away from or converge toward the null point in the erstwhile ignorable direction (making it a positive or negative Y-null). A pair of Y-type null points at the edges of a TD of finite breadth, as in Figure 6, have the same topological degree (Greene, 1993) as a single regular null point which is either positive or negative. In both two and three dimensions it is possible to create the null pair continuously by deforming a regular null point (Syrovatskii, 1971; Longcope and Cowley, 1996).

The two-dimensional current sheet equilibrium proposed by Green (1965) and Syrovatskii (1971) is current-free everywhere except the current sheet. Such a structure can be described by a potential $A(x, y)$ which is the real (or imaginary) part of a complex potential analytic except at a branch cut defining the current sheet. This powerful technique has been used to construct equilibria resembling realistic coronal current sheets (Priest and Raadu, 1975; Tur and Priest, 1976; Hu and Low, 1982). General formulations developed by Aly and Amari (1989) and Titov (1992) permit the construction, and evolution, of equilibria of arbitrary complexity, containing numerous current sheets.

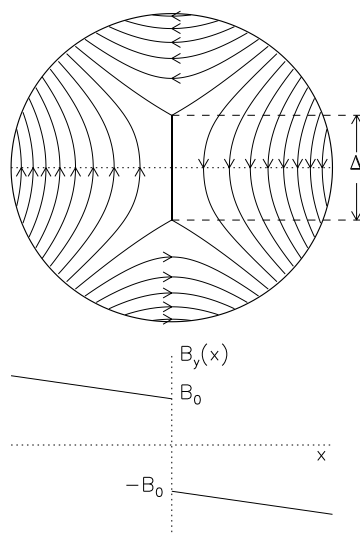


Figure 6: A tangential magnetic discontinuity of the Greene–Syrovatskii type, in a two-dimensional magnetic field. Lines show magnetic field lines which are contours of a flux function $A(x, y)$, arrows indicate the field’s direction. The field direction reverses across the current sheet of width Δ . The vertical field along the x -axis is plotted at the bottom. The Y-type null points are located at the tips of the current sheet: $(x, y) = (0, \pm\Delta/2)$.

2.5 Topological changes: Reconnection

Field lines may be found for any magnetic field whatsoever, by integrating Equation (1) from a set of initial points. Only, however, in cases with frozen field lines (i.e. a perfect conductor) can a given field line be unambiguously followed in time (Newcomb, 1958). In the frozen-field-line case each field line moves with the plasma itself. Provided the flow field $\mathbf{v}(\mathbf{x}, t)$ is reasonably continuous,

each field line will be continuously deformed by the flow. Continuous deformation precludes any topological changes. This means, for example, a closed field line will always remain closed and an isolated positive null point will always remain an isolated positive null point. Herein lies the utility of field line topology: Each field line's topology is preserved by arbitrary plasma motion, provided the plasma is a perfect conductor.

As soon as the assumption of perfect conductivity is abandoned it becomes impossible to unambiguously follow field line from one time to the next, and topology loses its practical utility⁸. Since plasmas are generally very good at eliminating electric fields it is common to retain the assumption of perfect conductivity everywhere with the possible exception of a few localized regions where $\mathbf{E}' \neq 0$. The perfectly conducting approximation can be justified by estimating the magnitudes of each term which might balance \mathbf{E}' in the generalized Ohm's law (see Vasyliunas, 1975, for one discussion of this scaling). Such estimates assume that all fields, including \mathbf{B} , vary on length scales comparable to those of the global geometry. In certain cases, however, the self-consistent dynamical solution will spontaneously develop localized structure on much smaller scales, such as a shock or a tangential discontinuity. Revised estimates using this much smaller length scale reveal that significant electric fields are possible within these localized structures. We will not delve into the literature (already substantial and rapidly expanding) concerning the self-consistent generation of \mathbf{E}' due to various terms in Ohm's law. Instead we will merely assume that it is possible for $\mathbf{E}' \neq 0$, but only within localized *non-ideal* regions.

In this modified picture a field line may be followed up to the time it encounters, along some part of its length, a non-ideal region. During this encounter, the field line is "cut" into two distinct pieces, each ending at the outside of the non-ideal region, and moving with the flow outside. When these pieces later decouple from the region each will most likely find itself connected to some other partial field line. This is the topological manifestation of *reconnection*: Field lines are "cut" and then "reconnected" to other segments (Vasyliunas, 1975; Hesse and Schindler, 1988). The discontinuous change, the cutting and reconnecting, must occur within the non-ideal region since that is the only place not bound by the frozen flux rule.

While it is not possible to follow a field line identified within the non-ideal region, it is possible to trace field lines into this region, which gain their identity from outside. Doing so provides a view of *kinematic reconnection*, capturing the topological change in action (Greene, 1988; Hesse and Schindler, 1988; Lau and Finn, 1990; Priest *et al.*, 2003). This generalization of field line evolution can provide valuable insight into reconnection, but one should always bear in mind that the field-line motion within the non-ideal region is basically a useful fiction. One consequence of the ambiguity inherent in this fiction is the following. Field lines traced from one side of the non-ideal region evolve differently from those traced from the other side.

⁸There may, nevertheless, be some utility in adopting some definition whereby field lines evolve in time. Hesse and Schindler (1988), and Priest *et al.* (2003) present such definitions.

3 Footpoints and Footpoint Mappings

3.1 Anchoring and line tying

A particularly simple domain is one where field lines cannot encounter a boundary, either because there are none (the plasma extends infinitely in all directions) or because the field is everywhere tangent to the boundaries ($\hat{\mathbf{n}} \cdot \mathbf{B} = 0$). In such cases field lines can end only at null points, and the vast majority do not end at all. A field line with no end must either form a closed curve, extend to infinity in both directions (when the volume is unbounded) or wander ergodically forever within a fixed volume (Greene, 1992). This “endless” situation is a common one in laboratory plasma experiments, which are specifically designed to ensure that $\hat{\mathbf{n}} \cdot \mathbf{B} = 0$ at the experiment wall. Consequently, fusion plasma literature is rife with discussions of periodic, quasi-periodic and ergodic field lines (see, for example, Lichtenberg and Lieberman, 1983). Many astrophysical fields can also be considered to be unbounded, however, in these astronomically vast cases, the distinction between a field line which is ergodic and one which closes only after a very long distance is unlikely to be physically meaningful in any of the manners discussed in Section 2.2. For this reason there is less emphasis on topological characterization of astrophysical field lines than in either laboratory or space plasmas. It should be noted that while *topology* is of little concern, there is a rich literature concerning the *structure* of galactic fields, as characterized for example by the spectrum of their fluctuation, which has a significant effect on, e.g., the propagation of cosmic rays (Jokipii, 1966).

Many space physics applications are modeled as a magnetized plasma with at least one boundary $\partial\mathcal{V}$ where the field’s normal component $B_n = \hat{\mathbf{n}} \cdot \mathbf{B}$ does not vanish. (The surface normal $\hat{\mathbf{n}}$ will herein be defined to point *inward*, toward the plasma, rather than outward as other conventions might have it.) The solar corona is the prototypical case, with its lower boundary at the denser layers of the atmosphere. In the simplest coronal models these layers are combined into a single mathematical surface and given the catch-all name “photosphere”. Models of the low corona consider the corona unbounded from above, while some more global models, most notably *Source Surface Models* (Altschuler and Newkirk Jr, 1969; Schatten *et al.*, 1969, discussed in more depth in Section 8 of this review), include a computational upper boundary to the corona, which the field also crosses. Models of the heliospheric field generally take same source surface as their *inner* boundary and extend outward to infinity. The present section introduces some basic concepts common to all field models with at least one boundary, but will often refer specifically to the coronal case.

Field lines intersecting the photospheric boundary are said to be *anchored* and the point of intersection is termed a *footpoint*. Field lines anchored at both ends to the photospheric boundary are said to be *closed*⁹. Closed field lines appear to account for the majority of an active region’s corona. *Open field lines*, such as in coronal holes, are those with one footpoint in the photosphere and the other end in the source surface or extending to infinity. To interpret the term “open” in cases of real magnetic field lines we recall the physical significance of field line topology discussed in Section 2.2. A field line is open for all practical purposes if it does not return to the photosphere within the mean-free path of high-energy electrons (so no diagnostic could detect its other end) or if it extends beyond the radius of super-Alfvénic solar wind speeds, outside of which dynamical perturbations propagate only outward.

A footpoint can have dynamical as well as topological significance. We will draw this distinction by hereafter distinguishing between the concepts of *anchoring* and *line-tying*. Anchoring, as just described, refers only to the topology of the field line: It ends at a boundary. This is contrasted to line-tying, where the footpoint is assumed to either remain motionless or to move in a prescribed

⁹This term is in common use in solar physics, although it risks confusion with the contradictory usage in unbounded systems.

manner – prescribed independent of the field. According to this usage a field line remains *anchored* even if its footpoint moves in an unspecified manner across the photosphere. Unfortunately, the literature seems to use these two terms interchangeably, and often fails to distinguish between the topological and dynamical aspects of footpoints. Since the present review is primarily concerned with topology, it becomes necessary to modify the terminology in order to make this important distinction.

A natural reason to consider the photosphere as the lower boundary of the coronal magnetic field is that *magnetographs* provide spatially resolved measurements at that particular surface. It is beyond the scope of this review to discuss details of the various polarimetric schemes for making magnetograms¹⁰. Our purpose will be adequately served by assuming that with a magnetogram it is possible to deduce the field's normal component, $B_n = \hat{\mathbf{n}} \cdot \mathbf{B}$, over some portion of the photospheric surface. Many of the widely-used magnetographs measure only the component along the line of sight which matches the vertical only at the center of the solar disk. In these cases the normal field B_n can be derived only after making assumptions about the field's actual direction. These assumptions become increasingly questionable near the solar limb where the line-of-sight and the vertical become orthogonal to one another. For this reason it is customary to find B_n from line-of-sight measurements only away from the limb.

3.2 Field extrapolation

Topological coronal models generally use magnetic fields extrapolated into the corona from photospheric data or an assumed photospheric distribution. The models themselves are independent of the extrapolation technique: They describe topological properties common to all magnetic fields. Nevertheless, since much of the literature is cast in terms of specific extrapolation methods, we briefly review their basics below. A typical procedure is to extrapolate the field upward from photospheric values after making some assumption about the state of the coronal field. (For concreteness we phrase the following discussion in terms of Cartesian coordinates with $z = 0$ being the photospheric plane; most of the discussion can be translated into spherical coordinates with only minor complications.)

The most common assumption made in extrapolation, that the coronal magnetic field is in force-free equilibrium

$$\mathbf{B} \times (\nabla \times \mathbf{B}) = 0, \quad z > 0, \quad (13)$$

is motivated by the corona's general calm and relatively small values of $\beta \equiv 8\pi p/B^2$, at least above the chromosphere. Under the least restrictive assumption, Equation (13) may be satisfied by any solution of

$$\nabla \times \mathbf{B} = \alpha \mathbf{B}, \quad (14)$$

where $\alpha(\mathbf{x})$ is arbitrary except for the requirement $\mathbf{B} \cdot \nabla \alpha = 0$, in order to preserve $\nabla \cdot \mathbf{B} = 0$.

Equation (14) is nonlinear since both \mathbf{B} and α are formally unknown, and is therefore difficult to solve for arbitrary boundary conditions. It is almost never used except in large-scale numerical solutions (see McClymont *et al.*, 1997, for a review of these techniques). Making the additional restriction that α is spatially uniform leads to a special case called the linear force-free field or the constant- α field (Nakagawa and Raadu, 1972; Chiu and Hilton, 1977; Gary, 1989). This additional restriction can be justified by an appeal to minimization of energy and conservation of helicity (Woltjer, 1958), but it is most often adopted simply for expediency. Governed by the linear Helmholtz equation, $(\nabla^2 + \alpha^2)\mathbf{B} = 0$, the constant- α field is significantly easier to find, although it can behave unphysically in unbounded domains (Nakagawa and Raadu, 1972).

The system can be made easier still by assuming $\alpha = 0$, which is equivalent to assuming the coronal field contains no current density. This ultimate simplification leads to the so-called

¹⁰Many of these details can, however, prove to be important in modeling magnetic topology.

potential field model which is by far the simplest, most frequently used, and most often criticized. For a potential field $\nabla \times \mathbf{B} = 0$ and $\nabla \cdot \mathbf{B} = 0$, making the magnetic field a direct analog of an electrostatic field in a charge-free region. This analogy is exploited by writing the magnetic field in terms of a scalar potential, $\mathbf{B} = -\nabla\chi$, which can be found directly from the boundary data (Schmidt, 1964). For a planar photosphere, unbounded above, the scalar potential is

$$\chi(x, y, z) = \frac{1}{2\pi} \int \frac{B_z(x', y') dx' dy'}{\sqrt{(x-x')^2 + (y-y')^2 + z^2}} \quad (15)$$

by analogy to Coulomb's law. In spherical geometry one uses a spherical harmonic expansion to solve Laplace's equation, $\nabla^2\chi = 0$, in the region $r > R_\odot$. The inner boundary, $r = R_\odot$, is constrained by magnetograms; source surface models impose the homogeneous Dirichlet condition, $\chi = 0$, at the outer boundary $r = R_S$, making the magnetic field purely radial there.

In the potential field model the normal component $B_z(x, y, 0)$ is the boundary data necessary and sufficient for unique solution. This means the photospheric horizontal field, $B_x(x, y, 0)$ and $B_y(x, y, 0)$, can be found from $B_z(x, y, 0)$. If these differ from measurements of those components (and they almost always will) then the field is evidently not potential. It is not so easy to know how much data is necessary for a unique solution of the less restrictive models, constant- α or general force-free equilibria.

In the case of a potential field the normal photospheric field plays the role of a surface magnetic charge density, analogous to an electrostatic surface charge. A localized magnetic region, such as a sunspot, therefore appears as a *magnetic charge*, and the leading order in their multipole expansion (Jackson, 1975) will be their monopole term. It is commonly held that there are no actual magnetic charges in the universe, and the present situation does not contradict this belief. Rather each localized photospheric region is the end of a sub-photospheric flux tube (Parker, 1955) which only *appears* as a charge in the coronal half-space $z > 0$ ¹¹. The magnetic charge of a given source is proportional to the flux in the tube, $Q_{\text{mag}} = \Phi/(2\pi)$. Nor is the concept of magnetic charge unique to potential field extrapolation. Since coronal field lines are anchored at the photosphere, the photospheric normal field $B_z(x, y, 0)$ is the *source* of field lines, regardless of what form the coronal field takes.

3.3 Footpoint mapping as a dynamical constraint

A field line anchored to the photospheric surface is either closed (it has two footpoints) or open (it has only one). A model photosphere may be partitioned into regions of open-field footpoints and closed-field footpoints; some models contain a third type of region where $B_n = 0$, in which there are no footpoints. The coronal field provides a *mapping* between positive and negative portions of the closed-field photospheric regions.

This mapping maps one footpoint, $\mathbf{x}_+ = (x_+, y_+)$ in a positive photospheric region to a point $\mathbf{X}_- = (X_-, Y_-)$ in a negative portion. (These are assumed to be photospheric footpoints, so they are given by x and y coordinates in the $z = 0$ plane.) Topological coronal field models generally concern the footpoint mapping, meaning the entire function $\mathbf{X}_-(\mathbf{x}_+)$, or its inverse mapping from negative to positive regions, $\mathbf{X}_+(\mathbf{x}_-)$.

The photospheric mapping can be found from the coronal field \mathbf{B} , however, the inverse is not possible; one cannot deduce the coronal field based on its footpoint mapping alone. Such a problem can have no unique solution since coronal field lines can be deformed in many ways without moving their footpoints. This hypothetical process for physically exploring multiple magnetic configurations also suggests a method for finding an equilibrium coronal field corresponding to

¹¹Some theoretical investigations of hypothetical magnetic monopole particles, most notably by P.A.M. Dirac, treat them as the termini of semi-infinite solenoids. This artificial construction is remarkably reminiscent of the actual configuration of solar flux tubes.

a given mapping. The method was proposed by Arnold (1974) (see also Moffatt, 1985) for un-anchored fields and adopted by various authors in the present coronal context (Parker, 1987; Antiochos, 1987; van Ballegoijen, 1988). Beginning with some coronal field consistent with the mapping, allow the coronal plasma to undergo dissipative dynamics, such as with viscosity, without pressure. During this relaxation the magnetic field must evolve according to ideal induction and line-tying $\mathbf{v} = 0$ at $z = 0$, so that the field line mapping is preserved. When the system ceases to evolve it will be in a force-free equilibrium consistent with the original footpoint mapping.

A numerical implementation of this scheme, called the magneto-frictional method (Yang *et al.*, 1986; Craig and Sneyd, 1990), uses friction rather than viscosity since it provides simpler dynamics which are still dissipative. Such schemes may be designed to preserve the frozen field lines exactly, but still suffer from limitations due to representing the continuous mapping with a finite number of variables. It is still difficult to know if a given field line mapping might admit more than one equilibrium coronal field. The existence of equilibria subject to ideal instabilities do, however, imply that some mappings admit multiple equilibria.

An even more subtle problem, proposed by Parker (1972) and subsequently dubbed “The Parker Problem”, concerns when continuous mappings admit discontinuous coronal magnetic fields. If the vector field $\mathbf{B}(\mathbf{x})$ is discontinuous across some TD, it follows from Equation (1) that the field lines will be discontinuous across that surface. This fact was used by several authors (van Ballegoijen, 1990; Longcope and Strauss, 1994) to argue that a continuous footpoint mapping admits only continuous coronal equilibria. While it is clear that a tangential discontinuity introduces a discontinuity into the incomplete field line mapping – the mapping to some surface in the corona – it has been argued that it is possible for this discontinuity to be “mended” into a continuous mapping at the opposite photosphere (Parker, 1990). After all it is possible to tear a curtain without affecting the top or bottom hems. Indeed, some examples have been found of discontinuous equilibria with continuous footpoint mappings (Parker, 1994). The present focus of this ongoing line of work concerns whether such equilibria are special cases, rather common, or almost ubiquitous, within the hypothetical space of “typical photospheric mappings” (Parker, 2004).

3.4 Topological models of anchored fields

Much of the literature on the topology of anchored magnetic fields concerns the properties of the footpoint mapping. Most of this literature cleaves into two categories according to the assumed form of the photospheric normal field and the level of detail with which the mapping is represented. Some models, hereafter called *pointwise mapping models*, consider the detailed structure of the point-to-point footpoint mapping $\mathbf{X}(\mathbf{x})$. The alternative, called *Magnetic Charge Topology* (MCT), reduce the mapping to its *connectivity* between distinct photospheric sources: regions of unipolar photospheric flux surrounded by a strictly field-free “sea” ($B_n = 0$)¹². Some models make a further simplification by replacing each region with a point magnetic charge – the leading order in its multipole expansion. In contrast to this intermittent distribution, pointwise mapping models generally assume the normal photospheric field is a generic, non-intermittent function on the surface, vanishing only along curves known as *polarity inversion lines* (PILs).

It is useful to organize the existing literature into these categories, because their different approaches lead to different concepts of topology and different topological elements; for example they use mutually inconsistent definitions of separatrices. While both seek to describe, in their own way, a common underlying reality, they do so using subtly different conceptual frameworks. The situation is further muddled by their use of the same terms, such as separatrix, to denote different things. One rather popular model, which we call the *submerged poles model*, appears to defy this categorization. In fact, this one model is used by some authors as an MCT model and

¹²The term “field-free” refers to the absence of the *normal* component of the magnetic field in these regions. There can be non-vanishing horizontal field, at least when defined as the limit from above.

by others as a pointwise mapping model. We find that formulating rigorous frameworks for each of category, MCT in Section 4 and pointwise mapping models in Section 5, leads to a relatively clear presentation of most existing literature. We refer briefly to the submerged poles model with the MCT models, but defer its full presentation to a separate section, Section 6, since it draws elements from both categories.

The need for two model categories arises partly from the diversity of data. The quiet Sun, for example, is revealed by line-of-sight magnetograms (see top panel of Figure 7 for an example) to have an intermittent photospheric field consisting of small unipolar regions, called magnetic elements, separated by distances far exceeding their own diameters (see Zwaan, 1987, for a review of the hierarchy of photospheric magnetic fields). This suggests that the magnetic charge topology model would be a good approximation for this portion of the solar atmosphere. Almost all modeling of the quiet Sun magnetic field uses some version of an MCT model.

Detailed chromospheric models suggest that the magnetic field expands above these isolated features until it merges at a *merging height* or canopy to form a volume-filling coronal field (Kopp and Kuperus, 1968; Gabriel, 1976). More careful studies of the apparently field-free sea surrounding the elements (Livingston and Harvey, 1971; Lin and Rimmele, 1999) reveals that it contains an even finer inter-mixture of smaller positive and negative flux elements. To date this further complication in the quiet Sun field has been modeled by MCT models with smaller charges (i.e. points with less magnetic charge, see Schrijver and Title, 2003). It is not clear if future efforts will turn to pointwise mapping models or be forced to discard topology altogether due to the higher collisionality, shorter time scales and lower Alfvén speeds in this very complex layer of the solar atmosphere.

Active region photospheric fields (see bottom panel of Figure 7), on the other hand, are less clearly separated into distinct unipolar structures and are consequently less amenable to MCT models. The alternative is to assume the photospheric magnetic field is a non-intermittent function vanishing only along the PILs. Models of this type consider the point-to-point mapping function from positive to negative regions. This is almost always the model used when analyzing time-dependent numerical simulations of active region evolution. The observed active region field does, nevertheless, appear to be organized into distinct positive and negative regions. Therefore, the literature includes both MCT and pointwise mapping model analyses of active regions.

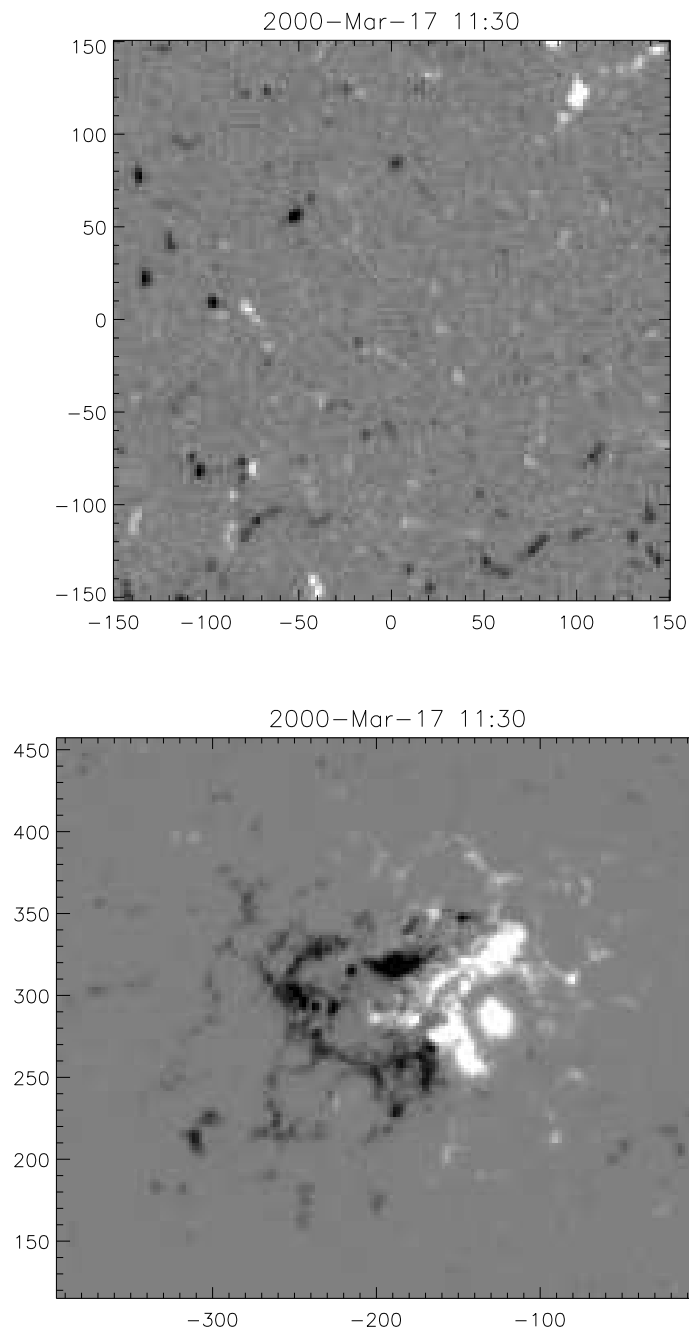


Figure 7: Two small sections of a full-disk magnetogram made on 2000 March 17 by the SOI/MDI instrument on the SOHO spacecraft (Scherrer *et al.*, 1995). The grey-scale shows the component of the magnetic field along the line of sight: Black is negative (away from the detector), white is positive, and grey is zero. Axes are labeled in arc seconds from the center of the solar disk. The top panel is a small (214 Mm on a side) region of the quiet Sun. Black and white specks are unipolar magnetic elements, each roughly 3×10^{18} Mx, with maximum field strengths $|B_{\text{los}}| \sim 150$ G; the grey-scale extends from -150 G to $+150$ G. Bottom is a small, young active region (NOAA 8910) plotted on a grey-scale extending from -1000 G to $+1000$ G.

4 Magnetic Charge Topology Models

All Magnetic Charge Topology (MCT) models share two basic assumptions. First, they assume the photospheric field can be partitioned into distinct unipolar regions. Second, they consider any two field lines with both their footpoints in the same regions to be topologically equivalent. The most natural partitioning occurs when each unipolar region is surrounded by a field-free “sea”, or is a point magnetic source located at $z = 0$. MCT’s definition of topological equivalence is most natural with point charges since there is only one footpoint location for each region: the charge itself.

A related class of models use the potential field from a set of *submerged* ($z < 0$) charges or dipoles to produce a smooth photospheric field (Seehafer, 1986; Gorbachev and Somov, 1988; Démoulin *et al.*, 1992). Photospheric regions are then defined by the mapping from submerged poles and may be delineated by curves mapping from fans of submerged null points. These submerged pole models share many elements with MCT and many authors consider them to be the category’s prototype. They differ from the MCT models, as defined here, in several critical respects. The flux Φ_a in photospheric region a depends on how many field lines from its source “reach” the photosphere. This value will change as source locations evolve, so the model does not constrain the fluxes of its regions. This fact is also responsible for the seeming arbitrariness in the definition of their separatrices: The separatrix extends from a photospheric curve whose actual definition is not topological, but depends on the modeling of the photosphere. Finally, submerged poles models are often used to analyze properties of the point-for-point mapping $\mathbf{X}(\mathbf{x})$. This means they include bald patches and quasi-separatrix layers, which are not elements of MCT as it is defined here. We therefore defer the discussion of submerged poles models to a separate section, Section 6, after the discussion of pointwise mapping models. Hereafter we apply the term MCT only to models whose photospheric field consists of *separated* unipolar regions or point charges located at $z = 0$.

In contrast to the intermittent photospheric field, the coronal field, $z > 0$, is assumed to be continuous and volume-filling, vanishing at only isolated points¹³. There is therefore a unique field line passing through every point in the corona, except the null points. Almost all field lines can be assigned to one of a countable number of equivalence classes according to source regions at each footpoint. Open field lines are considered to have a footpoint at infinity, which therefore counts as another source region. This divides the corona into sub-volumes, known as *domains* or cells.

A separatrix, as defined in MCT models, is any surface between two field-line domains. A separatrix surface must consist of field lines, and by definition these must have at least one end which is not at a source; it must end at a magnetic null point. We have excluded those models, such as submerged poles models, where photospheric source regions might be separated by a curve with footpoints of its own; there are no footpoints in the field-free sea. Therefore, *each separatrix in an MCT model is the fan surface of a null point*¹⁴. The fan surfaces of null points divide the coronal field into domains. Longcope and Klapper (2002) present a systematic method for constructing the separatrices and domains of an arbitrary potential magnetic field.

Sweet (1958b) proposed the first MCT model for a hypothetical flaring active region consisting of two positive and two negative sources interconnected by four domains of field lines, as shown in Figure 8. Sweet’s configuration has been thoroughly studied by subsequent authors using coronae consisting of potential fields (Baum and Bratenahl, 1980; Seehafer, 1986; Gorbachev *et al.*, 1988), linear force free equilibria (Hudson and Wheatland, 1999; Brown and Priest, 1999b; Petrie and Lothian, 2003), time-dependent numerical solutions (Longcope and Magara, 2004), and approximate semi-analytic equilibria (Longcope, 1996). In most models of Sweet’s configuration there

¹³In this respect, the photospheric surface, $z = 0$, actually represents the merging layer at which the pressure-confined flux tubes expand into a volume-filling coronal field.

¹⁴According to the foregoing definition of topological equivalence not all fan surfaces are separatrices since some separate field lines having the same footpoints which thus lie in the same domain.

are two magnetic null points located in the photospheric plane, one positive and one negative (see Figure 8). The fan surface from the positive null separates those field lines originating in $P1$ from those originating in $P2$. The negative fan divides the field lines ending at $N3$ from those ending at $N4$. The intersection between the two separatrices forms a separator lying at the junction of all four domains at once.

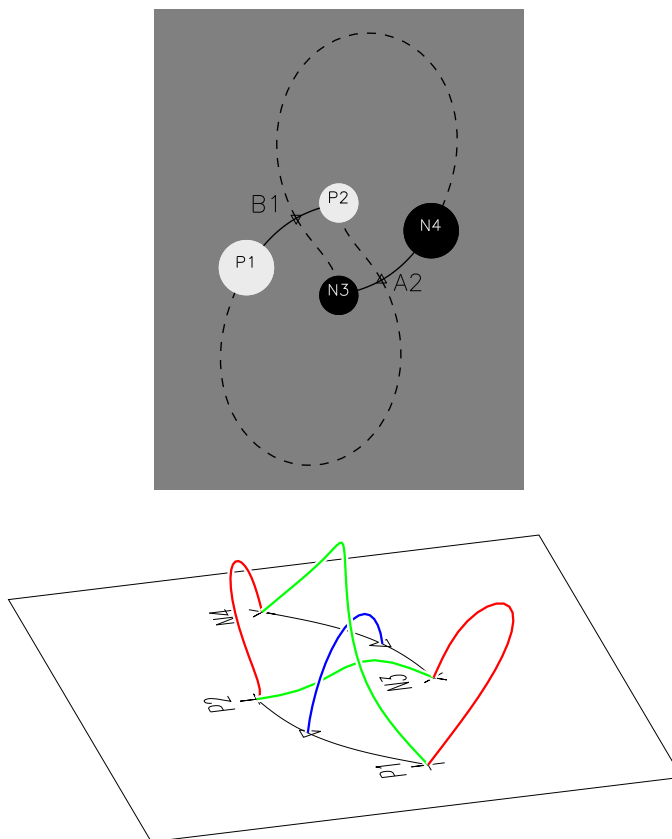


Figure 8: A version of Sweet's original model of four interacting flux domains (cells) from four discrete photospheric sources. The top panel shows the locations of the 2 positive (white) and two negative (black) sources. The two magnetic null points, $B1$ and $A2$ are shown by triangles. Dashed and solid lines are fans and spines, respectively. On the bottom is a perspective view of one representative field line from each of the four flux domains: $P1-N3$ and $P2-N4$ (red) and $P1-N4$ and $P2-N3$ (green). The blue line is the field's separator, running from the positive to negative null. Black lines are the spines from the two nulls.

A field line undergoes topological change in the MCT model when the source region at one of its footpoints changes. This occurs kinematically when two field lines, from different domains, approach the separator, temporarily join the spine-separator-spine combination, and then emerge in the other two domains (Greene, 1988; Lau and Finn, 1990). This occurs in Sweet's configuration when, for example, field lines from domains $P1-N4$ and $P2-N3$ are converted, through some non-ideal process, into field lines in domains $P1-N3$ and $P2-N4$.

The rate of reconnection in Sweet's configuration can be quantified as the time rate of change of the flux in domain $P2-N3$. According to Faraday's law this changing flux is proportional to the voltage drop along the separator (Sweet, 1958b; Longcope, 1996). Of course, since a perfect

conductor is an equipotential, this requires some departure from the ideal induction equation. Longcope and Klapper (2002) show that the flux changes in each domain in an MCT field of arbitrary complexity is linearly related to a vector composed of voltage drops across each of its separators.

4.1 The photospheric field

The extended photospheric region with no normal field, $B_z = 0$, heretofore called “field-free”, plays an important role in MCT models. Taking the limit of the coronal field just above gives values for $B_x(x, y, 0)$ and $B_y(x, y, 0)$ within the plane. Alternatively, one may define the photospheric field by reflecting the coronal field into the half-space $z < 0$ (the mirror corona) and requiring continuity everywhere outside photospheric source-regions. Either construction shows that, in general, $B_x(x, y, 0)$ and $B_y(x, y, 0)$ vanish only at isolated points called *photospheric null points*.

Since $z = 0$ is a plane of symmetry, field lines will remain within it, and they will have a two-dimensional topology of their own. The topology of photospheric fields was first analyzed in a methodical fashion by Molodenskii and Syrovatskii (1977). Recalling that the photospheric plane actually represents the merging layer, we can equate its topology with the topology of chromospheric features such as $H\alpha$ fibrils (Filippov, 1995). The topology of the photospheric field is characterized by the *footprint* (Welsch and Longcope, 1999), showing the sources (+s and \times s for positive and negative), the photospheric null points (∇ s and Δ s for positive and negative nulls) along with their spines (solid lines) and the photospheric lines of their fans (dashed lines). Figure 8 shows the footprint of Sweet’s configuration in the grey field-free sea, while Figure 9 shows the footprint of a slightly more complex example.

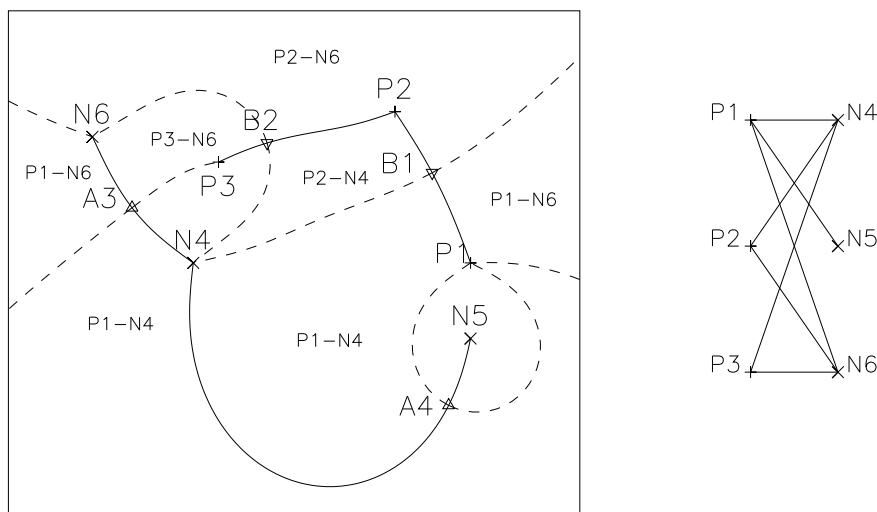


Figure 9: Left: The footprint of a potential field from 6 photospheric sources, labeled, e.g., $P1$, $P2$, etc. The 4 null points are labelled $B1$, $B2$, etc. Fan traces and spines (dashed and solid curves, respectively) divide the plane into 7 domains, which are labeled $P1-N4$, $P1-N6$, etc. On the right is a schematic depiction of the connectivity, called a domain graph.

Due to reflectional symmetry $\hat{\mathbf{z}}$ must be an eigenvector of a photospheric null point’s Jacobian matrix. This vertical eigenvector will be either the spine or part of the fan, making an *upright* or a *prone* null, respectively (Longcope and Klapper, 2002; Beveridge *et al.*, 2003). Prone nulls form hyperbolic (saddle) points in the photospheric field; they resemble two-dimensional X-points but

are in fact generic three-dimensional nulls. The four photospheric field lines connecting to a prone null include two spines and two field lines from the fan, called *fan traces*. These are rendered in a footprint diagram, such as Figure 9, by solid and dashed lines respectively. Due to their vertical orientations upright nulls have no spines or fan traces in a footprint diagram. They may, however, connect to spines or fan traces from prone null points.

The photospheric magnetic field is a two-dimensional vector field with sources, sinks and hyperbolic saddle points. Positive sources and positive upright nulls are sources, negative sources and negative upright nulls are sinks, and prone nulls are saddle points. The number of sources S (including ∞ if the net charge is not zero) is related to the number of upright and prone nulls n_u and n_p through the Poincaré index theorem (Molodenskii and Syrovatskii, 1977; Inverarity and Priest, 1999),

$$S + n_u - n_p = 2. \quad (16)$$

This relationship is invaluable for analyzing the topology of the photospheric magnetic field.

The footprint is divided into domains by the spines and fan traces of prone nulls. Any prone null whose fan traces both go to the same source is an unbroken fan which will most often enclose a single domain. For example, null *A4* in Figure 9 has an unbroken fan enclosing domain *P1–N5*. Each spine and fan trace from the remaining prone nulls are edges of this partitioning. Euler characteristic of this construction shows the number of photospheric domains to be

$$D_\phi = 2n_p - n_{uf}, \quad (17)$$

(Longcope and Klapper, 2002), when there are n_{uf} nulls with unbroken fans, assumed to each enclose a single domain, or to recursively enclose other domains of unbroken fans. For example, Figure 9 has $n_p = 4$ nulls, of which only *A4* has an unbroken fan, $n_{uf} = 1$, therefore there are $D_\phi = 7$ domains in the footprint.

When all nulls have unbroken fans, Equation (16) yields $D_\phi = n_p$, which is too small by one. Eliminating the unbroken fans in this pathological case leaves a trivial configuration with two sources, one domain and no edges, not consistent with Euler's characteristic.

Upright nulls of a given sign seem to occur most frequently surrounded by sources of the opposing sign. A study of potential fields generated by uniform, random distributions of point sources shows that the density of upright nulls is proportional to the density of sources. The constant of proportionality depends on the distribution of source magnitudes and on the imbalance of flux in each sign, reaching a maximum of 0.03 when all sources are of the same sign and magnitude (Beveridge *et al.*, 2002). Using this in Equation (16) shows that the density of prone nulls will be $\simeq 1.1$ times the density of sources in the case with only one sign of source.

4.2 Skeletons

A complete topological description of a three-dimensional MCT field is provided by its *skeleton* (Priest *et al.*, 1997), comprising all of its null points, spines, fans and separators. The footprint described above is the photospheric slice of the full skeleton. Longcope and Klapper (2002) present a systematic method for analyzing the skeleton of a potential field by “scanning” each null point: tracing its spines and then tracing the fan lines originating in each direction from the local fan plane. Since all MCT separatrices originate in null points this process yields the complete skeleton of the field.

The field's domain graph (Longcope, 2001) provides a schematic summary of the field's connectivity. The right panel of Figure 9 shows the domain graph of the field from six sources, while the left panel is the footprint of the field's skeleton.

The skeletons of the simplest non-trivial system, the potential field arising from three photospheric point sources, were completely cataloged and characterized by Brown and Priest (1999a).

A different and more systematic method for cataloging the skeletons was introduced by Pontin *et al.* (2003) and applied to these same three-source configurations. Considering all possible locations, magnitudes and signs of three sources there are eight different skeletons. Since the sum of photospheric fluxes from the three sources does not necessarily vanish, there will in general be a fourth balancing source at infinity. The sign of the balancing source (opposite to the sign of the sum) will match the signs of M_{Σ} of the photospheric sources, where M_{Σ} can be zero, one or two. Two of the eight skeletons correspond to $M_{\Sigma} = 0$, three to $M_{\Sigma} = 1$, and three to $M_{\Sigma} = 2$. The cases $M_{\Sigma} = 0$ and $M_{\Sigma} = 2$ have trivial domain graphs with one source (possibly infinity) connecting separately to each of the other three. The case $M_{\Sigma} = 1$ corresponds to a version of Sweet's configuration where one of the four sources has been removed to infinity. Depending on relative strengths there may be three or four flux domains.

Four photospheric sources offer many more possibilities, which have not yet been so methodically cataloged. Baum and Bratenahl (1980) pioneered the field by constructing the skeleton of a potential field from Sweet's configuration (two positive and negative sources, all of equal magnitude). Seehafer (1986) considered all possible configurations of these four equiflux sources and ruled out coronal null points except in very special arrangements such as perfect rectangles. Gorbachev *et al.* (1988) performed a comprehensive analysis of more general configurations in which the sources have arbitrary magnitudes so long as the two positives cancelled the two negatives. They showed that only two generic domain graphs were possible, shown in Figure 10. The first, case A, has four domains and a separator, while the second, case B, has only three, and no separator. The separator in case A is a single curve composed of either one or two null-null lines encircling one domain (Figure 8 shows one possibility). The photospheric field always includes exactly two prone nulls; some case A configurations also include a coronal null linked by separators to each prone null. Subsequent investigations (Brown and Priest, 2001; Beveridge *et al.*, 2002) have characterized the broader realm of four-source configurations including cases with net flux in the photosphere (including infinity, these are actually five-source systems).

The topology of a field is a robust property which will not change, in general, as the field is continuously deformed or changed. When a change of topology does occur during some continuous process, say non-ideal time evolution or hypothetical parameter variation, it is a singular event known as a *bifurcation*. Bifurcations are designated either local or global following the nomenclature from ordinary differential equations (Guckenheimer and Holmes, 1983). Local bifurcations, discussed further in Section 7, create or destroy null points without changing the domain structure of the field. Global bifurcations change the domain structure by changing global elements of its skeleton – fans, spines and separators – without affecting the null points themselves. The most important of these are the *global separator bifurcation* and the *spine-fan bifurcation* (Brown and Priest, 1999a), each of which is an analog of a two-dimensional heteroclinic saddle bifurcation (Guckenheimer and Holmes, 1983).

In a global separator bifurcation the fans of two opposing nulls encounter one another creating a pair of separators at their intersections. Gorbachev *et al.* (1988) describe such a bifurcation between two prone nulls which converts a three-domain case B field to Sweet's four-domain field, case A (see Figure 10). When both are prone photospheric nulls one separator is in the mirror corona, while in all other cases both are coronal separators. In the former case, fan traces from each of the opposing null points will appear to sweep past one another, as shown in Figure 10. This process will create one or two new separators in the corona and must create an equal number of new domains in order to preserve the inter-relation between these two skeletal elements (this relationship is quantified below).

The other common bifurcation, a global spine-fan bifurcation (Brown and Priest, 1999a), occurs when the spine of one null passes through the fan of a like-signed null point. At the instant of bifurcation the spine of the first null ends at the second null; this is a structurally unstable configuration as any bifurcation must be (Hornig and Schindler, 1996). The final effect of a global

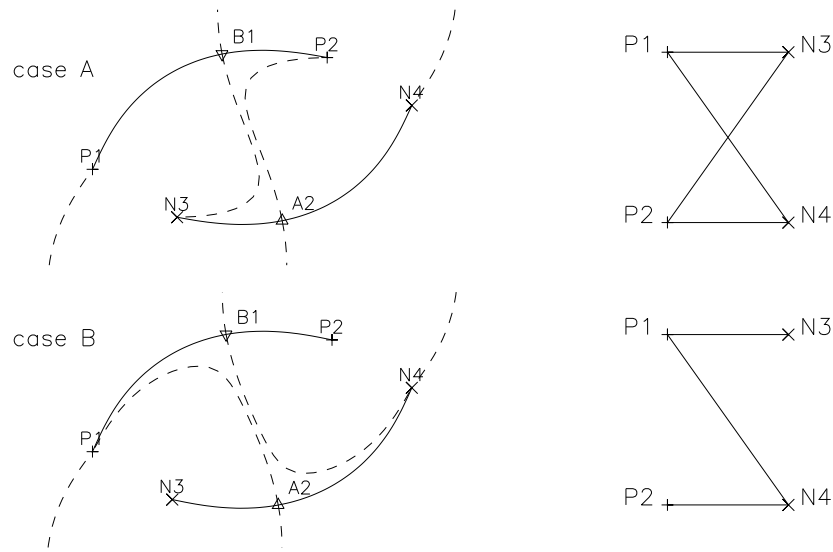


Figure 10: The two possible connectivities of Sweet's configuration. Footprints are shown on the left and corresponding domain graphs on the right. The top and bottom rows are cases A and B, respectively, of Gorbachev *et al.* (1988). Case A (topologically equivalent to Figure 8) has four domains, and the fan surfaces from the two nulls intersect along a separator (not shown), so both fans are *broken fans*. For example, the fan traces from $B1$ (∇) connect to $N3$ (downward) and to $N4$ (upward, although the complete fan trace is not shown). In case B (bottom row) the fans from null points $B1$ and $A2$ are unbroken enclosing domains $P1-N3$ and $P2-N4$, respectively. For example, both fan traces (dashed lines) from null $B1$ connect to $N4$. A potential field will switch from case B to case A through a *global separator bifurcation* as sources $P2$ and $N3$ approach one another.

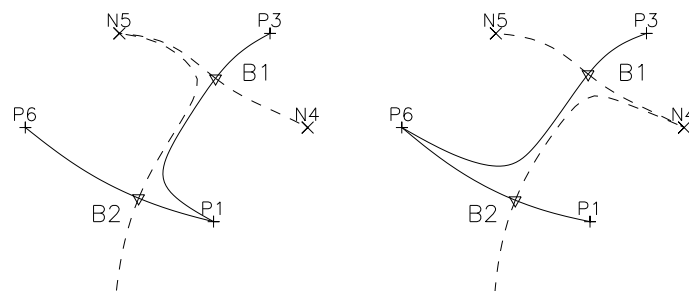


Figure 11: An example of a global spine-fan bifurcation. The two panels show a portion of the footprint of the field before (left) and after (right) the bifurcation. The bifurcation occurs as the spine (solid curve) of null point $B1$ sweeps across the fan (dashed curve) of null point $B2$. As a consequence the spine source of $B1$ switches from $P1$ to $P6$, and the fan trace of $B2$ sweeps from $N5$ to $N4$. At the instant of bifurcation (not shown) the spine from $B1$ is part of the fan of $B2$.

fan spine bifurcation is to swap the spine sources of one null, and create and destroy separators linking to the other null (see Figure 11). This will result in complicated changes to the skeleton and thereby to the domain graph. Maclean *et al.* (2005) present a detailed analysis of the bifurcation and present a systematic prescription for predicting the changes to the field's skeleton.

These two global bifurcations account for most of the topological transitions which fields undergo under continuous change. Any coronal field, be it potential or not, equilibrium or dynamic, will change its connectivity either through a global separator bifurcation or a global spine-fan bifurcation. Events involving the creation of new connections, as in the breakout model of coronal mass ejections (Antiochos, 1998), must occur through a global bifurcation. In a topological analysis of breakout in three dimensions, Maclean *et al.* (2005) show that it is most often the result of a global spine-fan bifurcation, although some are due to global separator bifurcation.

4.3 Connectivity

MCT models characterize a field's connectivity by quantifying the amount of flux interconnecting each pair of photospheric sources. This is not possible in either pointwise mapping models or submerged poles models. The domain graph of a field with D domains and S sources has D edges connecting S vertices (Longcope, 2001). This defines an incidence matrix M_{ar} which is 1 when domain r connects to source a , and 0 otherwise. The domain matrix relates domain fluxes ψ_r to source fluxes Φ_a ,

$$\Phi_a = \sum_{r=1}^D M_{ar} \psi_r. \quad (18)$$

These $S - 1$ relations¹⁵ leave only $D - S + 1$ domain fluxes undetermined (Longcope, 2001). Sweet's configuration, with $D = 4$ and $S = 4$, thus has only one domain flux not fixed by the sources. This one degree of freedom is set by the flux passing through its one separator, which can be varied through reconnection without changing any source fluxes. It can be shown in general that relation (18) augmented with the fluxes through all separators uniquely determines all domain fluxes (Longcope and Klapper, 2002). A direct consequence of this is that domain fluxes can only change from changing source fluxes, due to emergence or submergence, or from transferring field lines across separators, through separator reconnection.

There is not yet a method for enumerating the domains in a general MCT field, however, Longcope and Klapper (2002) present a method for enumeration in potential fields and those topologically equivalent to them, and Beveridge and Longcope (2005) generalize it. A field with X' separators, n nulls, n_{uf} with unbroken fans, and S sources has $D' = S + X' - n + n_{\text{uf}}$ domains, including those in the mirror corona¹⁶. Assuming there are no upright nulls (which introduce such complications as fans and separators in the photosphere) we set the number of coronal separators to $X = X'/2$ and subtract off half of the domains not present in the footprint (the number of footprints is given by Equation [17]) to find the total number of domains D not counting those in the mirror corona. Designating by n_c the number of coronal nulls gives (Beveridge and Longcope, 2005)

$$D = S + X - n_c - 1, \quad (19)$$

once n_p has been eliminated using Equation (16). Furthermore, the number of purely coronal domains, those without footprints, is $D_c = X - (n - n_{\text{uf}}) + 1$, equal to the number of independent circuits formed by coronal separators (Longcope and Klapper, 2002). This is a consequence of the fact that each purely coronal domain must be engirdled by a unique circuit of separators.

¹⁵Since infinity is a balancing source, the rows will sum to zero demonstrating that there are not S independent relations.

¹⁶Longcope and Klapper actually excluded unbroken fans along with the sources and domains they enclosed. Beveridge and Longcope (2005) added them back in, and made certain less restrictive assumptions.

4.4 Applications

The literature includes only a few cases where the connectivity of an active region is analyzed using strictly MCT methods, here again distinguished from submerged poles models. Longcope and Silva (1998) partition the active region complex 6993/6994 (1998 January 7) into 13 regions, each of which is represented by a point charge. The potential field from this field has 12 nulls, all photospheric and prone, 24 photospheric domains and 4 additional coronal domains. Equation (19) predicts $X = 15$ separators, of which Longcope and Silva (1998) report 12 (the remaining 3 can, however, be found from their reported configuration). Longcope and Klapper (2002) exhibit an example of a small, diffuse active region (1993 June 5) modeled using 20 sources plus a balancing source at infinity. The complete skeleton of the potential field includes 19 nulls (all prone and photospheric), 28 separators and 33 domains, 16 of which are purely coronal.

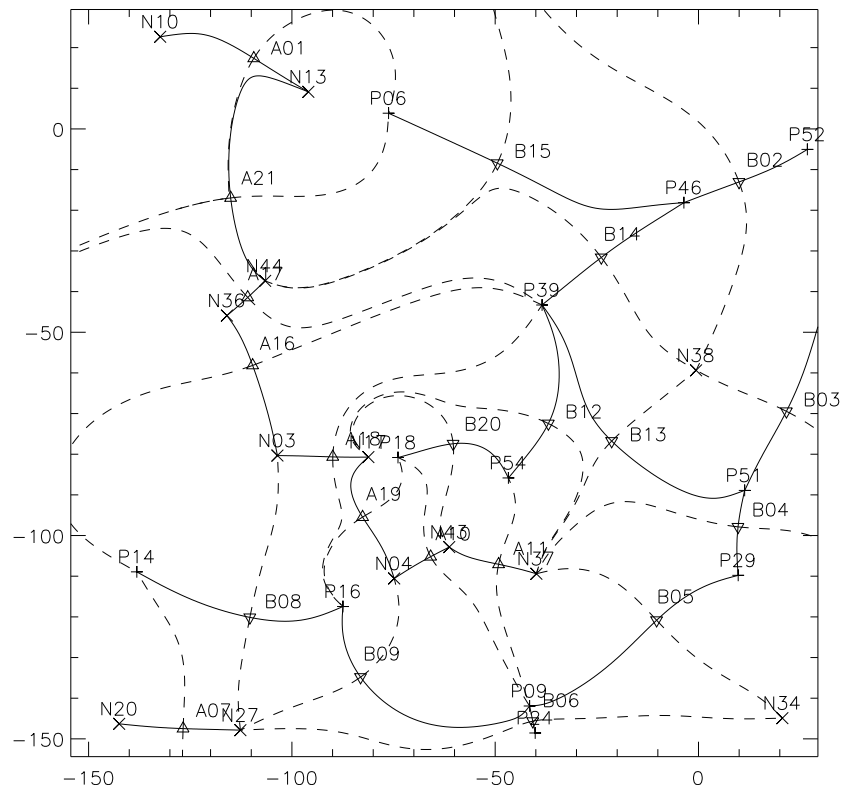


Figure 12: The footprint of a potential field modeling the lower left quadrant of the quiet Sun field shown in Figure 7.

Most applications of pure MCT models have been to the quiet Sun corona. Even a small patch of the quiet Sun will have a connectivity far more complex than the three-source and four-source prototypes. Figure 12 shows the footprint of the potential field generated from the lower left quadrant of the quiet Sun magnetogram in Figure 7. Aside from verifying general relationships among topological elements, it is not clear that anything would be learned from an intensive study of a single example of the quiet Sun. Consequently, studies have tended to characterize the quiet Sun topology statistically.

Schrijver and Title (2002) modeled the quiet Sun by randomly distributing 288 point sources over a square region and assigning them fluxes from a random distribution with zero mean (the net

flux in the region was forced to vanish). Using a potential field anchored in these sources they found the connectivity of each one by tracing selected field lines from it. To reduce the effects of edges, connectivity was determined only for sources within the central one-ninth of the square. From 200 realizations of this type they concluded that elements connect, on average, to 8.0 opposing elements, although a given element might connect to as many as 32 or as few as one. Of the 8.0 domains linking a given source, roughly half (3.8) are photospheric; the remainder are coronal domains. The majority of flux is found in short connections to the nearest 2–6 neighbors, however, there are some very long connections to distant sources. Schrijver and Title (2002) then compare 171 Å and 195 Å EUV coronal images made by TRACE (Handy *et al.*, 1999) with magnetograms from SOHO/MDI (Scherrer *et al.*, 1995), finding evidence for only the shortest connections predicted by the potential field model.

Close *et al.* (2003) studied two overlapping regions in a high resolution magnetogram of the quiet Sun from June 13, 1998. They extrapolated potential fields from each 264 Mm × 264 Mm region, and characterized the connectivities between source regions (not point charges) within the central one-ninth. The first region analyzed contained 375 sources (defined by $|B_z| > 20$ G) within the central 88 Mm × 88 Mm, with approximate flux balance. Each source connected on average to 5 others, although one particular source connected to 65. The second region contained 414 sources in its central region, with a 1:2 mix of positive:negative flux. The majority (negative) sources averaged 6.7 connections while the minority averaged 3.7. In both the balanced and unbalanced cases a source's single largest connection accounted, on average, for two-thirds of its net flux (69% and 65% in the balanced and unbalanced regions, respectively).

Beveridge *et al.* (2003) used a Monte Carlo approach to model a long coronal loop whose footpoints comprised numerous small elements. They modeled each footpoint by randomly distributing point sources with one sign of flux but with a distribution of magnitudes. The footprint of such a region had an average of 0.1 upright nulls and 1.1 prone null point for each source. Mapping the footprints between the two ends they found 18 separatrix intersections, meaning 18 separators, for each prone null. Applying these statistical findings to Equation (19) implies that each source connects to an average of 20 opposing sources at the other end of the loop. The tendency of the separatrices to cluster together led to bundles of many dozen separators. Consequently, many of the 20 connections to an average source would have very little flux in them; so little flux that they would never occur in any random selection of field lines such as those used by Schrijver and Title (2002) or Close *et al.* (2003).

5 Pointwise Mapping Models

The alternative to the MCT is a class of models concerned with the point-to-point photospheric mapping $\mathbf{X}(\mathbf{x})$. Each field line can be considered to be topologically unique, since every footpoint is distinct from every other. Some authors prefer instead to think of every field line as topologically equivalent by allowing footpoints to be continuously moved except across PILs. In either case, separatrices in these models are defined by discontinuities in the footpoint mapping. This definition opens the door for the *quasi-separatrix layer* (QSL, see Section 5.2), where the mapping is “almost” discontinuous.

5.1 Mapping discontinuities: Coronal fans and bald patches

It is possible for a continuous coronal field, one for which spatial derivatives of $\mathbf{B}(\mathbf{x})$ are defined and bounded everywhere, to generate discontinuities in its footpoint mapping. One significance of such mapping discontinuities is that they are natural locations for the *formation* of magnetic discontinuities in an initially continuous field (Low, 1987; Low and Wolfson, 1988). While debate persists on the viability of magnetic discontinuities constrained by continuous mappings (see Section 3.3), there is no question that a discontinuous mapping is consistent with a discontinuous field. This means that if a field is initially continuous, but has a discontinuous footpoint mapping, then subsequent dynamics, even subject to strict line tying, may produce a discontinuous field. Indeed, analysis shows that line tied evolution will *almost always* lead to such discontinuities (Inverarity and Titov, 1997).

A mapping discontinuity is a curve across which neighboring footpoints, i.e. footpoints separated by an infinitesimally small distance, map to points a finite distance apart. This property means that spatial derivatives of the mapping functions $X_+(x_-, y_-)$ and $Y_+(x_-, y_-)$ are not defined at the discontinuity. Two types of structures in a continuous coronal field can lead to a discontinuous mapping. These are coronal null points and *bald patches* (Seehafer, 1986; Titov *et al.*, 1993; Bungey *et al.*, 1996), which are portions of PILs. In each case there is a surface in the corona, a separatrix, whose footpoints sit on the curve of mapping discontinuity (Bungey *et al.*, 1996).

Two field lines in contact across the separatrix surface will, by definition, be rooted in different footpoints. They almost certainly also differ in other physical characteristics such as their total length or their end-to-end Alfvén transit times (Lau, 1993). Since these properties are important factors in the line-tied dynamics and equilibrium of a field, it is hardly surprising that magnetic discontinuities tend to form along these separatrices.

In most pointwise mapping models the vertical photospheric field $B_z(x, y, 0)$ vanishes only along curves, i.e. PILs. Barring specially constructed cases there are no photospheric nulls in such models, since both components of the horizontal field will not, in general, vanish at the same point along a given PIL. Therefore, *all null points in a pointwise mapping model will be located in the corona.*

The fan of a coronal null will map to a photospheric curve which then defines a mapping discontinuity (see Figure 13). Footpoints on opposite sides of this curve will map to the ends of the null point’s two spines. One side of the discontinuity to the end of one spine, the other side to the end of the other spine. Points on the curve do not map to the photosphere at all, but end at the coronal null. The photospheric points to which the spines map will be singularities of the mapping, but not in the sense of a simple discontinuity: The neighborhood of this point will map to the entire region near the footpoints of the fan surface.

The other type of discontinuity comes from a portion of the PIL called a bald patch. When the horizontal field at a PIL crosses from the positive ($B_z > 0$) to negative ($B_z < 0$), called the *normal* sense, the field lines will be concave downward. This produces a mapping which simply “flips” a neighborhood across the PIL – a continuous operation. The opposite situation, when the horizontal

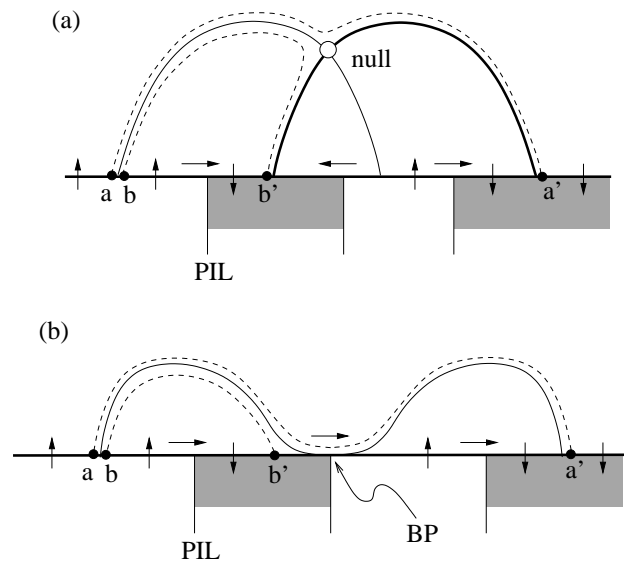


Figure 13: Two-dimensional illustrations of field line mappings exhibiting both types of mapping discontinuities. In each case neighboring footpoints a and b map to points a' and b' separated by considerable distance. Each time the photospheric field is quadrupolar with 3 PILs indicated by vertical lines. The negative (downward) photospheric regions are shaded, and vertical and horizontal arrows show the sense of the photospheric field. Panel a: a field with a coronal null point. Although it is a two-dimensional illustration we take the null to be negative, with spines indicated by dark solid lines and fan field lines by thinner solid lines. Footpoints a and b map from opposite sides of the fan surface to points near each of the spine field footpoints. Panel b: a bald patch where a coronal field line (solid) grazes the photospheric surface, crossing in the inverse sense, from negative to positive, as indicated by the horizontal arrow.

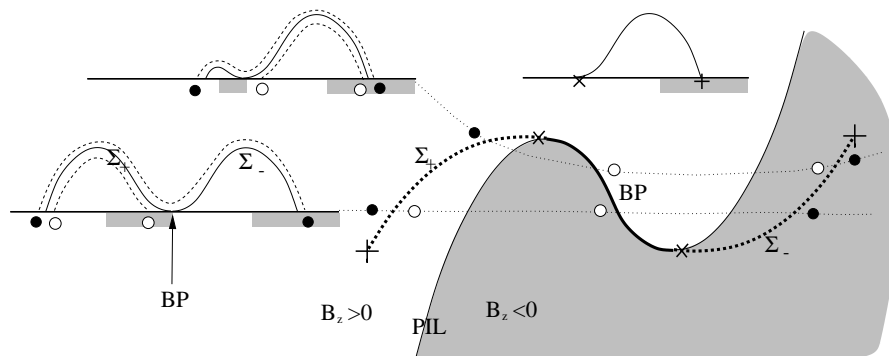


Figure 14: A schematic illustrating the photospheric features associated with a simple bald patch. The larger (lower right) figure shows the top-view of a sinuous PIL (solid) separating positive (white, $B_z > 0$) from negative (grey, $B_z < 0$) photospheric field. The bald patch is the darker portion extending between the two \times s: the points where $(\mathbf{B} \cdot \nabla)B_z = 0$. The dashed curves (Σ_+ and Σ_-) are footprints of the two separatrix surfaces. Three insets show elevation views of the BP separatrices (solid) and two field lines (dashed) which interconnect footpoints labeled as white or black circles. These views cut along the dotted curves in the main, plan view, along which the same circles show the footpoint locations. The lowest of these curves cuts near the center of the BP showing the correspondence with the two-dimensional version from Figure 13.

field crosses from negative to positive, called the *inverse* sense, produces concave upward field lines. The portion of the PIL where the horizontal field is inverse, and hence $(\mathbf{B} \cdot \nabla)B_z|_{z=0} > 0$, is called the *bald patch* (BP). Unless the PIL is closed, and entirely inverse, the bald patch will extend between points where the horizontal field is parallel to the PIL, $(\mathbf{B} \cdot \nabla)B_z|_{z=0} = 0$.

The mapping discontinuity occurs across the set of field lines which graze the surface at the BP (Seehafer, 1986; Titov *et al.*, 1993). These field lines form two surfaces, the BP separatrices, departing the PIL horizontally in opposite directions (see Figure 13) and mapping to curves of footpoints in the photosphere. A simple bald patch, which may occur in a potential or a non-potential field, has the characteristic structure shown schematically in Figure 14. The BP itself extends along the portion of the PIL between points where $(\mathbf{B} \cdot \nabla)B_z = 0$, marked by \times s in the figure. The two BP separatrices extend upward from this curve forming open shells over the “normal” PIL (thin solid). These surfaces intersect the photosphere along two footprints denoted by dashed curves connected to the ends of the BP (their ends are marked with a \times and a $+$). Separatrix Σ_+ has one footprint in the positive (white) region and maps to the negative (grey) side of the BP. Each BP separatrix has an open edge, the lip of the shell, extending between a \times and a $+$ as shown in the upper inset. The footprint mapping will be discontinuous across the entire three-part curve: Σ_+ -BP- Σ_- .

The BP separatrix is not a separatrix in the same sense as other separatrices, since it does not partition the field into separate domains or flux systems. It is evident from Figure 14 that the footprint of the separatrix Σ_+ -BP- Σ_- is not a closed curve. This is a general property of bald patch separatrices, which therefore do not completely enclose coronal sub-volumes. While the field lines on opposite sides of a BP separatrix have distinct properties, there is often a continuous set of field lines between these two, passing around the separatrix. It is analogous to a fence which, however solid it may be, cannot effectively pen an animal since it is not completely closed.

BP separatrices from different BPs may intersect to form a separator (Bungey *et al.*, 1996). The most common cases of BP separators occur where two BPs occur on the same PIL, such as in the field of Titov and Démoulin (1999). Unlike a null-null line, this separator is not associated with any null points, not even with submerged null points.

It is worth noting that the sense of concavity in a general field line is a geometric property, not a topological one. Locations of downward concavity, called “dips”, in field lines throughout the corona play a significant role in dynamic models of prominence formation (Tandberg-Hanssen, 1995). But a field line whose dip does not touch the photosphere can be continuously deformed into an undipped field line; the dip is therefore not a topological property. This is not possible when the dip grazes the photosphere since the photosphere is considered immovable. Thus a bald patch separatrix owes its infinitesimal thinness to the assumption that the photosphere is an infinitesimally thin surface. In models which treat the photospheric and chromospheric layers more realistically, BP separatrices become quasi-separatrices, defined similarly to quasi-separatrix layers in Section 5.2 (Karpen *et al.*, 1990; Billinghamurst *et al.*, 1993; Lau, 1993).

Perhaps the most well-studied three-dimensional field with bald patches is an analytic model, proposed by Titov and Démoulin (1999), of a twisted flux rope nested under a potential arcade. The Titov and Démoulin field is a general force-free equilibrium produced by a superposition of a toroidal current ring (major radius R and minor radius $a \ll R$, with current uniformly distributed inside it), a submerged line current (running along the axis of the ring at depth d), and two submerged point sources (sitting on the line current and separated by $2L$; see Figure 15). It is a four-parameter class of equilibria after imposing force balance and leaving free the size and strength scalings. Titov and Démoulin (1999) studied a one parameter quasi-static emergence scenario where the major radius R increases while its center’s depth d remains fixed.

The photospheric field from the above construction consists of a positive and a negative region separated by a single sinuous PIL (see Figure 16). Each region is concentrated where the current ring crosses the photosphere, giving the appearance of a classic bipolar active region. The field

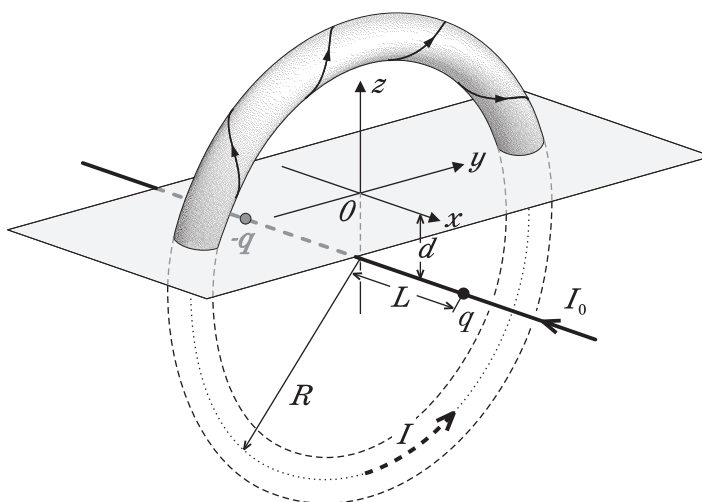


Figure 15: The elements composing the Titov and Démoulin (1999) model of a twisted flux rope under an overlying arcade. The figure depicts a current ring of radius R , a line current at depth d and a pair of point sources separated by $2L$ (reproduced from Titov and Démoulin, 1999).

contains no coronal nulls, so any separatrices must originate in BPs. Titov and Démoulin (1999) find that a BP forms at the center of the PIL when R first exceeds a critical value $R = R_a$. The BP then grows as its endpoints (where $\mathbf{B} \cdot \nabla B_z = 0$) move outward. The two separatrices from this single BP extend into the positive and negative region, respectively, where their footpoints (the separatrix traces) form an S-shaped (or inverse S-shaped) footprint when combined with the BP, as illustrated schematically in Figure 14. At a second critical value, $R = R_b$, the center of the PIL reverts to a normal sense, $\mathbf{B} \cdot \nabla B_z < 0$, meaning that the BP has bifurcated into two portions. These two BPs have a total of four separatrices, two of which intersect to form a separator.

The Titov and Demoulin field represents a twisted flux tube underneath an arcade. While these are distinct elements in the field's construction (a toroidal flux ring and a line-current, respectively) the resulting field cannot be unambiguously partitioned this way. Due to the open nature of a BP separatrix, discussed above, it does not separate the field into distinct flux systems which might be called "flux tube" or "arcade". It is fair to say the field just beneath the BP separatrix is part of the flux tube, and that field just above is part of the arcade. This distinction becomes less clear, however, with increasing distance from the BP separatrix.

Titov and Démoulin (1999) propose that the actual coronal field due an emerging twisted flux rope would have a similar topology and geometry, including the S-shaped, or inverse-S-shaped BP separatrices. If and when the field became dynamically unstable, they went on to argue, strong currents would naturally form along the separatrix surfaces. Numerical simulations (Fan and Gibson, 2003) have confirmed that free dynamical evolution leads to current sheets along the BP surfaces in fields of the Titov and Demoulin type.

This theorized configuration could explain the occurrence of soft X-ray sigmoids prior to the onset of eruptive flares (Canfield *et al.*, 1999). Observations show a strong preference for sigmoids to be S-shaped in the South and and inverse-S-shaped in the North. The Titov and Demoulin model attributes those shapes with flux ropes twisted in right-handed and left-handed helices, respectively, which are known to be the dominant magnetic chiralities in the South and North hemisphere (see, for example, Zirker *et al.*, 1997).

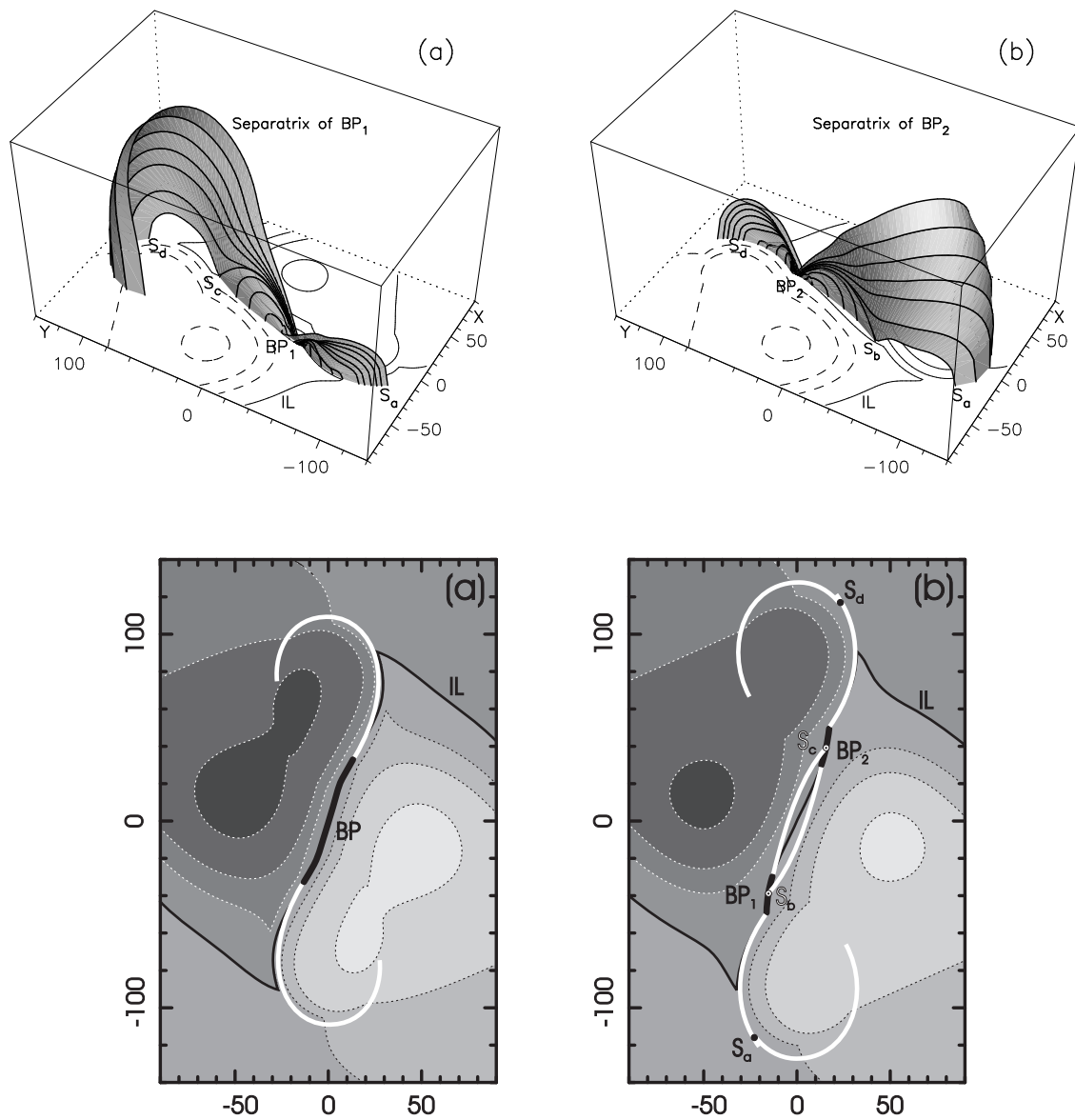


Figure 16: Bald patches and their separatrices in the Titov and Démoulin (1999) equilibrium. Bottom panels show the photospheric normal field (grey), PIL (thin black curve), BPs (thick black curves) and traces of the BP separatrices (white solid curves). Left is the state with one BP, $R_a < R < R_b$, which naturally has two separatrix traces. Right is the state after bifurcation, $R > R_b$, with two BPs and four separatrix traces. The top panels show perspective views of the BP separatrices from the two BPs of the bottom right case (reproduced from Titov and Démoulin, 1999).

5.2 Quasi-separatrix layers

Separatrices occur where the photospheric mapping is discontinuous. This discontinuity permits the generation, under line-tied coronal dynamics, of magnetic discontinuities at which the current density is formally infinite. If the footpoint mapping is continuous but severely distorted, it may preclude the formation of a genuine current sheet (*pace* Parker) but will not preclude current structures which are very thin and contain extremely large current densities (van Ballegoijen, 1985; Longcope and Strauss, 1994). This motivates the definition of a *quasi-separatrix layer* (QSL), defined as a region of large mapping distortion (Priest and Démoulin, 1995; Démoulin *et al.*, 1996) or “squashing” (Titov *et al.*, 2002).

An inherent ambiguity in the definition of QSL stems from specifying how much deformation should be considered “large”. Most useful definitions are given in terms of derivatives of the mapping functions, $\mathbf{X}_+(\mathbf{x}_+)$ and $\mathbf{X}_-(\mathbf{x}_-)$, collected into Jacobian matrices

$$\mathcal{D}_+(\mathbf{x}_+) \equiv \begin{bmatrix} \frac{\partial X_-}{\partial x_+} & \frac{\partial X_-}{\partial y_+} \\ \frac{\partial Y_-}{\partial x_+} & \frac{\partial Y_-}{\partial y_+} \end{bmatrix}, \quad \mathcal{D}_-(\mathbf{x}_-) \equiv \begin{bmatrix} \frac{\partial X_+}{\partial x_-} & \frac{\partial X_+}{\partial y_-} \\ \frac{\partial Y_+}{\partial x_-} & \frac{\partial Y_+}{\partial y_-} \end{bmatrix}. \quad (20)$$

These matrices are defined in the positive and negative photospheric regions, respectively. A straightforward estimate for the degree of local distortion is given by the norm of the Jacobi matrix (Priest and Démoulin, 1995; Démoulin *et al.*, 1996)

$$N_{\pm}(\mathbf{x}_{\pm}) = \left[\left(\frac{\partial X_{\mp}}{\partial x_{\pm}} \right)^2 + \left(\frac{\partial X_{\mp}}{\partial y_{\pm}} \right)^2 + \left(\frac{\partial Y_{\mp}}{\partial x_{\pm}} \right)^2 + \left(\frac{\partial Y_{\mp}}{\partial y_{\pm}} \right)^2 \right]^{1/2}. \quad (21)$$

A related but slightly more complicated definition, offered by Titov *et al.* (2002)

$$Q(\mathbf{x}_+) = \frac{N_+^2}{|\det(\mathcal{D}_+)|}, \quad Q(\mathbf{x}_-) = \frac{N_-^2}{|\det(\mathcal{D}_-)|}, \quad (22)$$

is directly related to the degree of squashing imposed by the mapping¹⁷. Moreover, this function takes the same value at conjugate footpoints of the same field line, $Q(\mathbf{x}_-) = Q[\mathbf{X}_+(\mathbf{x}_-)]$, which is not true of the norms. (The value of Q on a field line is the product of the norms from its two footpoints.)

Both the norm $N_{\pm}(\mathbf{x}_{\pm})$ and the squashing function $Q(\mathbf{x}_{\pm})$ designate QSLs in the same basic way. They are dimensionless, are smallest when the mapping is a rigid translation, rotation or inversion, and become larger with the degree of deformation. Plots of their values, or the logarithms of them, exhibit narrow areas of exceptionally large distortions which are the QSLs. Figure 17 shows a plot of $Q(\mathbf{x})$ for a submerged poles model of Sweet’s configuration taken from Titov *et al.* (2002). Two roughly horizontal strips have $Q \simeq 10^6$, roughly where the spine curves would be in an MCT model. For a precise definition one must define a threshold value of N or Q , and then all footpoints exceeding that value are part of a QSL.

The QSL is therefore a layer rather than an infinitesimal surface like a separatrix. Tracing the field lines of every footpoint at some threshold value of $Q(\mathbf{x})$, defines a surface enclosing the three-dimensional QSL. QSL with a particular X-shaped cross section are common and have been dubbed *hyperbolic flux tubes* (HFTs, Titov *et al.*, 2003).

Submerged poles models, discussed in the following Section 6, offer a link between pointwise mapping models and MCT as the depth of the submerged poles is reduced to zero. Each model

¹⁷The actual squashing degree is $(Q + \sqrt{Q^2 - 4})/2$.

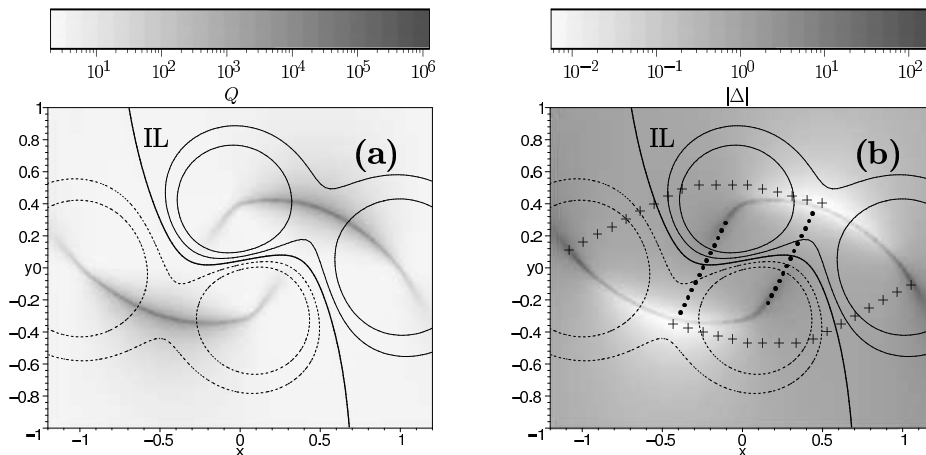


Figure 17: QSLs in a submerged pole model of Sweet's configuration. Contours show the photospheric field $B_z(x, y)$, with the dark line designating the PIL (here labeled IL). (Left) Grey scale shows $Q(\mathbf{x})$ on a logarithmic scale. (Right) Grey scale shows the degree of flux tube expansion for each footpoint. Pluses and dots indicate the principal locations of the four interacting flux systems. (Reproduced from Titov *et al.* (2002).)

with truly submerged poles has a non-intermittent photospheric field, and is thus a pointwise mapping model, containing only QSLs. In the limit that the poles reach the surface, the QSLs become genuine separatrices and the footpoints of a QSL lie approximately where the spines of the prone nulls will appear in that limit. In this same limit, a hyperbolic flux tube becomes a pair of positive and negative fan surfaces along with the null-null line. Its two ends become the spines of the two nulls linked by the null-null line. The X-shaped coronal portion of the HFT becomes the pair of separatrices and the separator at their intersection (Titov *et al.*, 2002).

Most instances where QSLs are invoked in reference to observations use a submerged poles model of the coronal magnetic field (see Démoulin *et al.*, 1997, for an example). Thus the QSLs provide a self-consistent explanation for the localization of current in an evolving active region field. These applications are discussed at the end of the following Section 6.

6 Submerged Poles Models

6.1 The method

One drawback of point charge MCT models is that they produce a photospheric magnetic field which is singular at each charge. This is not surprising in a multipole expansion which should not, after all, be used in the immediate vicinity of the sources. It means, however, that the field may not be directly compared to magnetograms. A solution introduced by Seehafer (1986), and then by Gorbachev and Somov (1988), is to place point charges below the photospheric surface. The charges themselves, and the field in the region $z < 0$, are artifacts of the modeling and not intended to represent the true sub-photospheric field. These original submerged poles models used a potential field from a set of point charges. They produce a vertical photospheric field

$$B_z(x, y, 0) = \sum_{i=1}^M \frac{q_i d_i}{[(x - x_i)^2 + (y - y_i)^2 + d_i^2]^{3/2}}, \quad (23)$$

which depends on the depths d_i , charges q_i and horizontal placements (x_i, y_i) of the M sources. By adjusting these parameters it is possible to approximate the vertical field observed by a magnetogram. The salient features of such representations are that each charge generates a smooth, circular flux concentration of radius comparable to its depth. The combination of poles produces a non-intermittent photospheric field with smooth PILs separating regions of opposing polarity.

To illustrate the method let us consider two different models of flaring active region 2776 on November 5, 1980, as shown in Figure 18. Gorbachev and Somov (1989) proposed a model with four charges all placed at $d = 4.4$ Mm (0.1 units), while Démoulin *et al.* (1994) produced a more accurate representation using 18 charges at depths ranging from $d_9 = 3.99$ Mm to $d_{14} = 102$ Mm. Gorbachev and Somov (1989) selected their charge distribution in order to produce a vertical field which resembled the basic appearance of AR 2776. Démoulin *et al.* (1994) employed an automated algorithm to define their parameters; the algorithm minimized the squared difference in vertical photospheric field between the model, Equation (23), and a vector magnetogram obtained at Marshall Space Flight Center (MSFC). Figure 18 illustrates how the use of more sources permits a more complex photospheric field and thereby permits a more faithful representation of observation.

The next step in a submerged poles model is to associate every photospheric footpoint with the pole to which it maps by the sub-photospheric model field. This process, at least in principle, partitions the photosphere into regions which serve the same function as in MCT models. The coronal field may now be divided into domains according to the regions at each footpoint, exactly as in MCT models. Separatrices are defined as the boundaries between such domains, and separators as the intersections of these separatrices.

This partitioning scheme resembles that of MCT models in that fan surfaces from null points produce separatrices. In this case the null points are frequently sub-photospheric, and map up to the photosphere to produce region boundaries. Figure 19 shows how a portion of one null's fan surface crosses the photosphere to produce a separatrix in the corona. The first crossing produces a photospheric boundary between regions approximately resembling the null's spine sources, in this case $N17$ and $N14$ (not shown). The region boundary forms the footpoints of a separatrix surface (solid curves) extending into the corona. The opposite footpoints, shown as dashed curves, complete the trace of this particular separatrix.

Submerged poles models differ from MCT models in that they have a non-intermittent photospheric field with a PIL and therefore can have bald patches (Seehafer, 1986). The skeleton of a submerged poles model must therefore include BP separatrices as well as the fan surfaces.

Submerged poles models serve an important role as a conceptual bridge between MCT models and pointwise mapping models. A set of submerged point charges, at depths d_i , may be converted to a point-source MCT model by simply taking each depth continuously to zero. Through this

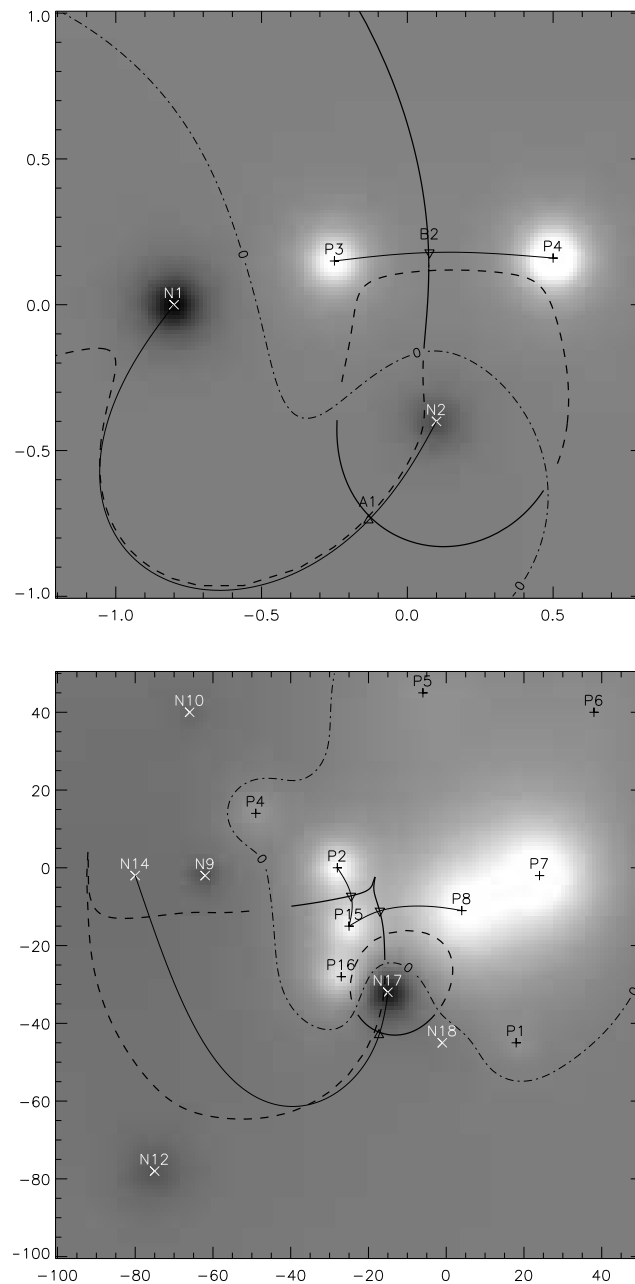


Figure 18: Two submerged poles models of AR 2776, November 5, 1980. The grey scale shows the vertical magnetic field at the photosphere from the collection of submerged poles. The top panel shows the 4-charge co-planar model by Gorbachev and Somov (1989). The bottom panel shows the 18-pole model by Démoulin *et al.* (1994). The axes are labeled in units used in that paper. The projected location of each charge is indicated. The PIL is a thin broken line, and several separatrix traces are shown as solid and dashed dark curves. The solid curve is the first intersection of the fan surface from the submerged null (triangle), the dashed curve is its second crossing. Thin solid lines show the sub-photospheric spines of the selected null points.

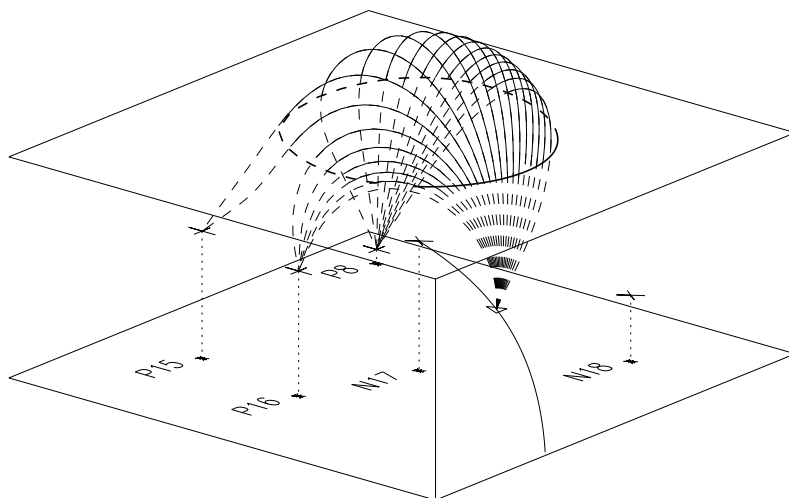


Figure 19: One of the separatrices in the 18-source model of Démoulin *et al.* (1994). A portion of the fan surface of a submerged negative null point (triangle), and its spine curves (solid), one extending to $N17$ and the other leaving the box. The box is a section of the region below the photosphere, showing charges at their respective depths as $+s$ and $\times s$. Dashed lines show field lines from the null's fan surface extending upward to the photosphere. A dark solid curve indicates where they cross $z = 0$, and the thin solid lines are the same field lines above the surface. A dark dashed line shows where the separatrix descends again below the photosphere, mapping to sources $P8$, $P15$ and $P16$. These same photospheric curves appear in the lower panel of Figure 18.

process the sequence of non-intermittent of photospheric fields will continuously approach the singular, intermittent MCT field. If the submerged sources are coplanar (all depths d_i are equal) then this is equivalent to moving the photospheric surface downward until it coincides with the charge-surface. In this case the actual magnetic field never changes, but certain features defined using the photosphere, such as PILs and BPs, do change. Separatrices from fan surfaces are the same in both models, while BPs will vanish in the MCT limit. Figure 20 shows the footprint of the MCT which results from taking the 4-charge co-planar model of Gorbachev and Somov (1989) to the photosphere. The correspondence is illustrated by comparing the footprint in Figure 20 to the separatrix trace from the submerged poles model in Figure 18.

Submerged dipoles were introduced by Démoulin *et al.* (1992) as an alternative to point charges. Dipoles with moments pointing either vertically upward or vertically downward produce positive and negative flux concentrations, respectively. These models promise improved representation of the photospheric field because their field is more vertical at the concentrations periphery, and there will automatically be a surrounding layer of opposing B_z (Démoulin *et al.*, 1992). When using potential fields it is often hard to see significant the differences in the photospheric fields produced by dipoles and monopoles (see Démoulin *et al.*, 1994, for example). An added complication which arises from dipoles is that a given dipole has terminations of both senses (i.e. the field goes both into and out of a dipole). This opens up numerous new, and often perplexing, possibilities for domains connecting like-signed poles or even connecting a pole to itself. With the new connections come new separatrices (Démoulin *et al.*, 1992).

Submerged sources can generate constant- α force free fields as well as potential fields. Démoulin and Priest (1992) proposed a submerged poles model using force-free dipoles. In spherical coordi-

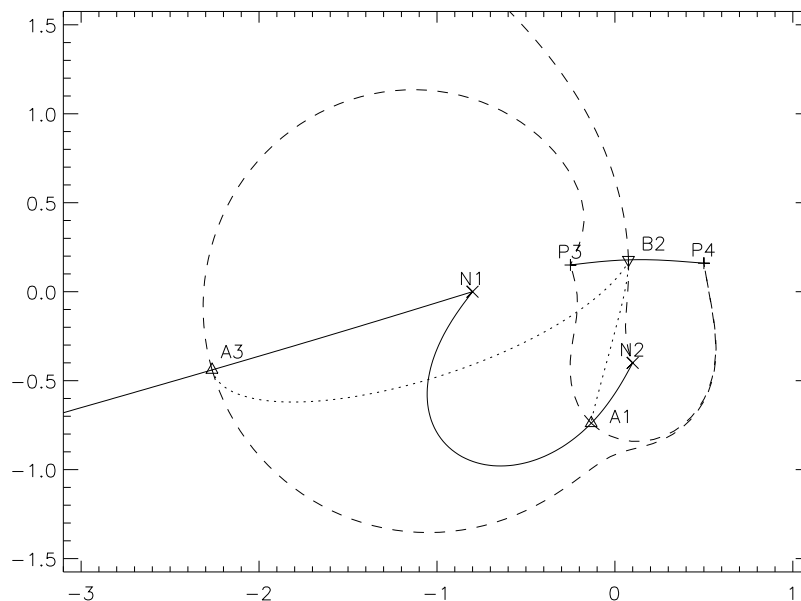


Figure 20: The footprint of the 4-charge co-planar model of Gorbachev and Somov (1989) after source-depths are taken to zero. Symbols are the same as MCT footprints. Dotted lines are the field's two separators. The top panel of Figure 18 is the central portion of this footprint. This is identical to Figure 4 in Gorbachev and Somov (1989).

nates centered on it, a single dipole with moment $\mathbf{m} = m\hat{\mathbf{z}}$ has the axi-symmetric field

$$\mathbf{B} = \nabla f \times \nabla \phi + \alpha f \nabla \phi, \quad (24)$$

where the flux function (see Section 2.1) is given by

$$f(r, \theta) = m \sin^2 \theta [\cos(\alpha r) + \alpha r \sin(\alpha r)]. \quad (25)$$

This matches the potential dipole in the center, $\alpha r \ll 1$, but falls off less rapidly at large distances. A full field is produced by superposing contributions from every dipole. The weak fall-off is somewhat unphysical, so the model should be restricted to distances $\lesssim 1/|\alpha|$ of all poles. Within that region the field will differ from a potential field principally by its overall twist, including shear at the PIL.

6.2 Comparisons with observations

Numerous investigators have compared flare observations with various types of submerged poles models. On the whole these investigations have shown that flare-related phenomena such as H α ribbons, HXR footprints and radio emission sources occur at sites corresponding, at least approximately, to some of the separatrix traces. Moreover, the separatrices involved in a given flare are those which intersect at a single separator across which reconnection appears to have occurred.

Topological studies using submerged poles models were performed on the oft-studied flares of November 5, 1980, first by Gorbachev and Somov (1989) and then by Démoulin *et al.* (1994). Gorbachev and Somov (1989) reported that locations of both H α ribbons from the flare at 22:26 UT corresponded with two separatrix curves from their 4-charge potential field model. (A larger flare at 22:33 UT had almost identical flare ribbon locations). The separatrices involved are the

dark dashed curves originating in nulls $A1$ and $B2$ in Figure 18. These separatrix traces lie very close to the spine curves from the same pair of nulls in Figure 20.

The association of $H\alpha$ ribbons with these two separatrices corroborates a general topological theory of two ribbon flares put forth by Gorbachev and Somov (1988). As interpreted by this theory, the November 5, 1980 event was powered by reconnection across the $A1$ – $B2$ separator converting $P3$ – $N1$ and $P4$ – $N2$ field lines into $P3$ – $N2$ and $P4$ – $N1$ field lines. The field lines in the vicinity of this reconnection site map back to the dashed separatrix traces, which are in turn close to the spines of the two nulls at the ends of the separator.

Démoulin *et al.* (1994) argued that the agreement between $H\alpha$ ribbons and separators of the 4-charge potential model was not good enough to be convincing by itself. They developed the more accurate 18-charge model of AR 2776 shown in Figure 18. Several of their poles were considerably deeper than those of Gorbachev and Somov (1989), resulting in separatrices which were not as close to the projections of spines. (Compare the thick dashed curves to the thin solid ones in each panel of Figure 18.) Even with this adjustment, however, Démoulin *et al.* (1994) found poor correspondence between the ribbons and the separatrices, in this case near the $N14$ – $N17$ spine and the $P15$ – $P8$ spine. A potential dipole model had almost identical separatrices, but a linear force free field with $\alpha = -0.019 \text{ Mm}^{-1}$ (a value found by comparison to $H\alpha$ fibrils) showed superior correspondence. Furthermore, a radio sources observed by VLA and two hard X-ray sources (16–30 keV) observed by HXIS were also located along the separatrix traces.

The constant- α model field was topologically equivalent to the potential field but had separatrix traces nearer to the PIL. This led to a better correspondence with flare signatures, but basically upheld the topological interpretation of Gorbachev and Somov (1989), although this time through the separator at the $P8/N17/P15/N17$ junction. The model pointed to the need for non-potential models from numerous submerged sources in order to achieve good geometrical correspondence with observation.

The benefit of more sources had first been established by Mandrini *et al.* (1991) and Mandrini *et al.* (1993) in a topological study of a series of homologous flares in AR 2372 between April 6 and 8, 1980. Vector magnetograms from MSFC were modeled as a potential field from submerged dipoles. While the active region could be crudely modeled using 4–6 submerged dipoles, reasonable correspondence with the locations of $H\alpha$ kernels required 17, 16 and 18 dipoles for flares on April 6, 7 and 8, respectively. In each case the dipoles could be grouped into a smaller number of families (4–6 families) corresponding to the dipoles of the cruder model. From the numerous separatrices present, only those separating different families were considered as possible sites of reconnection. These separatrices were topologically equivalent to separatrices present in the crude 4–6 dipole model, but the larger number of sources permitted better representation of the magnetic field’s geometry. This more accurate modeling proved critical in producing good correspondence between the separatrices and the observed flare signatures.

Each of the flares studied by Mandrini *et al.* (1991) and Mandrini *et al.* (1993) had five distinct kernels in off-band $H\alpha$ observations. These were widely separated, but all began and reached their peaks in unison, suggesting a common driver. Mandrini *et al.* (1991) showed that 4 of the 5 kernels lay on top of traces of two separatrices which intersected along a common separator. Moreover, there were four magnetic field lines, one from each of the four domains neighboring the separator, whose footpoints were found within the flare kernels, two footpoints in each kernel. This is still more evidence of magnetic reconnection at a separator causing a flare. All 5 $H\alpha$ kernels of the flares on April 7 and April 8 were found to lie on separatrix traces; all but one associated with field lines in the vicinity of a common separator (Mandrini *et al.*, 1993).

Several other applications of this technique provide still further evidence of the role of separator reconnection in solar flares (Démoulin *et al.*, 1993; van Driel-Gesztelyi *et al.*, 1994; Bagalá *et al.*, 1995; Mandrini *et al.*, 1995). When taken as a group these modeling efforts provide very strong evidence of the importance of magnetic field line topology in solar flares.

6.3 Separatrices and QSLs

In spite of the observational evidence of their significance, separatrices and separators in submerged poles models appear theoretically to have dubious relevance. Those separatrices which are the fan surfaces of sub-photospheric nulls have no characteristic in the photospheric or coronal fields which distinguish them as such. Since the sub-photospheric field is only an artifact of the modeling, it is unclear why topological features originating there would be physically meaningful.

The solution to this puzzle appears to lie in the concept of QSLs (see Section 5.2). Since a submerged poles model has a non-intermittent photospheric field it may be analyzed strictly as a pointwise mapping model, without regard to the sub-photospheric field. Doing so eliminates the separatrices from submerged nulls, and with them most of the photospheric regions. The footpoint mapping $\mathbf{X}(\mathbf{x})$ may be computed from photospheric footpoint \mathbf{x} to conjugate footpoint \mathbf{X} . From that may be found the derivative norms $N_{\pm}(\mathbf{x}_{\pm})$ or squashing function $Q(\mathbf{x})$ discussed in Section 5.2. Large values of either indicate severe local distortion in the footpoint map. The locus of point where $Q(\mathbf{x})$ exceeds a threshold may be used to define the QSLs.

Titov *et al.* (2002) performed this analysis for a submerged pole model of Sweet's configuration. They found two QSLs, shown in Figure 17, whose location corresponded with separatrices from the two submerged null points. They repeated this process for models with poles at decreasing depths and found that the maximum values of Q within the QSL became ever larger. They concluded that in the limit $d \rightarrow 0$, $Q \rightarrow \infty$, meaning the layers have become genuine discontinuities: they are separatrices.

Submerged poles models have proven particularly useful since they offer a fast and convenient means of predicting QSLs. At least with algorithms presently used, null points and fan surfaces can be found much faster than QSLs. Furthermore, the topology of submerged poles field will resemble that of an MCT field: separatrices partitioning the volume into a certain number of domains. Analysis of this partitioning gives an immediate indication of how many QSLs a field might therefore have.

The process of raising poles to $z = 0$ also serves as a bridge between the two classes of models. MCT models, described in Section 4, included one type of separatrix: fans from null points. Pointwise mapping models, on the other hand, had separatrices from coronal nulls and from BPs as well as QSLs and HFTs. In the process of starting with a continuous field generated by submerged poles, and raising the poles to the surface, the topological elements from one model are transformed into those of another model. Titov *et al.* (2002) showed that QSLs transform to genuine separatrices and Titov *et al.* (2003) showed that a HFT transforms to a separator and adjacent separatrices.

The two genuine separatrices in the pointwise mapping models suffer different fates in this limit. Nulls already in the corona when the poles are submerged will rise even higher into the corona as the poles are raised. Separatrices from fans of coronal nulls will therefore be the same in both models. Bald patches, however, are rooted in PILs which are absent from the intermittent fields of MCT models. As submerged poles are raised, the gradient ∇B_z in the vertical field at each PIL decreases in magnitude. In the limit $d \rightarrow 0$ the PILs expand and merge to form the field-free sea. The BP separatrices will, in general, disappear along with the PILs which they are rooted to. All separatrices in MCT models have closed footprints, and therefore enclose sub-volumes. The BP separatrices, on the other hand, do not enclose volumes so they have no counterpart in MCT models.

7 Coronal Null Points

In the idealized models of coronal field topologies treated here, coronal and photospheric nulls form distinct classes. Photospheric nulls only occur, in general, in the field-free photospheric regions of MCT models, and are absent from models with non-intermittent photospheric field. Coronal null points, on the other hand, are possible in all coronal models.

Enumeration of coronal null points in a given field is considerably more difficult than the enumeration of photospheric nulls. Formulae relating to photospheric null points, discussed in Section 4.1, follow from an application of Poincaré’s index theory to planar vector fields (Molodenskii and Syrovatskii, 1977). The sum of the indices of the sources (+1), upright nulls (+1) and prone nulls (−1) over the entire plane must equal the index of the asymptotic field which is either 1 or 2 for a field which is asymptotically monopolar or dipolar, respectively. Adding to the count one source at infinity in cases of monopolar field leads to Equation (16) for the number of photospheric null points of each type.

The *topological degree* (Molodenskii and Syrovatskii, 1977; Greene, 1993), which is the three-dimensional analog of Poincaré index, is somewhat less useful for enumeration of null points. A positive source and a negative null point have the same topological degree, +1, while negative sources and positive nulls each have topological degree −1. A volume containing S_{\pm} positive/negative sources and n_{\pm} positive/negative nulls will therefore have a topological degree $S_+ + n_- - S_- - n_+$. The topological degree can be established independently using only the field at the volume’s outer surface (Greene, 1993; Inverarity and Priest, 1999). A general formula follows from using a surface at infinity and evaluating the degree of the asymptotic field; this is +1, −1 or 0 when the net charge is positive, negative or zero. Unfortunately, this procedure requires enclosing both the corona and its mirror image, so the general formula (Inverarity and Priest, 1999)

$$S_+ - S_- = n_+ - n_- \quad (26)$$

effectively double-counts coronal nulls (infinity itself has once again been included as a source when the photospheric sources do not balance). Nor is Equation (26) useful for bounding the number of null points since it depends on the difference between positive and negative nulls.

In a field undergoing topological changes, either due to non-ideal evolution (see Section 2.5) or hypothetical parameter variation, null points are created and destroyed only through local bifurcations. According to the general theory (see, for example, Guckenheimer and Holmes, 1983) singular points of a divergence-free field may change either through saddle-node bifurcation or, in cases of symmetry, through pitchfork bifurcation or Hopf bifurcation.

In a saddle-node bifurcation two singular points of opposite degree are created simultaneously. In the reverse bifurcation the two annihilate one another. A saddle-node bifurcation in a magnetic field, called a *local separator bifurcation* (Brown and Priest, 2001), creates one positive and one negative null. The two spines and the line of initial separation are all three mutually orthogonal. This means that there is a separator connecting the two nulls immediately following their formation. A local separator bifurcation can occur in the corona, where it automatically satisfies Equation (26), or within a field-free portion of the photosphere, where it creates one prone null and one upright null of the opposite sign in order to satisfy Equation (16) as well (see Figure 21).

A pitchfork bifurcation occurs only within field-free photospheric regions, and therefore is only relevant to MCT models. This bifurcation involves the transformation of one null into three, two with the same sign as the original null. Such a scenario is structurally unstable under general conditions where it would prefer to be a saddle-node bifurcation in the vicinity of an existing null point. In cases where symmetry forbids this generic version, however, such as at the $z = 0$ plane, the bifurcation must occur as a pitchfork. In MCT models, where it is called a *local double separator bifurcation* (Brown and Priest, 2001), a prone photospheric null point, say it is positive, will bifurcate into a negative prone null, and a positive coronal null. The third null is the mirror

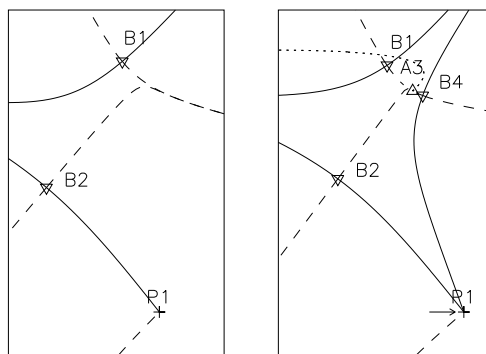


Figure 21: A local separator bifurcation. Footprints of the potential field generated by two configurations. The left configuration has two positive prone null points, B1 and B2, whose fan traces asymptote to the same line. In the right configuration one positive source, P1, has been moved to the right (arrow) leading to a local separator bifurcation. This bifurcation creates a new positive prone null, B4, and a negative upright null, A3, whose coronal spine is shown as a dotted line. Fan traces from B1, B2 and B4 all connect to the upright null A3.

image of the coronal null which is therefore also positive, making the total, two positive and one negative, in compliance with Equation (26). The spines of the coronal null will be parallel to those of the original photospheric null, and orthogonal to those of the new photospheric null (see Figure 22). The fan of the new photospheric null will follow underneath the coronal null's spines.

There is one final mechanism which, while not a proper bifurcation, transforms photospheric nulls into coronal nulls, while observing Equations (16, 26) and reflectional symmetry. A prone and an upright null of the same sign can collide and “scatter” from the photosphere into the corona and mirror corona (Graham Barnes, private communication). Both the coronal null and its mirror image have the same sign as the original pair, so Equation (26) is obeyed. The simultaneous loss of a prone and an upright null from the photosphere satisfy Equation (16).

General MCT models have far fewer coronal nulls than photospheric nulls. Coronal nulls require complex source configurations. For instance they will not occur in distributions where it is possible to draw a straight line dividing the positive from the negative sources (Seehafer, 1986). This means that a minimum of four sources are required. Typical is a kind of δ -spot configuration with one source surrounded by three of opposite sign. This leads to a coronal null of the same sign as the central source whose fan surface forms a dome.

Nulls in submerged poles models are either sub-photospheric or coronal; only accidentally will one occur exactly at $z = 0$. The sources in these models are not co-planar, but restricted to a sub-photospheric layer. The likelihood of coronal nulls therefore depends on the extent to which nulls extend outside the source-layer (Bungey *et al.*, 1996). Démoulin *et al.* (1994) posed the question “Are magnetic nulls important in solar flares?”, and ultimately concluded the answer must be “No”. In this work they used various placements and strengths of four submerged poles to model a variety of flaring active regions. They found that null points occurred above the photosphere very rarely, and that their inferred presence or absence was unrelated to properties of the flares observed.

There is some observational evidence for coronal null points especially above a photospheric magnetic concentration surrounded by opposing polarity. Filippov (1999) reported EUV observations (171 Å and 284 Å from SOHO/EIT) of AR8113 close to the west limb in which loops exhibited a very clear “saddle” configuration. The shape of the coronal loops suggested a coronal null point located approximately 65 Mm above a small positive region which had emerged into a dispersed

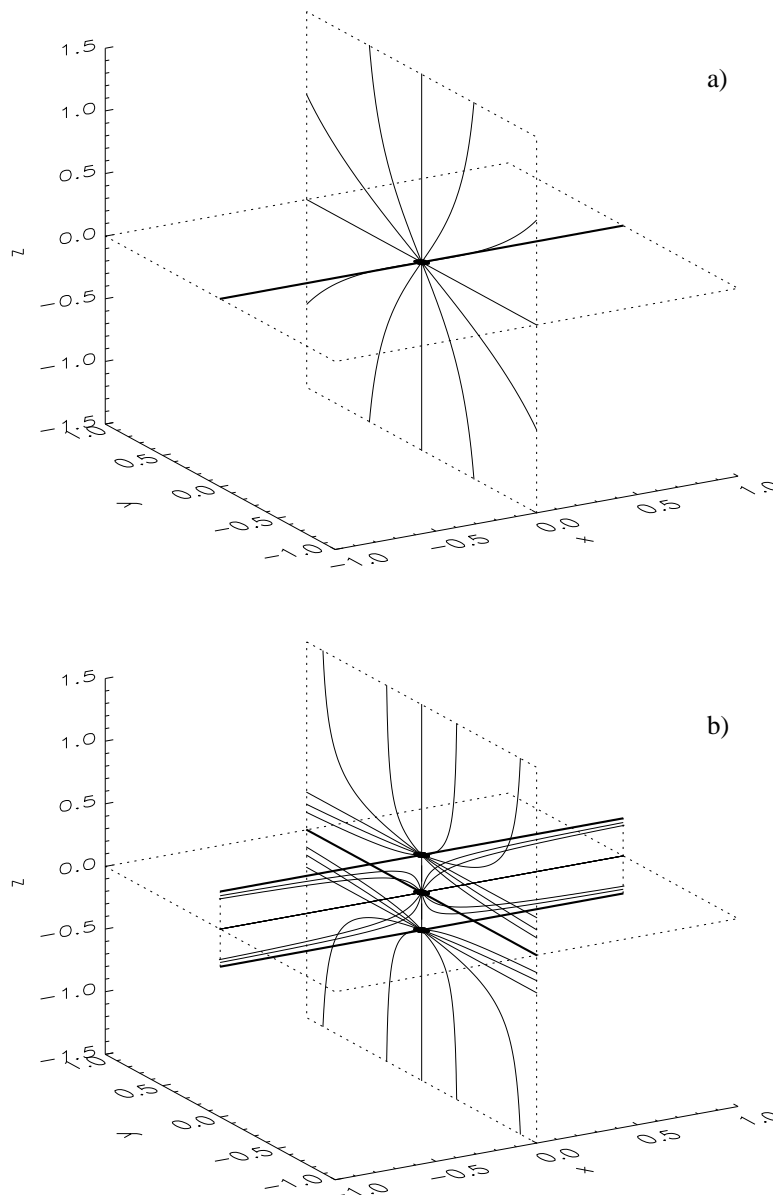


Figure 22: A local double separator bifurcation. Panel a: a single prone null located at the origin. The spines (solid dark line) run along the x axis, lying in the photospheric plane (horizontal dotted square). Thin lines show a selection of fan field lines in the corona ($z > 0$), mirror corona ($z < 0$) and in the photosphere (i.e. the fan traces). Panel b: the structure of the field after bifurcation. The null at the origin has reversed sign, so its spines now form the x axis. New nulls now appear above and below the origin on the z axis. Their fans lie in the $y = 0$ plane, and their spines extend horizontally in the $\pm \hat{y}$ direction. These spines form the top and bottom edges of the fan surface of the prone null. The three fans intersect along a pair of separators running along the z axis between the null points (reproduced from Brown and Priest, 2001).

negative polarity. There is no evidence in the EUV data for energy release or reconnection at this null point.

There is also evidence that magnetic null points do play a role in a few solar flares. Fletcher *et al.* (2001) study an M-class flare which occurred in AR8524 on 3 May, 1999. Magnetograms shows that a small bipole emerged in the trailing (negative) polarity of the existing active region just prior to the flare. In a potential field extrapolations from a point source representation of the magnetogram there is a coronal null point just above the surrounded positive pole; this feature is, however, absent from extrapolations which use the full magnetogram. Based on this and the morphology of TRACE EUV (171 Å) and *Yohkoh* SXT observations, Fletcher *et al.* (2001) conclude that the flare was initiated by reconnection at the coronal null point.

Evidence is also found, by Aulanier *et al.* (2000), for a coronal null at the initiation of the flare on July 14, 1998 (the first Bastille Day flare). The magnetic configuration in which this occurs (AR8270) is a δ -type sunspot. These are often characterized by a surrounded polarity, and as a general configuration they are well known to produce the largest solar flares (Zirin and Liggett, 1987). In this case, Aulanier *et al.* (2000) perform potential extrapolations from line-of-sight magnetograms (KPNO) and find a null point in the corona.

In models of random magnetic fields with homogeneous isotropic statistics it is possible to calculate an average density of null points. The density of null points in a general field with three-dimensional homogeneity depends on the spectral energy density (Albright, 1999). Null points will have a volume density

$$\sim \left[\frac{\langle (\partial B_i / \partial x_j)^2 \rangle}{\langle B^2 \rangle} \right]^{3/2}, \quad (27)$$

where the numerator is the mean square of a typical spatial derivative. This means that in smooth magnetic fields nulls will be spaced by roughly the length over which the field is globally structured. It is theoretically possible for the field's spectrum to be so hard that $\langle (\partial B_i / \partial x_j)^2 \rangle$ diverges, in which case an unlimited number of nulls form self-similar fractal clusters (Albright, 1999).

A coronal magnetic field is unlikely to be entirely homogeneous since it is anchored to the photosphere. For a potential-field extrapolation from $z = 0$ the scale of structuring gets progressively smoother with height, causing the null density to fall dramatically (Schrijver and Title, 2002). For a homogeneous photospheric field composed of an equal mixture of positive and negative elements the null density has the universal form $\simeq 0.05z^{-3}$, independent of the sizes or density of the photospheric elements (Longcope *et al.*, 2003). When the mixture is uneven the nulls become restricted to a thin layer, but with slightly higher overall column density. In most cases there is roughly one coronal null point for every ten photospheric sources (Schrijver and Title, 2002; Longcope *et al.*, 2003). This means that nulls are relatively rare in the corona and get rarer still as one goes higher.

8 Topology of the Heliospheric Magnetic Field

8.1 The solar wind

The solar wind consists of outward flowing plasma whose radial velocity is roughly constant with distance causing its density to fall as $\rho \sim r^{-2}$. By the time it reaches the Earth (at 1 AU) the density has dropped to $n_e \sim 3\text{--}10 \text{ cm}^{-3}$. During solar minimum the overall structure is the clearest, and high and low heliospheric latitudes exhibit different characteristic speeds giving rise to the terms “fast” and “slow” solar wind. The fast solar wind at high latitudes is very steady at $700\text{--}800 \text{ km s}^{-1}$ with very little variation over a solar cycle (Phillips *et al.*, 1995). At low latitudes the wind is sometimes fast and sometimes slow ($300\text{--}500 \text{ km s}^{-1}$).

The magnetic field embedded in the solar wind appears very weak ($B \sim 5 \times 10^{-5} \text{ G}$ at 1 AU) when its energy density is compared to either the plasma’s pressure or kinetic energy density. The field is therefore readily deflected by the wind and generally lies parallel to the flow. In his early model Parker (1958) predicted that the outward solar wind would “open” the magnetic field into a split magnetic monopole: field lines directed outward in one hemisphere and inward in the other, with magnitude decreasing with distance as r^{-2} . Between the hemispheres the field reverses sign in a layer called the *heliospheric current sheet*. Magnetic observations made within the ecliptic, from the Earth for example, show reversals in the field direction as the heliospheric current sheet sweeps past, rotating with the Sun. These transitions are known as *sector boundaries*, as they divide sectors of inward and outward directed magnetic field. The current sheet is deformed to accommodate the complex field structure it separates, so there can be more than two sector boundary crossings per solar rotation.

A simultaneous measurement of the magnetic field within an entire hemisphere is not possible, since measurements are made at single points by spacecraft. Taking a typical measured value $B_r \simeq 3 \times 10^{-5} \text{ G}$ as the representative of the entire hemisphere gives a net flux $\Phi_{\text{open}} = 2\pi(1 \text{ AU})^2 B_r \sim 4 \times 10^{22} \text{ Mx}$. Because they are anchored to a rotating Sun, the field lines in each hemisphere sweep backward in a pattern called the *Parker spiral*. *In situ* measurements of the magnetic field vectors by various spacecraft confirm the average field to be oriented in good agreement with the Parker spiral: $\simeq 45^\circ$ from radial in the ecliptic plane at 1 AU.

The connection of an interplanetary field line to the Sun can be experimentally inferred by the presence of a uni-directional high-energy electron population called “strahl” (Feldman *et al.*, 1975). Such measurements generally corroborate the picture that almost all field lines in the solar wind connect back to the Sun at one end and are open to interplanetary space at the other¹⁸. Notable exceptions are transient events known as magnetic clouds which appear to be ropes of closed field lines (both ends anchored to the Sun) whose apices are entrained in the solar wind (Burlaga *et al.*, 1981) discussed further below. A more serious challenge to the simple Parker spiral picture came from the Ulysses spacecraft which flew to very high heliospheric latitudes and observed populations of electrons and ions typically associated with low latitude activity. These observations suggest either that the electrons are capable of diffusing across field lines much more readily than expected or that heliospheric field lines are not confined to latitudinal cones as they would be in a Parker spiral (Fisk, 1996).

The open field lines which compose the solar wind must all have footpoints located somewhere on the solar photosphere. X-ray images of the solar corona revealed extensive dark regions, generally near the poles, dubbed coronal holes. It was quickly understood that coronal holes probably corresponded with the open field lines from which the out-flowing solar wind originated. The plasma density on these field lines would be lower than on the closed active region field lines, causing them to appear darker in soft X-rays. While they are typically confined to high latitudes,

¹⁸It is important to recall that this definition of topology arises from the high-energy electrons which have a large but not infinite mean free path.

the boundaries of coronal holes can be complex near solar maximum, sometimes even crossing the equator.

8.2 Open/closed boundaries

Locating the photospheric source of the solar wind requires some kind of magnetic model extending through the low solar corona, where $\beta \ll 1$, into the super-Alfvénic solar wind. The key topological elements in any such model are the boundaries between open and closed field lines. Yeh (1978) presented a general discussion of the possible topologies of the open/closed separatrices. We neglect at this point those separatrices between different regions of closed fields since they are topologically identical to cases without open field discussed at length in the foregoing sections. In the remaining cases, Yeh concluded that separatrices could either separate open field lines from closed field lines, or they could separate the two polarities of open field lines. A given closed flux region can either have a compact footprint or its footprint can surround one or more regions of open field lines (compare Panels a and b in Figure 23). A compact footprint (one which includes no open field regions) will be enclosed by two separatrices, connected by a separator contacting the photosphere at two points, as in Panel a. When the closed region surrounds a section of open flux, as in Panel b, it will form a “crater-like” enclosure, with separatrices inside and outside intersecting along a closed coronal separator (Yeh, 1978).

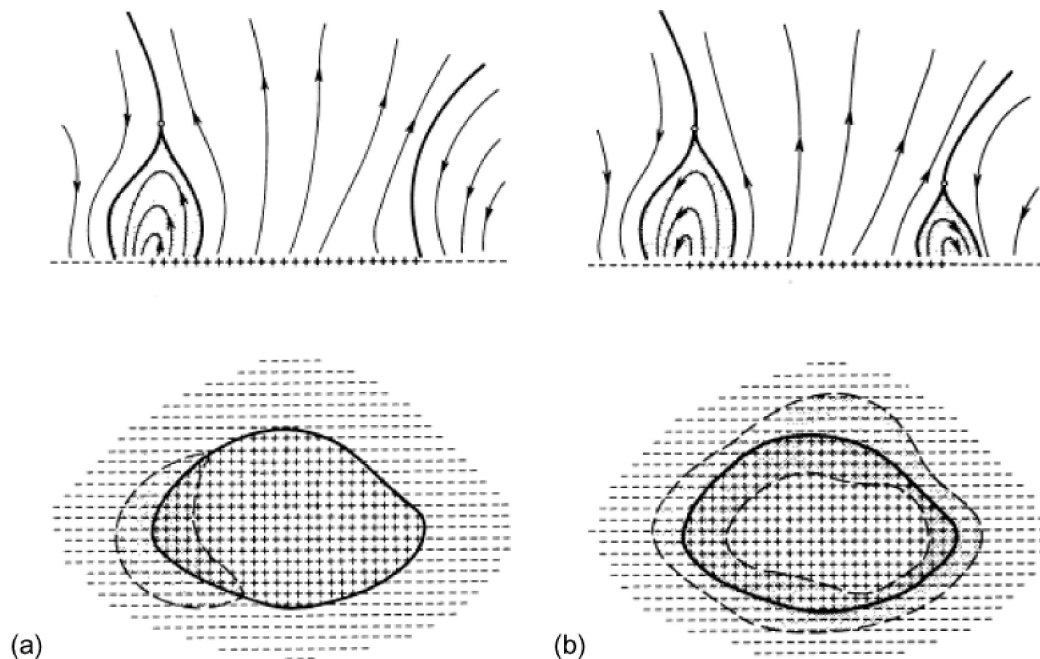


Figure 23: Possibilities for topological boundaries with open field lines. Lower panels show the photospheric field in relation to the PIL (dark solid curve) and separatrices (dashed). In each case, the positive field (+s) forms a compact region separated from the surrounding negative region by the PIL. Top panels are elevation views of the field lines (thin curves) and separatrices (dark curves) anchored to the positive and negative regions denoted with +s and -s. Panel a: a closed separatrix enclosing a compact region of closed field. Panel b: a “crater-like” enclosure where the closed field region surrounds open field (reproduced from Yeh, 1978).

The most common quantitative model of the global corona is the Potential Source Surface

(PSS) model first introduced by Schatten *et al.* (1969) and Altschuler and Newkirk Jr (1969), and refined by subsequent investigators. The field is taken to be potential, $\mathbf{B} = -\nabla\chi$, in the region between the photosphere and an outer shell at $r = R_S$ called the source surface (see Figure 24). The solenoidal condition, $\nabla \cdot \mathbf{B} = 0$, means that the scalar potential must be harmonic, $\nabla^2\chi = 0$, within the range $R_\odot < r < R_S$. The upper boundary, $r = R_S$, is meant to represent the base of the true solar wind, in which all field is open and approximately radial. The appropriate boundary condition for this purpose is $\chi(R_S, \theta, \phi) = 0$, which makes all field purely radial ($B_\theta = B_\phi = 0$) on the surface. The general solution to Laplace’s equation satisfying this boundary condition is

$$\chi(r, \theta, \phi) = \sum_{\ell=1}^{\infty} \sum_{m=0}^{\ell} \left[\left(\frac{R_S}{r} \right)^{\ell+1} - \left(\frac{r}{R_S} \right)^{\ell} \right] P_\ell^m(\cos \theta) [g_\ell^m \cos(m\phi) + h_\ell^m \sin(m\phi)], \quad (28)$$

where $P_\ell^m(x)$ is the associated Legendre polynomial¹⁹. The coefficients g_ℓ^m and h_ℓ^m are fixed using the lower boundary condition from the photospheric magnetic field. This boundary condition can, for example, be formulated in terms of a sequence of magnetograms covering one complete solar rotation (Altschuler and Newkirk Jr, 1969)²⁰.

In a complete magnetic field model the outside of the potential field from Equation (28) is matched to the inside of a heliospheric field. The latter typically consists of field lines tracing Parker spirals outward or inward along cones from $r = R_S$, as shown in Figure 24. The radial field at the source surface, $B_S(\theta, \phi) = B_r(R_S, \theta, \phi)$, therefore serves as the “source” of the heliospheric field. The outward and inward sectors are anchored where $B_S > 0$ and $B_S < 0$, respectively.

The curve along which $B_S = 0$ thereby defines the base of the heliospheric current sheet separating the heliospheric sectors: It is the sector boundary (see Figure 25). At radii approaching the source surface from below, Equation (28) becomes strongly dominated by its lowest poles, $\ell = 1$ and $\ell = 2$, corresponding to the photosphere’s overall dipole and quadrupole. One consequence of its low-order nature is that $B_S(\theta, \phi) = -\partial\chi/\partial r|_{r=R_S}$ tends to be very smooth, vanishing along a single closed curve dividing the $r = R_S$ sphere in two. Thus, at least at its base the heliospheric current sheet is not a discontinuity since B_r passes continuously through zero.

The sector boundary is defined by the curve or curves on the source surface where $B_S = 0$, as shown in Figure 25. Were the field purely dipolar the sector boundary would be a great circle on the source surface, although it would only coincide with the rotational equator in the case $g_1^1 = h_1^1 = 0$. It is the influence of the quadrupole (and the higher poles to a lesser extent) which deforms the heliospheric current sheet, sometimes resulting in four sector crossings per rotation or even multiple distinct unipolar regions (Hoeksema *et al.*, 1983). Examples of particularly complex configurations are shown in Figure 26.

Since both B_θ and B_ϕ vanish everywhere over the source surface, the sector boundary, $B_r = 0$, is a curve of genuine magnetic null points. Such a one-dimensional continuum of nulls is one of the constructions expressly discounted in the foregoing section (2.4) since it is non-generic. It owes its appearance now to the definition of the source surface as a surface on which B_θ and B_ϕ vanish simultaneously (in general circumstances, these functions would vanish on separate surfaces which would generically intersect transversally only along curves). These null points are neither positive nor negative but are all X-type nulls whose neutral direction (along the eigenvector corresponding to the $\lambda_2 = 0$ eigenvalue) is parallel to the sector boundary curve. Each null point has two distinct separatrix curves extending downward into the current-free corona: one forward and one backward (see Figures 24 and 25). For each closed sector curve on the source surface the forward separatrix

¹⁹In practice the expansion includes a pre-factor $\sim (R_S/R_\odot)^\ell$, and $P_\ell^m(x)$ is defined using the Schmidt normalization in order to keep all coefficients of roughly comparable magnitude. Equation (28) is intended only to indicate the basic form of the potential.

²⁰Ideally this would require knowledge of the field over the full solar surface, including the North and South poles, at one instant. Information from the “back” side is obtained by letting solar rotation bring it to the front; information about the poles is more difficult to obtain (see Hoeksema *et al.*, 1982).

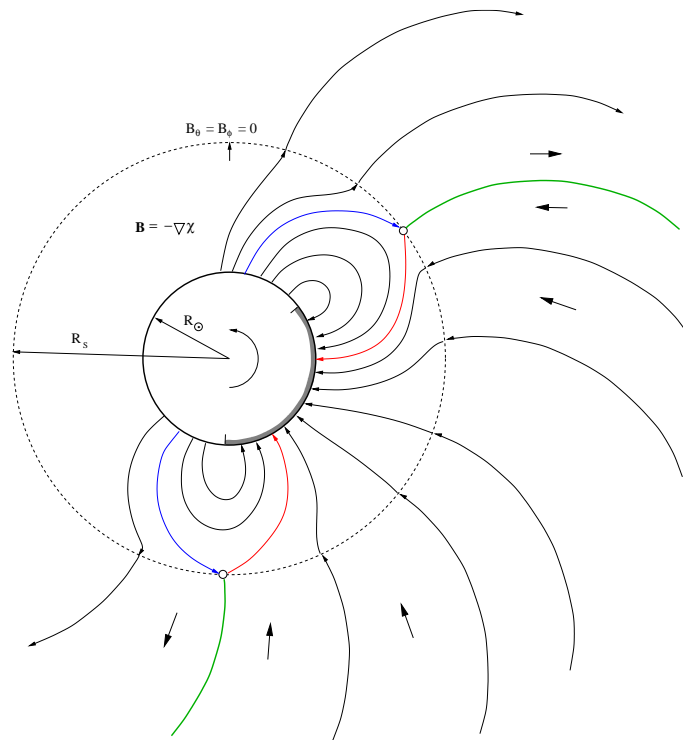


Figure 24: A schematic depiction of a source-surface model as viewed from above the Sun's North pole (the sense of rotation is indicated by a semi-circular arrow). A dashed circle shows the source surface at $r = R_S$. The field is made purely radial at this surface by setting $B_{\theta} = B_{\phi} = 0$. Between the source surface and the solar surface, $r = R_{\odot}$, the magnetic field is potential: $\mathbf{B} = -\nabla\chi$. Field lines anchor to the photosphere in a negative region (shaded segment) and positive regions. Outside the source surface the field is swept back in a Parker spiral. Two null points (X-points) are shown as circles on the source surface. The upward and downward separatrices are shown in blue and red, respectively. The sector boundaries are shown as green curves.

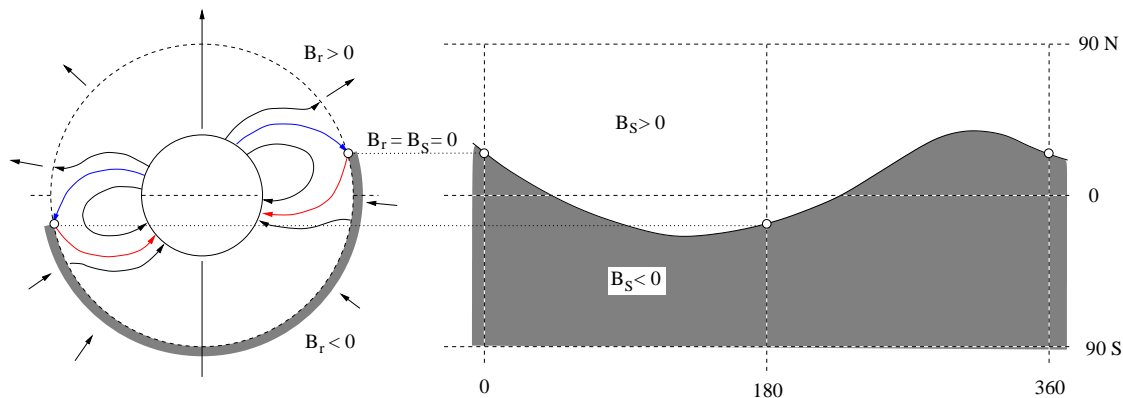


Figure 25: A schematic depiction of the sector boundary defined by the potential source surface model. On the left is a view of the coronal field, $R_{\odot} < r < R_S$, in the meridional plane using the same scheme as Figure 24. The X-points at the source surface are shown by circles. From them originate one downward separatrix (red) and one upward separatrix (blue). The map on the right is the source surface itself ($r = R_S$) plotted as sine of latitude versus longitude. The dark curve is the sector boundary, $B_S = 0$, separating the outward sector ($B_S > 0$, white) from the inward sector ($B_S < 0$, grey). The dashed vertical lines at 0° and 180° correspond to the two meridional slices on the left.

curves form a continuous separatrix surface mapping downward to negative polarity photospheric regions; this is the red curve on the right part of Figure 27. The backward separatrices form independent separatrix surfaces mapping to positive regions (the blue curve). These surfaces are the separatrices between open and closed magnetic field lines. Their footpoints trace photospheric curves which are the theoretical manifestation of coronal hole boundaries in the PSS model. The coronal field becomes increasingly complex at decreasing radii and can also contain isolated coronal null points at radii $R_{\odot} < r < R_S$. Thus the separatrices leaving the smooth sector boundary may map to fairly complex coronal hole boundaries.

The topology of a heliospheric field model may be tested against several types of observation. The model was first developed by Schatten *et al.* (1969) for comparison to the magnetic sectors observed by spacecraft at 1 AU. This showed that setting $R_S = 1.6R_{\odot}$ gave a model whose predictions of mean field strength, sector duration and smoothness in $B_r(t)$ was in good agreement with the average values observed by spacecraft. Hoeksema *et al.* (1982) compared observations to time histories of radial field direction (inward or outward) predicted by source surface models over 18 solar rotations (1976–1977). The observations showed four sector boundary crossings per rotation, implying a rather complex heliospheric current sheet. The PSS model produced a time history agreeing with the observations with a correlation coefficient of $\simeq 0.63$; the maximum correlation occurred when $R_S = 2.35R_{\odot}$. Burton *et al.* (1994) compared a PSS model to sector crossings of the ISEE-3 spacecraft and found that not only were the transitions correctly predicted, but so was the inclination of the current sheet at the crossings (with a correlation coefficient of 0.96). An independent test was provided by Bruno *et al.* (1984), who observed a correlation between the predicted location of the heliospheric current sheet and the location of maximum K-corona brightness observed from the Mauna Loa coronagraph.

Originally developed to model the heliospheric magnetic field, the PSS model has also proven useful in studies of large-scale coronal topology. The separatrices extending downward from the sector boundary, $B_S = 0$, form the boundary between open and closed coronal field lines. There is evidence in support of this interpretation and of the correspondence between open field lines and

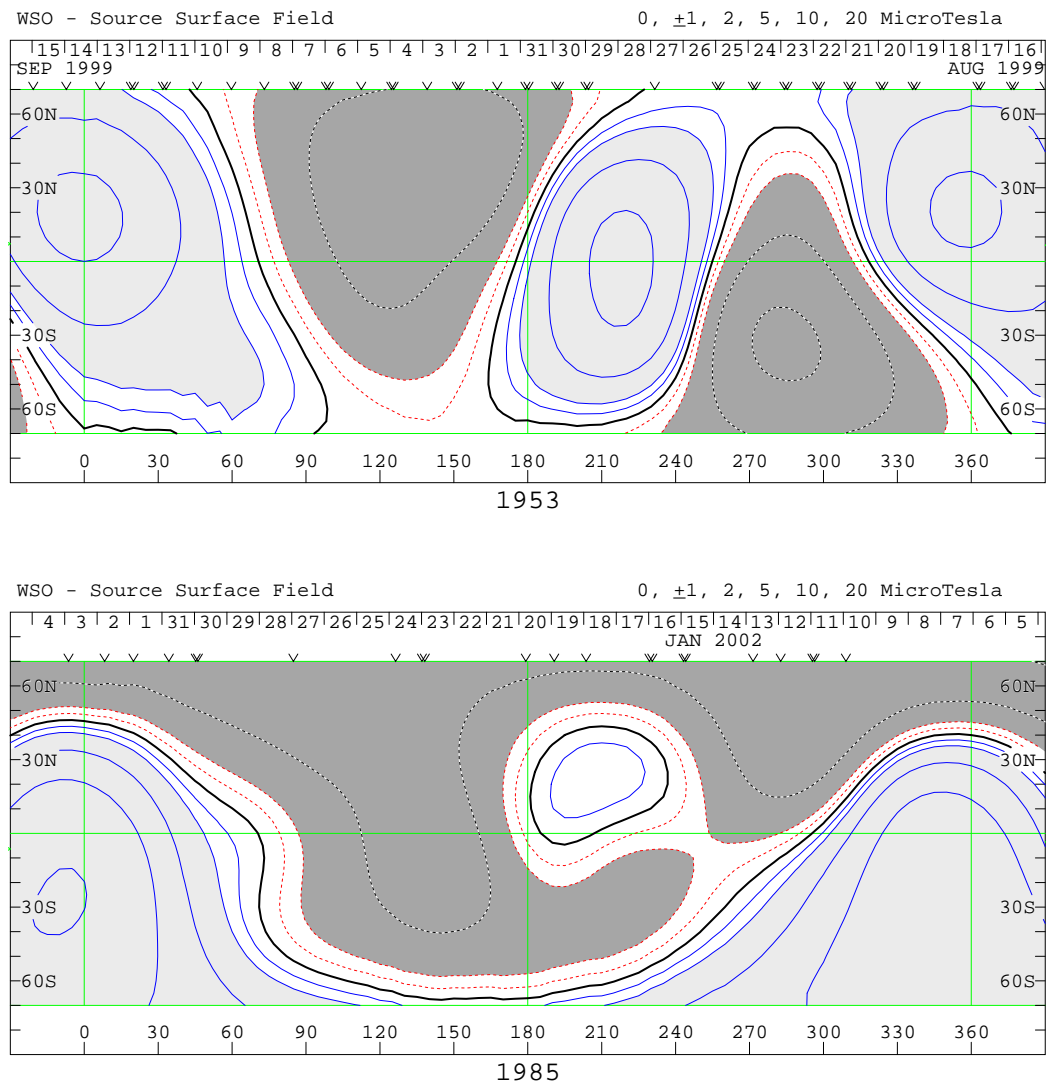


Figure 26: Examples of particularly complex sector boundaries. These are contour plots of $B_S(\theta, \phi)$ at the source surface, $R_S = 2.5R_\odot$, versus Carrington longitude (horizontally) and latitude (vertically) similar to the format of Figure 25. Dark solid curves show the sector boundary, $B_S = 0$, separating inward sectors (partially grey with red contours) from outward sectors (blue contours). The top panel is from September 1999, as the Sun's dipole is reversing and the quadrupole moment is dominant. There are four sector boundary crossings along the solar equator. The bottom panel is from January 2002, when the Northern hemisphere is mostly inward but includes a patch of outward flux enclosed by a second sector boundary. (Courtesy of J.T. Hoeksema and Wilcox Solar Observatory).

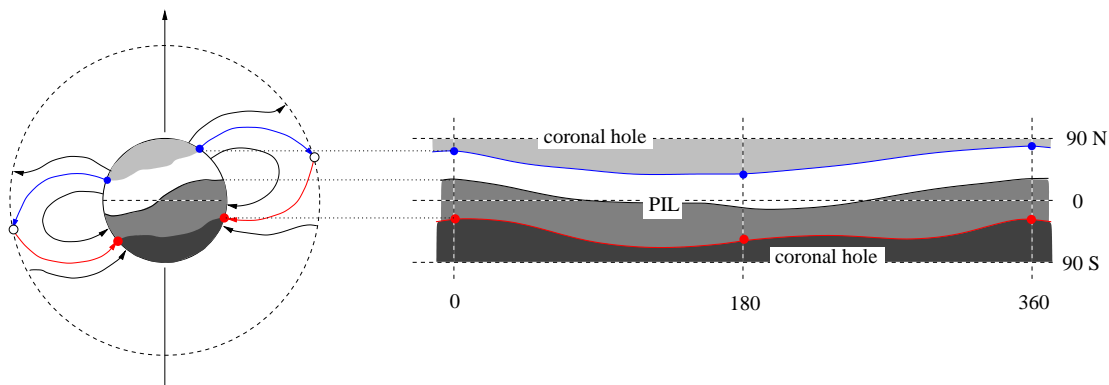


Figure 27: A schematic depiction of the coronal hole boundaries defined by the source surface model. The left is the same meridional view as in Figure 25. The right part now shows the solar surface ($r = R_{\odot}$) plotted as sine of latitude versus longitude. The blue and red curves are the footprints of the upward and downward separatrices, respectively; the black curve is the PIL. The shaded regions are (from top to bottom) the outward coronal hole (light grey), positive closed flux (white), negative closed flux (grey) and inward coronal hole (dark grey). The same colors on the left part indicate how these regions might appear on the disk.

coronal holes. Coronal holes are defined observationally by their lower X-ray or EUV emission or by a lack of chromospheric network in He II emission at 304 \AA or $10,830 \text{ \AA}$. Levine (1982) found very good agreement between open/closed boundaries (separatrices) in a PSS model and observed coronal hole boundaries, especially in the period near solar maximum.

The PSS model has been used to study the evolution of the large-scale corona including its coronal holes (Sheeley Jr *et al.*, 1987; Wang and Sheeley Jr, 1993; Wang *et al.*, 1996; Luhmann *et al.*, 1998). Evolution of the photospheric field leads to changes in the overlying coronal field extending all the way to the source surface. The open/closed boundaries extend from the source surface, so the motion of their photospheric footprint need not coincide with photospheric motions. This was found to give a compelling explanation for the fact that coronal holes were observed to rotate rigidly in spite of the photosphere's differential rotation (Levine, 1982; Sheeley Jr *et al.*, 1987). The implication of this model is that field lines anchored to the photosphere undergo reconnection in order to open or close as the separatrix sweeps over them. While the need for such reconnection is predicted by the PSS model, its dynamics cannot be studied in a quasi-static model (Wang and Sheeley Jr, 2004). There has been observational confirmation of reconnection occurring at coronal hole boundaries (Madjarska *et al.*, 2004). Luhmann *et al.* (1998) propose that CMEs are a more dramatic manifestation of the need to open magnetic fields.

A still more global consequence of this application is its prediction of how the net open flux Φ_{open} responds to the photospheric field. The open flux in the PSS model can be calculated by integrating $|B_S|$ over the entire source surface. The field at the source surface will evolve over the solar cycle, principally in response to the lowest moments of the photospheric flux. As a consequence Φ_{open} tends to reach its maximum when the dipole moment is largest some time near solar minimum (Wang *et al.*, 2000). This is in close agreement with observations (King, 1979), which must infer the total flux from a few point measurements as discussed above. Once again the quasi-static model cannot be used to determine *how* the open flux is changed, only to predict that it will change. One possibility for increasing the open flux, discussed further below, is that coronal mass ejections leaving the corona drag open previously closed field lines (Gosling, 1975). The subsequent reduction in open flux after solar minimum could occur only through the reconnection

of open field lines to produce more closed flux.

8.3 Magnetic clouds and coronal mass ejections

An important departure from the steady or quasi-static picture presented above occurs as coronal mass ejections (CMEs) drag closed magnetic loops with them into the solar wind. *In situ* observations show occasional features called *magnetic clouds* (MCs, Burlaga *et al.*, 1981) which appear to be the interplanetary manifestation of CMEs. Magnetic clouds are regions $\simeq 3\text{--}6 \times 10^7$ km in diameter (at 1 AU) in which the density and temperature are significantly lower, and magnetic field strength is significantly greater, than in the ambient solar wind. These properties suggest that the MC is a distinct magnetically dominated structure ($\beta \leq 0.1$, Bothmer and Schwenn, 1998), which has expanded on its journey from the Sun. The arrival at 1 AU of a MC can often be associated with a previous prominence disappearance or CME at the solar surface (Bothmer and Schwenn, 1994). In a few cases, the trailing portion of a MC has been observed to contain a density enhancement whose properties could be associated with filament material.

Magnetic clouds are often marked by the presence of high-energy electrons flowing in both directions along the magnetic field. Such instances of *bidirectional heat flux* indicate that the magnetic field lines remain anchored at both ends (Gosling *et al.*, 1987; Larson *et al.*, 1997). The MC is therefore believed to be a closed magnetic flux rope entrained in the solar wind. Since the wind is supersonic (and super-Alfvénic) at 1 AU, magnetic tension will not be able to retract the flux and it will ultimately be dragged ever outward. The continual occurrence of CMEs will thereby tend to increase the Sun's open magnetic flux (Gosling, 1975). Observational evidence indicates, however, that the net open flux does not monotonically increase, but rather varies up and down by a small amount in approximate phase with the photosphere's magnetic cycle (King, 1979; Wang *et al.*, 2000). This indicates either that CMEs do not actually open any flux, or that the opening is opposed by closing down previously open field lines, perhaps at different places and times.

The topology of solar wind field lines is inferred from the direction in which the high-energy (halo) electron population is conducting heat. Uni-directional heat flux indicates connection at one end (open) and bi-directional heat flux indicates connection at both ends (closed). The natural signature of a field line open at both ends (a U-loop) would be an absence of heat flux electrons, known as a *heat flux drop-out*. McComas *et al.* (1989) found 25 instances of heat flux dropout in ISEE-3 plasma data covering the last 4.5 months of 1978. These events were often found near sector boundaries, making it even more likely that they signified the creation of a U-shaped magnetic loop through reconnection. Lin and Kahler (1992) re-investigated these events using data from electrons of still higher energy (2–8.5 keV) which they took to be more reliable indicators of connectivity. This data revealed that at least 8 of the heat flux dropouts identified by McComas *et al.* (1989) were in fact connected to the solar surface, and only 2 remained unambiguously U-shaped. They attributed the discrepancy to the presence of enhanced scattering which made the field lines appear open, at least to electrons of low enough energies.

Based on the observed variation in radial field strength at 1 AU (King, 1979) it is believed that the total open flux does vary over the solar cycle. This requires the introduction of new open field lines during the rising phase, and their subsequent destruction during the declining phase. There is clear evidence that CMEs carry closed field lines into interplanetary space, thereby increasing the open flux. It is not yet clear, however, where, when or how open field lines are closed down in the declining phase.

9 Conclusion

The foregoing has reviewed some of the topological methods developed to study solar magnetic fields. It sought to organize the concepts, review their development and show how they have been applied. In the interest of a manageable scope, it focused on topological methods with some application to magnetic fields of the solar corona. It did not, however, touch on the extensive literature concerning *magnetic helicity*, a fruitful topological technique on its own. A monograph devoted to this topic edited by Brown *et al.* (1999) provides an excellent resource for this purpose. Finally, the many consequences that magnetic topology has on the dynamical evolution of the coronal field were neglected all together. It is hoped, however, that reviewing the topology alone has provided a valuable first step toward this more important subject.

10 Acknowledgements

The author wishes to thank Gunnar Hornig, Slava Titov, Colin Beveridge, Eric Priest and an anonymous referee for comments on the manuscript. This material is based upon work supported by the National Science Foundation under grant No. ATM-0416340.

References

- Albright, B.J., 1999, “The density and clustering of magnetic nulls in stochastic magnetic fields”, *Phys. Plasmas*, **6**, 4222–4228. 7, 7
- Alfvén, H., 1943, “On the existence of electromagnetic-hydrodynamic waves”, *Ark. Mat. Astron. Fys.*, **29**, 1–7. 5
- Altschuler, M.D., Newkirk Jr, G., 1969, “Magnetic fields and the structure of the solar corona. I: methods of calculating coronal fields”, *Solar Phys.*, **9**, 131–149. Related online version (cited on 01 November 2005):
http://adsabs.harvard.edu/cgi-bin/bib_query?1969SoPh...9..131A. 3.1, 8.2, 19
- Aly, J.J., Amari, T., 1989, “Current sheets in two-dimensional potential magnetic fields. I. General properties”, *Astron. Astrophys.*, **221**, 287–294. Related online version (cited on 01 November 2005):
http://adsabs.harvard.edu/cgi-bin/bib_query?1989A&A...221..287A. 7
- Antiochos, S.K., 1987, “The topology of force-free magnetic fields and its implications for coronal activity”, *Astrophys. J.*, **312**, 886–894. Related online version (cited on 24 November 2005):
http://adsabs.harvard.edu/cgi-bin/bib_query?1987ApJ...312..886A. 3.3
- Antiochos, S.K., 1998, “The Magnetic Topology of Solar Eruptions”, *Astrophys. J. Lett.*, **502**, L181–L184. Related online version (cited on 01 November 2005):
<http://arXiv.org/abs/astro-ph/9806030>. 4.2
- Arnold, V.I., 1973, *Ordinary Differential Equations*, MIT Press, Cambridge, U.S.A. 1, 2.4
- Arnold, V.I., 1974, “Asymptotic Hopf bifurcation and its applications”, in *Trans. of All-Union School on Differential Equations, Yerevan, 1974*, pp. 229–256, Armenian SSR Academy of Science, Yerevan, Armenia. In Russian; English translation in *Selecta Math. Sov.* 5 (1986) 4, 327–346. 3.3
- Aulanier, G., DeLuca, E.E., Antiochos, S.K., McMullen, R.A., Golub, L., 2000, “The Topology and Evolution of the Bastille Day Flare”, *Astrophys. J.*, **540**, 1126–1142. 7
- Axford, W.I., 1984, “Magnetic field reconnection”, in *Magnetic Reconnection in Space and Laboratory Plasmas*, (Ed.) Hones Jr, E.W., Papers presented at a Chapman Conference on Magnetic Reconnection, held at Los Alamos National Laboratory, October 3–7, 1983, vol. 30 of Geophysical Monograph, pp. 1–8, American Geophysical Union, Washington, U.S.A. 5
- Bagalá, L.G., Mandrini, C.H., Rovira, M.G., Démoulin, P., Hénoux, C.H., 1995, “A topological approach to understand a multiple-loop solar flare”, *Solar Phys.*, **161**, 103–121. Related online version (cited on 24 November 2005):
http://adsabs.harvard.edu/cgi-bin/bib_query?1995SoPh...161..103B. 1, 6.2
- Bastian, T.S., Benz, A.O., Gary, D.E., 1998, “Radio Emission from Solar Flares”, *Annu. Rev. Astron. Astrophys.*, **36**, 131–188. 2.2
- Baum, P.J., Bratenahl, A., 1980, “Flux linkages of bipolar sunspot groups: a computer study”, *Solar Phys.*, **67**, 245–258. Related online version (cited on 24 November 2005):
http://adsabs.harvard.edu/cgi-bin/bib_query?1980SoPh...67..245B. 1, 14, 4.2
- Beveridge, C., Longcope, D.W., 2005, “On Three-Dimensional Magnetic Skeleton Elements due to Discrete Flux Sources”, *Solar Phys.*, **227**, 193–206. 15, 16

- Beveridge, C., Priest, E.R., Brown, D.S., 2002, “Magnetic topologies due to two bipolar regions”, *Solar Phys.*, **209**, 333–347. 4.1, 4.2
- Beveridge, C., Longcope, D.W., Priest, E.R., 2003, “A theoretical model for elemental coronal loops”, *Solar Phys.*, **216**, 27–40. 4.1, 4.4
- Billinghurst, M.N., Craig, I.J.D., Sneyd, A.D., 1993, “Current-sheet formation in two-dimensional coronal fields”, *Astron. Astrophys.*, **279**, 589–598. Related online version (cited on 24 November 2005):
http://adsabs.harvard.edu/cgi-bin/bib_query?1993A&A...279..589B. 5.1
- Bothmer, V., Schwenn, R., 1994, “Eruptive prominences as sources of magnetic clouds in the solar wind”, *Space Sci. Rev.*, **70**, 215. Related online version (cited on 24 November 2005):
http://adsabs.harvard.edu/cgi-bin/bib_query?1994SSRv...70..215B. 8.3
- Bothmer, V., Schwenn, R., 1998, “The structure and origin of magnetic clouds in the solar wind”, *Ann. Geophys.*, **16**, 1–24. Related online version (cited on 24 November 2005):
http://adsabs.harvard.edu/cgi-bin/bib_query?1998AnGeo...16...1B. 8.3
- Braginskii, S.I., 1965, “Transport processes in a plasma”, in *Reviews of Plasma Physics*, (Ed.) Leontovich, M.A., vol. 1 of Reviews of Plasma Physics, pp. 205–311, Consultants Bureau, New York U.S.A. 2.2
- Brown, D.S., Priest, E.R., 1999a, “Topological bifurcations in three-dimensional magnetic fields”, *Proc. R. Soc. London, Ser. A*, **455**, 3931–3951. 4.2, 4.2
- Brown, D.S., Priest, E.R., 1999b, “The Topological Behaviour of Stable Magnetic Separators”, *Solar Phys.*, **190**, 25–33. 14
- Brown, D.S., Priest, E.R., 2001, “The topological behaviour of 3D null points in the Sun’s corona”, *Astron. Astrophys.*, **367**, 339–346. 4.2, 7, 7, 22
- Brown, M.R., Canfield, R.C., Pevtsov, A.A. (Eds.), 1999, *Magnetic Helicity in Space and Laboratory Plasmas*, no. 111 in Geophysical Monograph, American Geophysical Union, Washington, U.S.A. 9
- Bruno, R., Burlaga, L.F., Hundhausen, A.J., 1984, “K-coronameter observations and potential field model comparison in 1976 and 1977”, *J. Geophys. Res.*, **89**, 5381–5385. 20
- Bungey, T.N., Titov, V.S., Priest, E.R., 1996, “Basic topological elements of coronal magnetic fields”, *Astron. Astrophys.*, **308**, 233–247. 5.1, 5.1, 7
- Burlaga, L., Sittler, E., Mariani, F., Schwenn, R., 1981, “Magnetic loop behind an interplanetary shock - Voyager, Helios, and IMP 8 observations”, *J. Geophys. Res.*, **86**, 6673–6684. 18, 8.3
- Burton, M.E., Crooker, N.U., Siscoe, G.L., Smith, E.J., 1994, “A test of source-surface model predictions of heliospheric current sheet inclination”, *J. Geophys. Res.*, **99**, A1–A9. 20
- Canfield, R.C., Hudson, H.S., McKenzie, D.E., 1999, “Sigmoidal morphology and eruptive solar activity”, *Geophys. Res. Lett.*, **26**, 627. 5.1
- Chiu, Y.T., Hilton, H.H., 1977, “Exact Green’s function method of solar force-free magnetic-field computations with constant α . I. Theory and basic test cases”, *Astrophys. J.*, **212**, 873–885. Related online version (cited on 24 November 2005):
http://adsabs.harvard.edu/cgi-bin/bib_query?1977ApJ...212..873C. 3.2

- Close, R.M., Parnell, C.E., Mackay, D.H., Priest, E.R., 2003, “Statistical Flux Tube Properties of 3D Magnetic Carpet Fields”, *Solar Phys.*, **212**, 251–275. 4.4
- Cowley, S.C., Longcope, D.W., Sudan, R.N., 1997, “Current sheets in MHD turbulence”, *Phys. Rep.*, **283**, 227–251. 2.3, 2.3
- Craig, I.J.D., Sneyd, A.D., 1990, “Nonlinear development of the kink instability in coronal flux tubes”, *Astrophys. J.*, **357**, 653–661. Related online version (cited on 24 November 2005): http://adsabs.harvard.edu/cgi-bin/bib_query?1990ApJ...357..653C. 3.3
- Démoulin, P., Priest, E.R., 1992, “The properties of sources and sinks of a linear force-free field”, *Astron. Astrophys.*, **139**, 535–541. Related online version (cited on 24 November 2005): http://adsabs.harvard.edu/cgi-bin/bib_query?1992A&A...258..535D. 6.1
- Démoulin, P., Henoux, J.C., Mandrini, C.H., 1992, “Development of a topological model for solar flares”, *Solar Phys.*, **139**, 105–123. 4, 6.1
- Démoulin, P., van Driel-Gesztelyi, L., Schmieder, B., Hénoux, J.C., Csepura, G., Hagyard, M.J., 1993, “Evidence for magnetic reconnection in solar flares”, *Astron. Astrophys.*, **271**, 292–307. 1, 6.2
- Démoulin, P., Mandrini, C.H., Rovira, M.G., Hénoux, J.C., Machado, M.E., 1994, “Interpretation of multiwavelength observations of November 5, 1980 solar flares by the magnetic topology of AR 2766”, *Solar Phys.*, **150**, 221–243. 1, 6.1, 18, 19, 6.1, 6.2, 7
- Démoulin, P., Henoux, J.C., Priest, E.R., Mandrini, C.H., 1996, “Quasi-separatrix layers in solar flares. I. Method”, *Astron. Astrophys.*, **308**, 643–655. 5.2, 5.2
- Démoulin, P., Bagalá, L.G., Mandrini, C.H., Henoux, J.C., Rovira, M.G., 1997, “Quasi-separatrix layers in solar flares. II. Observed magnetic configurations.”, *Astron. Astrophys.*, **325**, 305–317. 17
- Dungey, J., 1953, “The motion of magnetic fields”, *Mon. Not. R. Astron. Soc.*, **113**, 679–682. 4, 5
- Fan, Y., Gibson, S.E., 2003, “The Emergence of a Twisted Magnetic Flux Tube into a Pre-existing Coronal Arcade”, *Astrophys. J. Lett.*, **589**, L105–L108. 5.1
- Feldman, W.C., Asbridge, J.R., Bame, S.J., Montgomery, M.D., Gary, S.P., 1975, “Solar wind electrons”, *J. Geophys. Res.*, **80**, 4181–4196. 2.2, 8.1
- Filippov, B., 1999, “Observation of a 3d Magnetic Null Point in the Solar Corona”, *Solar Phys.*, **185**, 297–309. 7
- Filippov, B.P., 1995, “The manifestation of topological singularities of solar magnetic fields in the chromospheric structure.”, *Astron. Astrophys.*, **303**, 242–248. 4.1
- Fisk, L.A., 1996, “Motion of the footpoints of heliospheric magnetic field lines at the Sun: Implications for recurrent energetic particle events at high heliographic latitudes”, *J. Geophys. Res.*, **101**, 15 547–15 554. 18
- Fletcher, L., Metcalf, T.R., Alexander, D., Brown, D.S., Ryder, L.A., 2001, “Evidence for the Flare Trigger Site and Three-Dimensional Reconnection in Multiwavelength Observations of a Solar Flare”, *Astrophys. J.*, **554**, 451–463. 7

- Gabriel, A.H., 1976, “A magnetic model of the solar transition region”, *Philos. Trans. R. Soc. London, Ser. A*, **281**, 339–352. 12
- Gary, G.A., 1989, “Linear force-free magnetic fields for solar extrapolation and interpretation”, *Astrophys. J. Suppl. Ser.*, **69**, 323–348. Related online version (cited on 24 November 2005): http://adsabs.harvard.edu/cgi-bin/bib_query?1989ApJS...69..323G. 3.2
- Gorbachev, V.S., Somov, B.V., 1988, “Photospheric vortex flows as a cause for two-ribbon flares: a topological model”, *Solar Phys.*, **117**, 77–88. Related online version (cited on 24 November 2005): http://adsabs.harvard.edu/cgi-bin/bib_query?1988SoPh..117...77G. 1, 4, 6.1, 6.2
- Gorbachev, V.S., Somov, B.V., 1989, “Solar flares of November 5, 1980, as the result of magnetic reconnection at a separator”, *Sov. Astron.*, **33**, 57–61. 1, 6.1, 18, 6.1, 20, 6.2
- Gorbachev, V.S., Kelner, S.R., Somov, B.V., Shvarts, A.S., 1988, “A new topological approach to the question of the trigger for solar flares”, *Sov. Astron.*, **32**, 308–314. 1, 14, 4.2, 4.2, 10
- Gosling, J.T., 1975, “Large-scale inhomogeneities in the solar wind of solar origin”, *Rev. Geophys. Space Phys.*, **13**, 1053–1058. 20, 8.3
- Gosling, J.T., Baker, D.N., Bame, S.J., Feldman, W.C., Zwickl, R.D., Smith, E.J., 1987, “Bidirectional solar wind electron heat flux events”, *J. Geophys. Res.*, **92**, 8519–8535. 2.2, 8.3
- Green, R.M., 1965, “Modes of annihilation and reconnection in magnetic fields”, in *Stellar and Solar Magnetic Fields*, (Ed.) Lust, R., IAU Symposium 22, pp. 398–404, North-Holland; Interscience, Amsterdam, Netherlands; New York, U.S.A. Related online version (cited on 24 November 2005): http://adsabs.harvard.edu/cgi-bin/bib_query?1965IAUS...22..398G. 7
- Greene, J.M., 1988, “Geometrical properties of three-dimensional reconnecting magnetic fields with nulls”, *J. Geophys. Res.*, **93**, 8583–8590. 1, 7, 8, 14
- Greene, J.M., 1992, “Locating three-dimensional roots by a bisection method”, *J. Comput. Phys.*, **98**, 194–198. 3.1
- Greene, J.M., 1993, “Reconnection of vorticity lines and magnetic lines”, *Phys. Fluids B*, **5**, 2355–2362. 5, 7, 7
- Guckenheimer, J., Holmes, P., 1983, *Nonlinear Oscillations, Dynamical Systems, and Bifurcations of Vector Fields*, vol. 42 of Applied Mathematical Sciences, Springer, New York, U.S.A. 6, 4.2, 7
- Handy, B.N., Acton, L.W., Kankelborg, C.C., Wolfson, C.J., Akin, D.J., Bruner, M.E., Carvalho, R., Catura, R.C., Chevalier, R., Duncan, D.W., Edwards, C.G., Feinstein, C.N., Freeland, S.L., Friedlaender, F.M., Hoffmann, C.H., Hurlburt, N.E., Jurcevich, B.K., Katz, N.L., Kelly, G.A., Lemen, J.R., Levay, M., Lindgren, R.W., Mathur, D.P., Meyer, S.B., Morrison, S.J., Morrison, M.D., Nightingale, R.W., Pope, T.P., Rehse, R.A., Schrijver, C.J., Shine, R.A., Shing, L., Strong, K.T., Tarbell, T.D., Title, A.M., Torgerson, D.D., Golub, L., Bookbinder, J.A., Caldwell, D., Cheimets, P.N., Davis, W.N., DeLuca, E.E., McMullen, R.A., Warren, H.P., Amato, D., Fisher, R., Maldonado, H., Parkinson, C., 1999, “The transition region and coronal explorer”, *Solar Phys.*, **187**, 229–260. 2.2, 4.4
- Hesse, M., Schindler, K., 1988, “A theoretical foundation of general magnetic reconnection”, *J. Geophys. Res.*, **93**, 5559–5567. 5, 2.2, 8

- Hoeksema, J.T., Wilcox, J.M., Scherrer, P.H., 1982, "Structure of the heliospheric current sheet in the early portion of sunspot cycle 21", *J. Geophys. Res.*, **87**, 10 331–10 338. 20, 20
- Hoeksema, J.T., Wilcox, J.M., Scherrer, P.H., 1983, "The structure of the heliospheric current sheet - 1978–1982", *J. Geophys. Res.*, **88**, 9910–9918. 20
- Hornig, G., Schindler, K., 1996, "Magnetic topology and the problem of its invariant definition", *Phys. Plasmas*, **3**, 781–791. 5, 2.2, 7, 4.2
- Hu, Y.Q., Low, B.C., 1982, "The energy of electric current sheets. I. Models with moving magnetic dipoles", *Solar Phys.*, **81**, 107–119. 7
- Hudson, T.S., Wheatland, M.S., 1999, "Topological Differences Between Force-Free Field Models", *Solar Phys.*, **186**, 301–310. 14
- Inverarity, G.W., Priest, E.R., 1999, "Magnetic Null Points due to Multiple Sources of Solar Photospheric Flux", *Solar Phys.*, **186**, 99–121. 4.1, 7
- Inverarity, G.W., Titov, V.S., 1997, "Formation of current layers in three-dimensional, inhomogeneous coronal magnetic fields by photospheric motions", *J. Geophys. Res.*, **102**, 22,285–22,293. 5.1
- Jackson, J.D., 1975, *Classical Electrodynamics*, Wiley, New York, U.S.A., 2nd edn. 3.2
- Jokipii, J.R., 1966, "Cosmic-Ray Propagation. I. Charged Particles in a Random Magnetic Field", *Astrophys. J.*, **146**, 480–487. Related online version (cited on 01 November 2005): http://adsabs.harvard.edu/cgi-bin/bib_query?1966ApJ...146..480J. 3.1
- Karpen, J.T., Antiochos, S.K., DeVore, C.R., 1990, "On the formation of current sheets in the solar corona", *Astrophys. J. Lett.*, **356**, L67–L70. Related online version: http://adsabs.harvard.edu/cgi-bin/bib_query?1990ApJ...356L..67K. 5.1
- King, J.H., 1979, "Solar cycle variations in the IMF intensity", *J. Geophys. Res.*, **84**, 5938–5940. 20, 8.3
- Kopp, R.A., Kuperus, M., 1968, "Magnetic fields and the temperature structure of the chromosphere-corona interface", *Solar Phys.*, **4**, 212–223. 12
- Lamb, H., 1932, *Hydrodynamics*, Cambridge University Press, Cambridge, U.K., 6th edn. Dover reprint. 3
- Larson, D.E., Lin, R.P., McTiernan, J.M., McFadden, J.P., Ergun, R.E., McCarthy, M., Rème, H., Sanderson, T.R., Kaiser, M., Lepping, R.P., Mazur, J., 1997, "Tracing the topology of the October 18–20, 1995, magnetic cloud with $\sim 0.1 - 10^2$ keV electrons", *Geophys. Res. Lett.*, **24**, 1911–1914. 8.3
- Lau, Y.-T., 1993, "Magnetic nulls and topology in a class of solar flare models", *Solar Phys.*, **148**, 301–324. 5.1, 5.1
- Lau, Y.-T., Finn, J.M., 1990, "Three-dimensional kinematic reconnection in the presence of field nulls and closed field lines", *Astrophys. J.*, **350**, 672–691. 1, 7, 7, 8, 14
- Levine, R.H., 1982, "Open magnetic fields and the solar cycle. I - Photospheric sources of open magnetic flux", *Solar Phys.*, **79**, 203–230. 20
- Lichtenberg, A.J., Lieberman, M.A., 1983, *Regular and Stochastic Motion*, vol. 38 of Applied Mathematical Sciences, Springer, New York, U.S.A. 3.1

- Lin, H., Rimmele, T., 1999, “The granular magnetic fields of the quiet sun”, *Astrophys. J.*, **514**, 448–455. 12
- Lin, R.P., Kahler, S.W., 1992, “Interplanetary magnetic field connection to the sun during electron heat flux dropouts in the solar wind”, *J. Geophys. Res.*, **97**, 8203–8209. 8.3
- Litwin, C., Rosner, R., 1993, “On the structure of solar and stellar coronae: loops and loop heat transport”, *Astrophys. J.*, **412**, 375–385. Related online version (cited on 24 November 2005): http://adsabs.harvard.edu/cgi-bin/bib_query?1993ApJ...412..375L. 2.2
- Livingston, W.C., Harvey, J., 1971, “The Kitt Peak Magnetograph. IV: 40-Channel Probe and the Detection of Weak Photospheric Fields”, in *Solar Magnetic Fields*, (Ed.) Howard, R., Proceedings of IAU Symposium No. 43, held at the College de France, Paris, France, August 31 to September 4, 1970, pp. 51–61, Reidel, Dordrecht, Netherlands. Related online version (cited on 23 November 2005): http://adsabs.harvard.edu/cgi-bin/bib_query?1971IAUS...43...51L. 12
- Longcope, D.W., 1996, “Topology and current ribbons: A model for current, reconnection and flaring in a complex, evolving corona”, *Solar Phys.*, **169**, 91–121. Related online version (cited on 24 November 2005): http://adsabs.harvard.edu/cgi-bin/bib_query?1996SoPh..169...91L. 1, 7, 14, 14
- Longcope, D.W., 2001, “Separator current sheets: Generic features in minimum-energy magnetic fields subject to flux constraints”, *Phys. Plasmas*, **8**, 5277–5290. 4.2, 4.3, 15
- Longcope, D.W., Cowley, S.C., 1996, “Current sheet formation along three-dimensional magnetic separators”, *Phys. Plasmas*, **3**, 2885–2897. 7, 7
- Longcope, D.W., Klapper, I., 2002, “A general theory of connectivity and current sheets in coronal magnetic fields”, *Astrophys. J.*, **579**, 468–481. 14, 14, 4.1, 4.1, 4.2, 15, 16, 4.4
- Longcope, D.W., Magara, T., 2004, “A comparison of the Minimum Current Corona to a magnetohydrodynamic simulation of quasi-static coronal evolution”, *Astrophys. J.*, **608**, 1106–1123. 14
- Longcope, D.W., Silva, A.V.R., 1998, “A current ribbon model for energy storage and release with application to the flare 1992 Jan. 7”, *Solar Phys.*, **179**, 349–377. 4.4
- Longcope, D.W., Strauss, H.R., 1994, “The form of ideal current layers in line-tied magnetic fields”, *Astrophys. J.*, **437**, 851–859. 3.3, 5.2
- Longcope, D.W., Brown, D.S., Priest, E.R., 2003, “On the distribution of magnetic null points above the solar photosphere”, *Phys. Plasmas*, **10**, 3321–3334. 7
- Low, B.C., 1987, “Electric current sheet formation in a magnetic field induced by continuous magnetic footpoint displacements”, *Astrophys. J.*, **323**, 358–367. 5.1
- Low, B.C., Wolfson, R., 1988, “Spontaneous formation of electric current sheets and the origin of solar flares”, *Astrophys. J.*, **324**, 574–581. 5.1
- Luhmann, J.G., Gosling, J.T., Hoeksema, J.T., Zhao, X., 1998, “The relationship between large-scale solar magnetic field evolution and coronal mass ejections”, *J. Geophys. Res.*, **103**, 6585–6593. 20

- Maclean, R., Beveridge, C., Longcope, D.W., Brown, D.S., Priest, E.R., 2005, “A topological analysis of the magnetic breakout model for an eruptive solar flare”, *Proc. R. Soc. London, Ser. A*, **461**, 2099–2120. 4.2
- Madjarska, M.S., Doyle, J.G., van Driel-Gesztelyi, L., 2004, “Evidence of magnetic reconnection along coronal hole boundaries”, *Astrophys. J. Lett.*, **603**, L57–L59. 20
- Mandrini, C.H., Démoulin, P., Hénoux, J.C., Machado, M.E., 1991, “Evidence for the interaction of large scale magnetic structures in solar flares”, *Astron. Astrophys.*, **250**, 541–547. Related online version (cited on 24 November 2005):
http://adsabs.harvard.edu/cgi-bin/bib_query?1991A&A...250..541M. 1, 6.2
- Mandrini, C.H., Rovira, M.G., Démoulin, P., Hénoux, J.C., Machado, M.E., Wilkinson, L.K., 1993, “Evidence for magnetic reconnection in large-scale magnetic structures in solar flares”, *Astron. Astrophys.*, **272**, 609–620. 1, 6.2
- Mandrini, C.H., Démoulin, P., Rovira, M.G., de La Beaujardiere, J.-F., Henoux, J.C., 1995, “Constraints on flare models set by the active region magnetic topology of AR 6233”, *Astron. Astrophys.*, **303**, 927–939. Related online version (cited on 24 November 2005):
http://adsabs.harvard.edu/cgi-bin/bib_query?1995A&A...303..927M. 6.2
- McClymont, A.N., Jiao, L., Mikic, Z., 1997, “Problems and progress in computing three-dimensional coronal active region magnetic fields from boundary data”, *Solar Phys.*, **174**, 191–218. 3.2
- McComas, D.J., Gosling, J.T., Phillips, J.L., Bame, S.J., Luhmann, J.G., Smith, E.J., 1989, “Electron heat flux dropouts in the solar wind - Evidence for interplanetary magnetic field reconnection?”, *J. Geophys. Res.*, **94**, 6907–6916. 8.3
- McComas, D.J., Gosling, J.T., Hammond, C.M., Moldwin, M.B., Phillips, J.L., Forsyth, R.J., 1995, “Reconnection on Open Field Lines Ahead of Coronal Mass Ejections”, *Space Sci. Rev.*, **72**, 129–132. 2.2
- Moffatt, H.K., 1978, *Magnetic Field Generation in Electrically Conducting Fluids*, Cambridge Monographs on Mechanics and Applied Mathematics, Cambridge University Press, Cambridge, U.K.; New York, U.S.A. 5
- Moffatt, H.K., 1985, “Magnetostatic equilibria and analogous Euler flows of arbitrary complex topology. Part 1: Fundamentals”, *J. Fluid Mech.*, **159**, 359–378. 3.3
- Molodenskii, M.M., Syrovatskii, S.I., 1977, “Magnetic fields of active regions and their zero points”, *Sov. Astron.*, **21**, 734–741. Related online version (cited on 24 November 2005):
http://adsabs.harvard.edu/cgi-bin/bib_query?1977SvA...21..734M. 4.1, 4.1, 7
- Nakagawa, Y., Raadu, M.A., 1972, “On practical representation of magnetic field”, *Solar Phys.*, **25**, 127–135. 3.2
- Newcomb, W.A., 1958, “Motion of magnetic lines of force”, *Ann. Phys. (N.Y.)*, **3**, 347–385. 5, 2.5
- Parker, E.N., 1955, “The formation of sunspots from the solar toroidal field”, *Astrophys. J.*, **121**, 491–507. 3.2
- Parker, E.N., 1957, “Sweet’s mechanism for merging magnetic fields in conducting fluids”, *J. Geophys. Res.*, **62**, 509–520. 1

- Parker, E.N., 1958, “Dynamics of the Interplanetary Gas and Magnetic Fields”, *Astrophys. J.*, **128**, 664–676. Related online version (cited on 24 November 2005):
http://adsabs.harvard.edu/cgi-bin/bib_query?1958ApJ...128..664P. 8.1
- Parker, E.N., 1972, “Topological dissipation and the small-scale fields in turbulent gasses”, *Astrophys. J.*, **174**, 499–510. 3.3
- Parker, E.N., 1979, *Cosmical Magnetic Fields: Their Origin and Their Activity*, International Series of Monographs on Physics, Clarendon Press; Oxford University Press, Oxford, U.K.; New York, U.S.A. 2.2, 5
- Parker, E.N., 1987, “Magnetic reorientation and the spontaneous formation of tangential discontinuities in deformed magnetic fields”, *Astrophys. J.*, **318**, 876–887. Related online version (cited on 01 November 2005):
http://adsabs.harvard.edu/cgi-bin/bib_query?1987ApJ...318..876P. 3.3
- Parker, E.N., 1990, “Spontaneous tangential discontinuities and the optical analogy for static magnetic fields. VI. Topology of current sheets”, *Geophys. Astrophys. Fluid Dyn.*, **53**, 43–80. 3.3
- Parker, E.N., 1994, *Spontaneous Current Sheets in Magnetic Fields: With Applications to Stellar X-Rays*, vol. 1 of International Series on Astronomy and Astrophysics, Oxford University Press, New York, U.S.A. 3.3
- Parker, E.N., 2004, “Tangential discontinuities in untidy magnetic topologies”, *Phys. Plasmas*, **11**, 2328–2332. 3.3
- Parnell, C.E., Smith, J.M., Neukirch, T., Priest, E.R., 1996, “The structure of three-dimensional magnetic neutral points”, *Phys. Plasmas*, **3**, 759–770. 6
- Petrie, G.J.D., Lothian, R.M., 2003, “An investigation of the topology and structure of constant-alpha force-free fields”, *Astron. Astrophys.*, **398**, 287–295. 14
- Petschek, H.E., 1964, “Magnetic field annihilation”, in *The Physics of Solar Flares*, (Ed.) Hess, W.N., Proceedings of the AAS–NASA Symposium, vol. SP-50 of NASA Special Publication, pp. 425–439, NASA, Washington, U.S.A. 1
- Phillips, J.L., Bame, S.J., Feldman, W.C., Goldstein, B.E., Gosling, J.T., Hammond, C.M., McComas, D.J., Neugebauer, M., Scime, E.E., Suess, S.T., 1995, “Ulysses Solar Wind Plasma Observations at High Southerly Latitudes”, *Science*, **268**, 1030–1033. 8.1
- Pontin, D.I., Priest, E.R., Longcope, D.W., 2003, “A Framework for Understanding the Topology of Complex Coronal Structures”, *Solar Phys.*, **212**, 319–342. 4.2
- Priest, E.R., 1982, *Solar Magnetohydrodynamics*, vol. 21 of Geophysics and Astrophysics Monographs, D. Reidel, Dordrecht, Netherlands; Boston, U.S.A. 5, 2.3
- Priest, E.R., Démoulin, P., 1995, “Three-dimensional magnetic reconnection without null points 1. Basic theory of magnetic flipping”, *J. Geophys. Res.*, **100**, 23,443–23,463. 5.2, 5.2
- Priest, E.R., Raadu, M.A., 1975, “Preflare current sheets in the solar atmosphere”, *Solar Phys.*, **43**, 177–188. 7
- Priest, E.R., Titov, V.S., 1996, “Magnetic reconnection at three-dimensional null points”, *Philos. Trans. R. Soc. London, Ser. A*, **354**, 2951–2992. 6

- Priest, E.R., Bungey, T.N., Titov, V.S., 1997, “The 3D topology and interaction of complex magnetic flux systems”, *Geophys. Astrophys. Fluid Dyn.*, **84**, 127–163. 4.2
- Priest, E.R., Hornig, G., Pontin, D.I., 2003, “On the nature of three-dimensional magnetic reconnection”, *J. Geophys. Res.*, **108**, 6–1. 8
- Rosner, R., Tucker, W.H., Vaiana, G.S., 1978, “Dynamics of the quiescent corona”, *Astrophys. J.*, **220**, 643–655. 2.2
- Schatten, K.H., Wilcox, J.M., Ness, N.F., 1969, “A model of interplanetary and coronal magnetic fields”, *Solar Phys.*, **6**, 442–455. 3.1, 8.2, 20
- Scherrer, P.H., Bogart, R.S., Bush, R.I., Hoeksema, J.T., Kosovichev, A.G., Schou, J., Rosenberg, W., Springer, L., Tarbell, T.D., Title, A.M., Wolfson, C.J., Zayer, I. (The MDI Engineering Team), 1995, “The Solar Oscillations Investigation – Michelson Doppler Imager”, *Solar Phys.*, **162**, 129–188. Related online version (cited on 01 November 2005): http://adsabs.harvard.edu/cgi-bin/bib_query?1995SoPh..162..129S. 7, 4.4
- Schmidt, H.U., 1964, “On the observable effects of magnetic energy storage and release connected with solar flares”, in *The Physics of Solar Flares*, (Ed.) Hess, W.N., Proceedings of the AAS–NASA Symposium, vol. SP-50 of NASA Special Publication, p. 107, NASA, Washington, U.S.A. 3.2
- Schrijver, C.J., Title, A.M., 2002, “The topology of mixed-polarity potential field, and inferences for heating of the quiet solar corona”, *Solar Phys.*, **207**, 223–240. 4.4, 7
- Schrijver, C.J., Title, A.M., 2003, “The magnetic connection between the solar photosphere and the corona”, *Astrophys. J. Lett.*, **597**, L165–L168. 12
- Seehafer, N., 1986, “On the magnetic field line topology in solar active regions”, *Solar Phys.*, **105**, 223–235. 4, 14, 4.2, 5.1, 5.1, 6.1, 6.1, 7
- Sheeley Jr, N.R., Nash, A.G., Wang, Y.-M., 1987, “The origin of rigidly rotating magnetic field patterns on the sun”, *Astrophys. J.*, **319**, 481–502. 20
- Sonnerup, B.U.O., 1970, “Magnetic field re-connexion in a highly conducting incompressible fluid”, *J. Plasma Phys.*, **4**, 161–174. 1
- Stern, D.P., 1966, “The motion of magnetic field lines”, *Space Sci. Rev.*, **6**, 147–173. 4, 5
- Stern, D.P., 1973, “A study of the electric field in an open magnetospheric model”, *J. Geophys. Res.*, **78**, 7292–7305. 1
- Sturrock, P.A., 1994, *Plasma Physics: An Introduction to the Theory of Astrophysical, Geophysical & Laboratory Plasmas*, Cambridge University Press, Cambridge, U.K.; New York, U.S.A. 5
- Sturrock, P.A., Woodbury, E.T., 1967, “Force-free magnetic field and solar filaments”, in *Plasma Astrophysics*, (Ed.) Sturrock, P.A., Proceedings of the International School of Physics “Enrico Fermi”, Course 39, held July 11–30, 1966, p. 155, Academic Press, New York, U.S.A. 4
- Sweet, P.A., 1950, “The effect of turbulence on a magnetic field”, *Mon. Not. R. Astron. Soc.*, **110**, 69–83. Related online version (cited on 01 November 2005): http://adsabs.harvard.edu/cgi-bin/bib_query?1950MNRAS.110...69S. 4, 5
- Sweet, P.A., 1958a, “The neutral point theory of solar flares”, in *Electromagnetic Phenomena in Cosmical Physics*, (Ed.) Lehnert, B., IAU Symposium 6, pp. 123–134, Cambridge University Press, Cambridge, U.K. 1

- Sweet, P.A., 1958b, “The production of high energy particles in solar flares”, *Nuovo Cimento*, **8**, 188–196. 1, 14, 14
- Syrovatskii, S.I., 1971, “Formation of current sheets in a plasma with frozen-in strong magnetic field”, *Sov. Phys. JETP*, **33**, 933–940. 7
- Tandberg-Hanssen, E., 1995, *The Nature of Solar Prominences*, vol. 199 of Astrophysics and Space Science Library, Kluwer, Dordrecht, Netherlands; Boston, U.S.A. 5.1
- Titov, V.S., 1992, “On the method of calculating two-dimensional potential magnetic fields with current sheets”, *Solar Phys.*, **139**, 401–404. 7
- Titov, V.S., Démoulin, P., 1999, “Basic topology of twisted magnetic configurations in solar flares”, *Astron. Astrophys.*, **351**, 707–720. Related online version (cited on 24 November 2005): http://adsabs.harvard.edu/cgi-bin/bib_query?1999A&A...351..707T. 5.1, 15, 5.1, 16
- Titov, V.S., Priest, E.R., Démoulin, P., 1993, “Conditions for the appearance of “bald patches” at the solar surface”, *Astron. Astrophys.*, **276**, 564–570. Related online version (cited on 24 November 2005): http://adsabs.harvard.edu/cgi-bin/bib_query?1993A&A...276..564T. 5.1, 5.1
- Titov, V.S., Hornig, G., Démoulin, P., 2002, “Theory of magnetic connectivity in the solar corona”, *J. Geophys. Res.*, **107**, 3–1. 5.2, 5.2, 17, 17, 6.3
- Titov, V.S., Galsgaard, K., Neukirch, T., 2003, “Magnetic Pinching of Hyperbolic Flux Tubes. I. Basic Estimations”, *Astrophys. J.*, **582**, 1172–1189. Related online version (cited on 24 November 2005): http://adsabs.harvard.edu/bin/nph-bib_query?2003ApJ...582.1172T. 17, 6.3
- Tur, T.J., Priest, E.R., 1976, “The formation of current sheets during the emergence of new magnetic flux from below the photosphere”, *Solar Phys.*, **48**, 89–100. Related online version (cited on 24 November 2005): http://adsabs.harvard.edu/cgi-bin/bib_query?1976SoPh...48...89T. 7
- van Ballegooijen, A.A., 1985, “Electric currents in the solar corona and the existence of magneto-static equilibria”, *Astrophys. J.*, **298**, 421–430. 5.2
- van Ballegooijen, A.A., 1988, “Force free fields and coronal heating”, *Geophys. Astrophys. Fluid Dyn.*, **41**, 181–211. 3.3
- van Ballegooijen, A.A., 1990, “Structure and equilibrium of coronal magnetic fields”, in *Basic Plasma Processes on the Sun*, (Eds.) Priest, E.R., Krishnan, V., Proceedings of the 142nd Symposium of the International Astronomical Union, held in Bangalore, India, December 1–5, 1989, pp. 303–308, Kluwer, Dordrecht, Netherlands; Boston, U.S.A. 3.3
- van Driel-Gesztelyi, L., Hofmann, A., Démoulin, P., Schmieder, B., Csepura, G., 1994, “Relationship between electric currents, photospheric motions, chromospheric activity, and magnetic field topology”, *Solar Phys.*, **149**, 309–330. Related online version (cited on 24 November 2005): http://adsabs.harvard.edu/cgi-bin/bib_query?1994SoPh..149..309V. 6.2
- Vasyliunas, V.M., 1975, “Theoretical models of magnetic field line merging. I”, *Rev. Geophys. Space Phys.*, **13**, 303–336. 1, 5, 8
- Wang, Y.-M., Sheeley Jr, N.R., 1993, “Understanding the rotation of coronal holes”, *Astrophys. J.*, **414**, 916–927. Related online version (cited on 24 November 2005): http://adsabs.harvard.edu/cgi-bin/bib_query?1993ApJ...414..916W. 20

- Wang, Y.-M., Sheeley Jr, N.R., 2004, “Footpoint Switching and the Evolution of Coronal Holes”, *Astrophys. J.*, **612**, 1196–1205. 20
- Wang, Y.-M., Hawley, S.H., Sheeley Jr, N.R., 1996, “The magnetic nature of coronal holes”, *Science*, **271**, 464–469. 20
- Wang, Y.-M., Lean, J.L., Sheeley Jr, N.R., 2000, “The long-term variation of the Sun’s open magnetic flux”, *Geophys. Res. Lett.*, **27**, 505–509. 20, 8.3
- Welsch, B. T., Longcope, D.W., 1999, “Statistical properties of magnetic separators in model active regions”, *Astrophys. J.*, **522**, 1117–1132. 4.1
- Winebarger, A.R., Warren, H.P., 2005, “Cooling active region loops observed with SXT and TRACE”, *Astrophys. J.*, **626**, 543–550. 2.2
- Woltjer, L., 1958, “A theorem on force-free magnetic fields”, *Proc. Natl. Acad. Sci. USA*, **44**, 489–491. Related online version (cited on 24 November 2005):
<http://www.pubmedcentral.gov/articlerender.fcgi?artid=528606>. 3.2
- Yang, W.H., Sturrock, P.A., Antiochos, S.K., 1986, “Force-free magnetic fields: the magneto-frictional method”, *Astrophys. J.*, **309**, 383–391. Related online version (cited on 24 November 2005):
http://adsabs.harvard.edu/cgi-bin/bib_query?=1986ApJ...309..383Y. 3.3
- Yeh, T., 1976, “Day side reconnection between a dipolar geomagnetic field and a uniform interplanetary field”, *J. Geophys. Res.*, **81**, 2140–2144. 1, 7
- Yeh, T., 1978, “Topological structure of coronal interplanetary magnetic field”, *Solar Phys.*, **56**, 439–447. Related online version (cited on 24 November 2005):
http://adsabs.harvard.edu/cgi-bin/bib_query?1978SoPh...56..439Y. 8.2, 23
- Zirin, H., Liggett, M.A., 1987, “Delta spots and great flares”, *Solar Phys.*, **113**, 267–281. Related online version (cited on 24 November 2005):
http://adsabs.harvard.edu/cgi-bin/bib_query?1987SoPh...113..267Z. 7
- Zirker, J.B., Martin, S.F., Harvey, K., Gaizauskas, V., 1997, “Global patterns or magnetic chirality”, *Solar Phys.*, **175**, 27–44. 5.1
- Zwaan, C., 1987, “Elements and patterns in the solar magnetic field”, *Annu. Rev. Astron. Astrophys.*, **25**, 83–111. Related online version (cited on 24 November 2005):
http://adsabs.harvard.edu/cgi-bin/bib_query?1987ARA&A...25...83Z. 12